NTNU
Norwegian University of
Science and Technology

The Applicability of Aluminium Alloys as Reinforcement Material in Concrete Constructions

Hans Sigurd Amundsen

Chemical Engineering and Biotechnology
Submission date: July 2018
Supervisor: Trond Furu, IMA
Co-supervisor: Hans Jørgen Roven, IMA
Oddvin Reiso, IMA

Norwegian University of Science and Technology
Department of Materials Science and Engineering

NTNU

Norwegian University of
Science and Technology

The Applicability of Aluminium Alloys as Reinforcement Material in Concrete Constructions

Master Thesis
TMT4900 Materials Technology
Spring 2018

Hans Sigurd Amundsen

Chemical Engineering and Biotechnology
Submission date: July 2018
Supervisor: Trond Furu, Hydro
Co-supervisor: Hans Jørgen Roven, IMA
Oddvin Reiso, Hydro

Norwegian University of Science and Technology
Department of Materials Science and Engineering

Preface

This master thesis is written at NTNU, Department of Materials Science and Engineering, during the spring of 2018. The thesis is written under the DARE2C research project. The project is led by the Norwegian aluminium producer Hydro with the cement producer Norcem, supported by HTC, the contractor Veidekke and the research institutions SINTEF and NTNU as partners. The work presented in this thesis is a continuation of the author's earlier work in the subject TMT4500. I hereby declare that this master thesis has been done independently and in accordance with regulations at NTNU.

Hans Sigurd Amundsen
NTNU, Trondheim
July 2018

Acknowledgements

First, my thanks go to my supervisor Trond Furu and my co-supervisors Hans Jørgen Roven and Oddvin Reiso. As a chemist, adventuring into the world of metallurgy was at first both an exciting and a little intimidating experience, but with their guidance, they have helped me to understand more about metallurgy than I could have imagined. I am grateful for all the help I have received from them and for all the constructive discussions we have had.

I would also like to take this opportunity to thank these people for their invaluable help in this master thesis:

- Elisabeth Kolberg, Eva-Marie Østbye and Åsne Takle Eide for amazing team work across field of studies, during our time in the DARE2C project. The work to casting concrete with aluminium reinforcement was a interesting process to be a part of and it would not have worked out as good as it did or been as fun without you.
- Harald Justnes for all the help in the laboratory and for sharing so much of his knowledge about concrete. I really hope that the DARE2C project will become a success story.
- All others involved in the DARE2C project.
- Geir Langelandsvik for his priceless guidance and help with the experimental work, fruitful discussions and entertaining coffee breaks. This master thesis wouldn't have been as good without his help.
- Pål Christian Skaret, Yingda Yu and Trygve Lindahl Schanche for tutorial guidance with experimental equipment.
- Helen Langeng for help with the extrusion work.
- Kristian Grøtta Skorpen and Martin V. Storlie for their help and expertise throughout long days of screw extrusion
- Øystein Gjervan Hagemo and his colleagues at Finmekanisk verksted Gløshaugen for their great craftsmanship and their many hours of machining aluminium.
- My dear friends Henrik G. Jenssen and Jonas S. Save for their help with the car engine and for both good academic and not so academic discussions during our 5 years together at NTNU.
- Herman Friele and the good workers at Evergood for supplying me and other tired students with high quality coffee
- And at last my family and friends for supporting and helping me with the master thesis.

Abstract

This thesis is a part of the DARE2C research project. The research projects primary objective is to develop a more environmentally-friendly type of concrete where more than 55% of the cement is replaced with less $CO_{2(g)}$ intensive supplementary cementitious materials (SCMs) and aluminium is used as reinforcement material, instead of steel. The major reason of why aluminium is not used as reinforcement material in concrete today is first and foremost because aluminium and its alloys will corrode in the highly alkaline environment that is produced in the concrete during the cement hydration reaction. Through a multidisciplinary collaboration together with three civil engineering students, a set of concrete beams incorporated with inhibitor protected Al-5Mg reinforcement were manufactured and subjected to a 4-point bend test. All of the reinforced concrete beams experienced anchorage failure where the reinforcement slipped inside the concrete due to poor adhesion but behaved mechanically similar as ordinary steel reinforcement before the failure. No corrosion was observed on the reinforcement surfaces which means the aluminium is chemically compatible with the concrete, but in order to conclude the applicability of aluminium as reinforcement further studies has to be conducted where the aluminium rebars need to be designed with a deformation pattern to obtain better adhesion.

An experimental procedure to measure gas development from the corrosion reaction was conducted on different alloys to determine the corrosion resistance with the inhibitor and its efficiency. The conclusion from this experiment was that a longer exposure time of the aluminium in the inhibitor solution seemed to increase the efficiency of the inhibitor and thereby increasing the corrosion resistance. Further studies must be performed to determine the mechanisms of the inhibitor and to identify the new protective oxide layer formed on the aluminium surface. Since this inhibitor is to be patented, the identity and possible mechanism will remain secret.

Two additional contributing reasons of why aluminium is not used as reinforcement material in concrete are firstly the inferior mechanical properties compared to steel and secondly high values of the coefficient of linear thermal expansion (CTE) in comparison to concrete. Aluminium has generally low stiffness and strength compared to steel, but by extruding the aluminium into specific geometries may compensate for the low Young's modulus. Improving the inhibitor may enable the use of alloys which are responsive to heat treatments and can obtain almost similar strength as compared to steel. Different CTE values between reinforcement materials and concrete exposed to large temperature differences can cause the reinforcement material to expand at higher rates than the concrete which may lead to loss of adhesion between the two materials and cracking and spalling of the concrete. The CTE was measured with use of a push-rod dilatometry technique and manual technique with an extensometer. The results obtained from the thermodilatometry was measured to be close to the literature values, but contained some uncertainties". Measuring CTE manually with an extensometer was unsuccessful. It was found that under normal operating temperature, CTE would not be a problem. Therefore, the focus should be directed to implementing high strength alloys rather than alloys with low CTE in concrete.

Two Al-Mg alloys and two Al-Si alloys were studied in this thesis, where they were subjected to thermomechanical processing, followed by examinations of their mechanical properties, microstructure and corrosion properties through a variety of metallurgical methods. In addition, a feasibility study was conducted where the possibility of recycling aluminium from old car engines through the novel method of screw extrusion and using it as reinforcement material in concrete was investigated. Insufficient cleaning of oil residue from the engine material and suboptimal run parameters resulted in poor quality of the surface of the produced profile. By improving the operating parameters during the screw extrusion process and improving the efficiency of the inhibitor, there is a possibility that this type of recycled material can be used as an environmentally friendly reinforcement material in concrete.

Sammendrag

Denne oppgaven er en del av DARE2C forskningsprosjekt. Forskningsprosjektets hovedmål er å utvikle en mer miljøvennlig betong hvor mer enn 55% av sementen er erstattet med mindre $CO_{2(g)}$ intensiv supplerende sement materialer (SCM) og aluminium brukes som forsterkningsmateriale, i stedet for stål. Hovedårsaken til hvorfor aluminium ikke brukes som forsterkningsmateriale i betong i dag, er først og fremst fordi aluminiumslegeringer vil korrodere i det svært alkaliske miljøet som produseres i betongen under sementhydreringsreaksjonen. Gjennom et tverrfaglig samarbeid sammen med tre bygg ingeniørstudenter, ble et sett betongbjelker støpt med inhibitorbeskyttet Al-5Mg armering produsert og testet i en 4-punkts bøyetest. Alle de aluminiumsarmerte betongbjelkene opplevde forankringsbrudd hvor forsterkningen skled inne i betongen på grunn av dårlig heft, men oppførte seg mekanisk likt som ordinær stålforsterkning før forankringsbruddet. Ingen korrosjon ble observert på forsterkningsflatene, noe som betyr at aluminium er kjemisk kompatibel med betong. For å kunne komme med en konklusjon på bruken av aluminium som forsterkning i konstruksjoner må det utføres flere studier hvor aluminiumsstengene må utformes med et deformasjonsmønster for å oppnå bedre heft.

En eksperimentell prosedyre for å måle gassutvikling fra korrosjonsreaksjonen ble utført på forskjellige legeringer for å bestemme korrosjonsmotstanden med inhibitoren og dens effektivitet. Konklusjonen fra dette eksperimentet var at lengre eksponeringstid av aluminiumslegeringene i inhibitoroppløsningen viste seg å øke effektiviteten til inhibitoren og dermed øke korrosjonsmotstanden. Flere studier må utføres for å bestemme inhibitorens mekanismer og å identifisere det nye beskyttende oksidlaget som blir dannet på aluminiumoverflaten. Siden denne inhibitoren skal patenteres, forblir identiteten og den mulige mekanismen hemmelig.

To ytterligere grunner til hvorfor aluminium ikke brukes som forsterkningsmateriale i betong er de dårligere mekaniske egenskapene i forhold til stål og høy termisk ekspansjon (CTE) i forhold til betong. Aluminium har generelt lav stivhet og styrke i forhold til stål, men gjennom å ekstrudere materialet med spesifikke geometrier kan dette kompensere for den lave Youngs modulen. Ved å forbedre inhibitoren kan det muliggjøre bruk av legeringer som kan varmebehandles og dermed oppnå omtrent like stor styrke stål. Ulike CTE-verdier mellom armering og betong kan ved store temperaturforskjeller føre til at forsterkningsmaterialet utvides raskere enn betongen, som kan forårsake tap av heft mellom de to materialene, og sprekkdannelse i betongen. CTE ble målt ved bruk av en push-rod dilatometer og ved manuell måling med et ekstensometer. De målte resultatene fra dilatometerforsøkene var nær litteraturverdiene, men på grunn av visse feilkilder førte det til usikkerheter i målingene. Det var mislykket å måle CTE manuelt med et ekstensometer. Det ble funnet ut at CTE under normal driftstemperatur ikke ville være et problem, og derfor bør det fokuseres på å implementere høystyrke legeringer fremfor legeringer med lav CTE i betong.

To Al-Mg legeringer og to Al-Si legeringer ble studert i denne oppgaven hvor de ble utsatt for termomekanisk prosessering. Deretter ble deres mekaniske egenskaper, mikrostruktur og korrosjonsegenskaper undersøkt gjennom en rekke metallurgiske metoder. I tillegg ble det gjennomført et mulighetsstudie i denne oppgaven, hvor muligheten for å gjenvinne

aluminium fra gamle bilmotorer gjennom bruk av den termomekaniske prosesseringsmetoden skrueekstrudering, og bruke det resulterende materialet som armering i betong. På grunn av utilstrekkelig rensing av motormaterialet for oljerester og lite ideelle kjøreparametere resulterte det i en dårlig kvalitet av overflaten til den produserte profilen. Ved å forbedre kjøreparametere under skrueekstruderingsprosessen og forbedre effekten av inhibitoren, er det en reell mulighet for at denne typen resirkulert materiale kan brukes som et miljøvennlig forsterkningsmateriale i betong.

Abbreviations

ASTM	American Society for Testing and Materials
CTE	Coefficient of linear thermal expansion
EDS	Energy-dispersive X-ray spectroscopy
DARE2C	Durable Aluminium Reinforced Environmentally-friendly Concrete Construction
HV	VIckers hardness
GP-zone	Guinier–Preston zone
IGC	Intergranular corrosion
LOM	Light optical microscopy
OPC	Ordinary Portland cement
PLC	Portevin-Le Chatelier
Rebar	Reinforcement bar for concrete
SCC	Stress corrosion cracking
SCM	Supplementary Cementitious Material
SE	Secondary electrons
SEM	Scanning electron microscope
TEM	Transmission electron microscope
TMP	Thermomechanical processes
UTS	Ultimate tensile strength
w/c	The water and cement mass ratio
wt.%	Weight percent
XRD	X-Ray Diffraction
XPS	X-ray photoelectron spectroscopy
ø10 mm	10 mm in diameter

Table of contents

Preface i

Acknowledgments iii

Abstract v

Sammendrag vii

Abbreviations ix

1 Introduction 1

2 Theoretical background 3
2.1 Aluminium alloy systems . . . 3
2.1.1 Al-Mg . . . 3
2.1.2 Al-Si . . . 6
2.2 Thermomechanical processes . . . 8
2.2.1 Extrusion . . . 8
2.2.2 Screw extrusion . . . 10
2.3 Microstructural evolution . . . 12
2.3.1 Recrystallisation . . . 12
2.4 Mechanical tests . . . 14
2.4.1 Tensile strength . . . 14
2.4.2 Hardness . . . 15
2.4.3 Coefficient of linear thermal expansion . . . 16
2.5 Concrete . . . 19
2.6 Corrosion of aluminium in alkaline media . . . 24

3 Experimental procedure 29
3.1 Materials . . . 29
3.1.1 Al-1Mg . . . 29
3.1.2 Al-5Mg . . . 30
3.1.3 Al-7Si-0.3Mg . . . 31
3.1.4 Al-12.7Si . . . 31
3.1.5 Engine block . . . 33
3.2 Grain structure characterisation . . . 36
3.2.1 Light optical microscopy (LOM) . . . 37
3.2.2 Scanning electron microscopy (SEM) . . . 37
3.3 Mechanical property measurements . . . 38
3.3.1 Hardness . . . 38
3.3.2 Tension test . . . 39
3.4 Techniques for measuring the coefficient of linear thermal expansion . . . 40
3.5 Extrusion . . . 42
3.6 Screw extrusion . . . 44
3.7 Hydrogen evolution measurement . . . 46

3.8 Casting and testing the aluminium reinforced concrete beams . . . 48

4 Results **53**
4.1 Hardness . . . 53
4.2 Tensile strength . . . 55
4.3 Coefficient of linear thermal expansion . . . 58
4.4 Observations made during screw extrusion trials . . . 62
4.5 Grain structure characterisation by LOM . . . 63
4.6 Particle characterisation by SEM . . . 72
4.7 Hydrogen-evolution of aluminium alloys in cement paste . . . 76
4.8 The 4-point bending test of the concrete beams results . . . 78

5 Discussion **79**
5.1 The effects of chemical composition and thermomechanical processing on the mechanical properties . . . 79
5.1.1 Hardness . . . 79
5.1.2 Tensile strength . . . 80
5.2 Grain structure observations of the thermomechanical processed alloys through LOM and SEM examinations . . . 82
5.3 The interpretation of the CTE data and its importance for reinforcement materials in concrete . . . 85
5.4 The durability and performance of the aluminium alloys in concrete . . . 88
5.5 Challenges and opportunities with recycling car engines through screw extrusion . . . 92

6 Conclusion **95**

7 Recommendation to further work **99**

References **101**

Appendices **105**

A Flowchart of the work and results obtained in this thesis **105**

B Extrusion log **106**

C Micrographs of anodised cross-sections **111**

D Micrographs of the samples before extrusion **113**

E CTE results **116**

F EDS analysis of the alloys before extrusion **123**

1 Introduction

Today concrete is one of the most commonly used materials in the building industry due to its versatility, user-friendliness, sturdiness and low-cost. Concrete can be defined, at the utterly most fundamental as gravel and sand bound together with cement and water to a structure. Only in Norway is the total annual consumption of cement approximately 1.5 million tons, [1]. Because of the energy-intensive processes which are involved in the manufacturing of ordinary cement and the immense quantity produced, this production has been shown to be one of the biggest global contributors to anthropogenic emissions of $CO_{2(g)}$, [2]. This is a challenge the industry takes seriously, where an example which can be drawn forth is the Norwegian cement producer Norcem which recently has made major investments in carbon capture technology, [3].

In order to additional increase the strength of the concrete, steel is most commonly used as reinforcement material since it is very compatible with concrete, strong, and is also easily accessible and an abundance of, which makes it relatively cheap. Although it seems that concrete and steel is a match made in heaven, it comes with some consequences. Steel is highly susceptible to corrosion attacks in the presence of chlorides and acidic environments. This is the basis for why concrete today is designed to protect embedded steel reinforcement from corrosion at the expense of potential strength and durability. This may be where aluminium can seize the opportunity to display its broad versatility as a construction material with its excellent corrosion protection and mechanical properties. Today, aluminium is already commonly used in many commercial areas such as marine applications and constructions, industry and not least in the automotive industry, [4]. With all this taken into account, this leads to the question:

Can aluminium be used in concrete?

The short answer to this question is no. Aluminium and its well known protective oxide layer would disintegrate in contact with the highly alkaline environment which concrete holds, in both fresh and hardened state. Using aluminium by itself as reinforcement would do nothing in terms of giving additional strength to the concrete and the corrosion products from the aluminium would just render the concrete susceptible to cracks and spalling. These reasons and the substantial hydrogen gas evolution have established the foundation of why aluminium as a structural component in concrete is not used and is even prohibited in certain fields due to HSE. The possibilities for a stronger and more environmentally friendly concrete through the use of other reinforcement materials became the driving force of investigating this opportunity, and through the DARE2C project it has now been developed a new protection system which has shown promising results in enabling the use of aluminium alloys with 5 wt.% Mg as reinforcement material in concrete, [2]. This corrosion protection system is based on replacing more than 50% of the cement clinker with less $CO_{2(g)}$ intensive materials and thereby reducing the pH in the concrete in the combination with treating the aluminium surface with an inhibitor. This master thesis is connected to this project and together with three master students, from the Department of Structural Engineering at NTNU shall through a multidisciplinary collaboration examine the behaviour of this Al-5Mg alloy in a scaled-down experiment, where it will be integrated as reinforcement in concrete beams.

By enabling the use of aluminium as reinforcement opens many new avenues of possibilities for new durable and environmentally friendly constructions. The combined weight reduction by replacing heavy steel with a lightweight metal such as aluminium which reduces the need for the concrete cover over the reinforcement bars leads to new super lightweight construction materials with high strength. Since aluminium is not susceptible to corrosion at relatively lower pH ranges, the concrete can thereby be designed to achieve higher strength by allowing faster carbonation of the concrete through higher porosity, [2]. In addition to obtaining higher strength, the concrete also becomes more durable and maintenance free. Faster carbonation of the concrete will also further contribute to a more $CO_{2(g)}$ neutral concrete.

Although aluminium displays many favourable properties as reinforcement material in concrete, there are some issues that have to be addressed. Aluminium alloys, in general, have approximately twice as high coefficient of thermal expansion than concrete, which means that during high temperature the aluminium can lose its adhesion to the concrete and crack. Despite pure aluminium having only $\frac{1}{3}$ of the density compared to iron, it also only has $\frac{1}{3}$ of the strength, so proper alloying of the aluminium to obtain high strength combined with good corrosion properties are of the utmost importance. The manufacturing method of the alloys also plays a crucial role for the corrosion, microstructural and mechanical properties. The work of implementing aluminium as a structural component in concrete implies that many disciplines need to be involved in order to form an overall picture of the applicability. Therefore will this thesis mainly focus on the metallurgical aspects of producing the aluminium reinforcement rods with the focus microstructure and mechanical properties, and the behaviour of different alloys in the concrete environment with the regards to corrosion, and to a certain extent tribology.

By improving the corrosion protection system to enable more aluminium alloys to be used as reinforcement, this introduces the possibility to use recycled aluminium as reinforcement. Today there are over 1 billion person cars globally on the road, and only in 2016 were over 70 million cars produced, [5]. With the steady increase in electric cars and other more environmentally-friendly transportation alternatives, and the today's bad reputation regarding emissions of diesel cars, are clear signs that traditional combustion engines are on its way to be phased out. Aluminium is a widely used material in cars, which altogether combined means that this can be an easily accessible and in abundance source for material which can potentially cover the need for reinforcement material in concrete. In order to truly optimise and further benefit the environment, a novel method of continuous extrusion of light metals has been developed in a cooperation between Hydro and NTNU, [6]. A recent study has shown that the screw extrusion process is more materials and energy efficient than remelting and other commercial extrusion processes, [7]. Together, this presents a golden opportunity to cover the demand for reinforcement material for concrete and to possible commercialise the screw extrusion process of light metals.

As the secondary objective of this thesis, the possibility of recycling aluminium from automobile engine parts through the novel method of continuous extrusion of light metals, and to use this processed material as reinforcement in concrete will be investigated.

2 Theoretical background

This chapter summarises the theoretical background necessary to give the reader insight into the analytical methods used for characterisation, material properties and mechanisms in the experimental work executed in this master thesis. The purpose is to combine the extracted experimental results with the presented theory with the goal to engage in a professional discussion. The sections 2.2.2, 2.4.1, 2.4.2, and 2.4.3 are based on the author's earlier work [8].

2.1 Aluminium alloy systems

Due to good corrosion properties, high strength to weight ratio and is one of the most common elements in the Earth´s crust makes aluminium one of today's most commonly used metals, [4]. The applicability of aluminium is very versatile with e.g. all from kitchen supply to industry and large marine applications. Aluminium is firstly divided into two major categories, casting alloys and wrought alloys, and are further divided into classes with respect to their principal alloying element.

The alloy classes which are studied in this thesis are presented in consecutive sections 2.1.1 and 2.1.2.

2.1.1 Al-Mg

Aluminium alloys in the 5xxx and 5xx.x series have Mg as their principal alloying element. Excellent corrosion properties, high strength to weight ratio and good weldability are properties which makes them an important material for marine-and-offshore applications, [9, 10]. The Al-Mg alloys are non-heat treatable and their strength comes from solid solution hardening and strain hardening, [4]. Compared to Al, Mg has a bigger atomic radius and as a solute atom in the Al lattice the impurity atom Mg will interact and decrease the mobility to dislocations, [11, 12]. The strength and the hardness of an alloy will increase by increasing the concentration of impurity atoms that go into solid solution (both substitutional and interstitial). With strain hardening, the strength will increase according to the degree of plastic deformation applied, but the ductility will consequently decrease. The dislocation density will increase during plastic deformation, which will cause the average distance between adjacent dislocations to decrease. Since the dislocation-dislocation strain field interactions are, on an average repulsive this will lead to restriction to the dislocation mobility. This means that more energy is required to enable dislocation movement which in other terms means that the aluminium will be stronger and harder. Compared to a metal in the annealed state, the yield strength of a heavily deformed metal can be 5-6 times higher, [13].

The precipitation sequence of $\beta - Al_2Mg_3$, which is described by Wei *et. al.* [15], is well accepted and occurs according to Equation 2.1. Guinier-Preston (GP) zones, β'' and β' are all metastable intermediate phases with the different crystal structure, morphology and chemical composition [16, 15]

The alloy classes which are studied in this thesis are presented in consecutive sections 2.1.1 and 2.1.2.

$$\text{Solid solution} \rightarrow \text{GP zones} \rightarrow \beta\text{''} \rightarrow \beta\text{'} \rightarrow \text{Stable } \beta\text{-phase } (Al_2Mg_3) \tag{2.1}$$

Commercial alloys in the 5xxx class tend to be alloyed with 3-6wt% Mg. Higher concentrations of Mg or slow cooling rate can lead to precipitation of stable $\beta - Al_2Mg_3$ along the grain boundaries, [18, 12]. This is unwanted since large particles in the microstructure will make the material brittle and depletion of the encircling Al-matrix with Mg will consequently decrease the strength of the material.

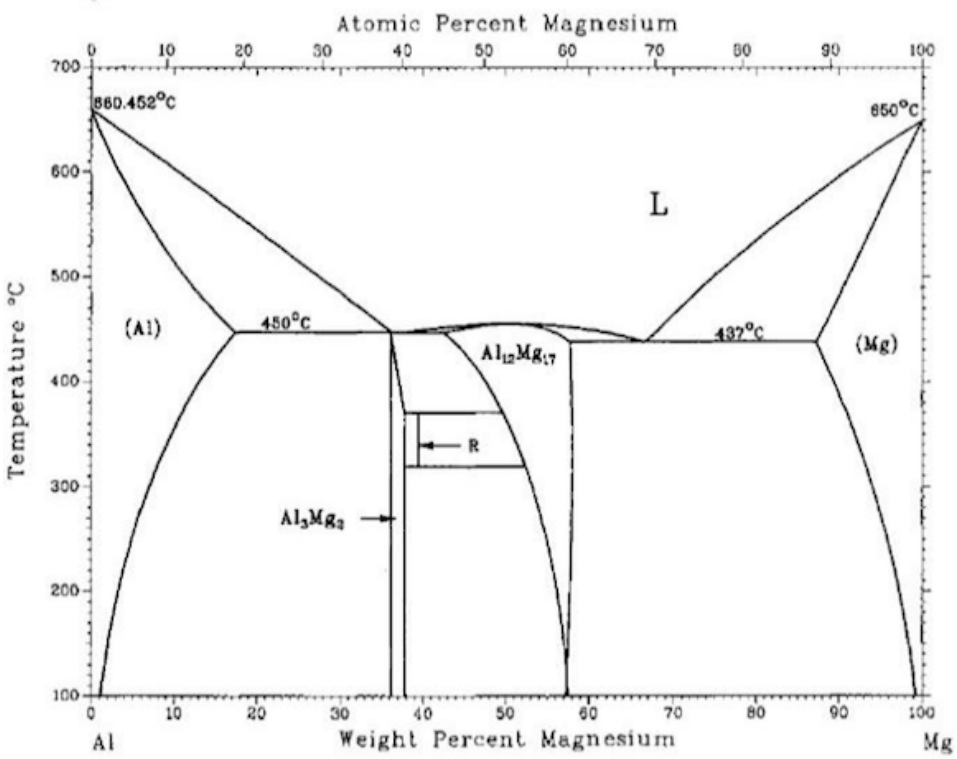

Figure 2.1.1: The binary phase diagram of Al-Mg, from reference [17].

In addition to the principal alloying element, alloys usually consist of smaller amounts of other alloying elements either to improve the properties of the alloy or just as an impurity from manufacturing. This may be e.g. Fe, Si, Cu, Mn and/or Cr. This may lead to precipitation of particles like $Al_6(Fe, Mn)$, $Al_{18}(Cr, Mn)_2Mg_3$ and Mg_2Si, [10].

The corrosion resistance of this alloy class is, as mentioned, excellent due to Mg which becomes a part of the protective oxide-film, [12]. The oxide layer on the surface will have a larger specific volume compared to aluminium alloys in other classes. However Al-Mg alloys with an Mg concentration exceeding 3 wt.% are susceptible to both intergranular corrosion (IGC) and stress corrosion cracking (SCC) when exposed to a corrosive environment at elevated temperatures ($\geq$50°C) over a prolonged amount of time, [15, 19]. This is due to the formation of $\beta - Al_2Mg_3$ precipitates along heterogeneities such as grain boundaries, which is anodic relative to the Al-matrix. according to Goswami *et. al.* [9] intergranular precipitation of $\beta - Al_2Mg_3$ will not contribute to ISC since it is not a part of the continuous grain boundary network, thus may also help to prevent ISC. "Scavenging" Mg before it reaches the grain boundary this may reduce the formation of the precipitates on the grain boundary.

2.1.2 Al-Si

Aluminium-silicon alloys hold a number of advantageous characteristics e.g. excellent castability, low density and favourable mechanical properties, [4]. This is a binary system with Si as the principal alloying element, and with the eutectic composition at 12.6 wt.%, as shown in Figure 2.1.2. Since Si is essentially insoluble in the Al matrix, the hypoeutectic microstructure will contain a soft and ductile Al phase and a hard and brittle Si phase at room temperature. The hard and brittle Si phase is which contributes to the good wear properties of this alloy class, where the vickers hardness of Si is approximately 1020 HV (10 GPa), [4].

For as-casted Al-Si alloys the ductility is controlled by the α-Al dendrite grain size of the and the morphology of β-Si particles [20, 21]. Large grain sizes of the α-Al-phase with sizeable elongated Si-particles with acicular morphology will yield a low ductility. By increasing the cooling rate during solidification, it will decrease the grain and particle sizes and consequentially increase the ductility as a result of increased nucleation. In an eutectic structure, large, coarse, lamellar-like plates of Si will be present in the aluminium matrix which will lead to the brittleness of the alloy [21]. The lamellar structure in the Al-Si eutectic is associated with the big anisotropy of the Si growth and too low interface energy between Si and Al.

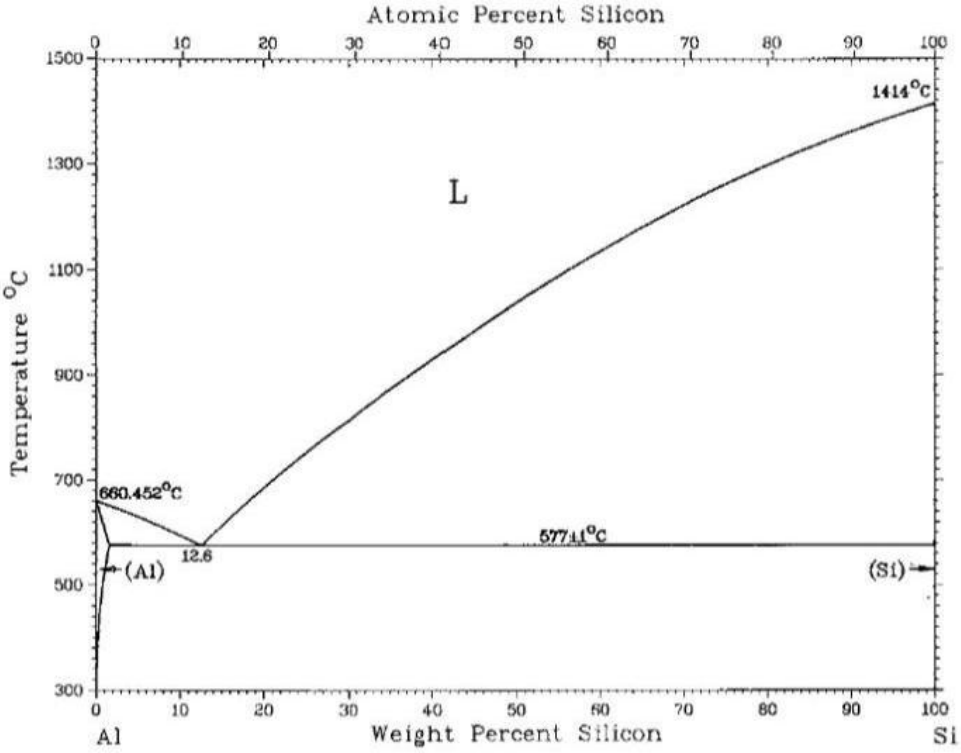

Figure 2.1.2: The binary phase diagram of Al-Si, from reference [17].

Commercial Al-Si alloys usually contain other alloying elements to further enhance and tailor their properties, [4, 20, 22]. Iron addition can be tolerated up to levels of 1.5

wt.% where its presence will modify the silicon phase by introducing different Al-Si-Fe phases. The α phase of this composition is present as a "Chinese script" morphology in the microstructure, while the less common β-phase is present as needles or platelets.
To increase the strength of the alloy, Mg will usually will precipitate into Mg_2Si particles in the matrix. The Mg may combine with insoluble Al-Fe phases which will result in a loss of strengthening potential. Cu is added to all the alloys to increase the wear resistance. The addition of Cu contributes to an additional strengthening of the matrix through ageing or precipitation-hardening by $AlCu_2$ or by modifying the brittle Al-Fe-Si phases through substitution. The strength of the alloy increases with increasing amounts of Cu, but at the expense of ductility and corrosion resistance. Mn is an important element which is added in small concentrations (<1 wt.%). The Mn in the matrix may reduce the solubility of Fe and Si in the aluminium matrix and modify the composition and morphology of the Al-Fe-Si phases. By supplementing with Mn the formation of phases like $Al_{12}(Fe, Mn)_3Si$ are rather favoured, with a less needle-like morphology than $Al_9Fe_2Si_2$. The β-Al_5FeSi-phase is the most harmful metallic phase [20]. It forms large, brittle plates that influence both mechanical properties and castability. Mg and Mn are added to reduce the formation of β-Al_5FeSi. In addition, to reducing the β phase, Mg also makes age hardening of the Al-Si alloys possible and may form a harmless π phase. Other alloying elements like Sr, Ca and Na are added as modifiers [23]. These modifiers repress the formation of Si primary crystals and produce a finer distribution of lamellar structure, which can displace the eutectic point to a higher Si content.

In addition to solid solution strengthening and strain hardening, some alloys may gain higher strength and hardness through specific heat treatments. This process is called precipitation hardening where the increased hardness and strength is obtained through the formation of extremely small, uniformly dispersed intermetallic particles of a second phase within the original phase matrix, [11]. The process involves an initial stage where quenching is applied after solid solution heat treatment to preserve the supersaturated solid solution at a maximum level in the matrix, and the final stage where the increase in hardness is obtained with heat treatments through the dissolution of soluble phases into precipitates, [4, 24]. The process gets its name from these small particles which is called precipitates. The strengthening mechanism from this process can be explained with the impeding of dislocation movement which is caused by these particles, [11]. Additions of Cu and Mg to the Al-Si alloy class enables precipitation hardening. The increase in strength over time, at room temperature is associated with the term ageing.

Excellent tribological properties, good corrosion resistance, castability desirable mechanical, and thermal properties are some of the reasons why Al-Si alloys with the addition of Cu and Mg are chosen as materials for automobile engine components. A high strength to weight ratio is needed to improve fuel efficiency and a low coefficient of linear thermal expansion is needed to reduce large residual stresses with the grey iron protective cylinders, [25]. Hypoeutectic Al-Si alloys with Cu and Mg additions are usually the choice of material when manufacturing aluminium engine blocks. Due to the Si, these alloys generally have excellent corrosion resistance. However, alloys containing Cu will have a lower corrosion resistance than Cu-free alloys, where the corrosion resistance will decrease according to the increasing amount of Cu, other impurities like Pb.

2.2 Thermomechanical processes

Thermomechanical processes (TMP) are a series of metal-forming processes such as rolling, forging and extrusion and, are often referred to as hot working operations, [26]. These are used in the first step of into converting cast ingots into a wrought product. They are carried out at high temperatures (usually above $0.6T_m$) and at high strain rates. The thermomechanical processes used in the work of this thesis is presented in consecutive sections 2.2.1 and 2.2.2.

2.2.1 Extrusion

Extrusion is a common industrial production method used to produce cylindrical bars, hollow tubes, and products with an irregular cross-section [26]. It was originally invented with the purpose of producing lead pipes, and then later to develop lead sheathed electrical cables. A block of metal is forced through a die or an orifice to a product with the desired shape and reduced cross-section, under high pressure. The billet is often extruded at high temperature to reduce the deformation resistance and flow stress. Due to the immense amount of plastic deformation which is introduced to the metal under extrusion, it is important to keep the top working temperature safely under the metal's melting point. The relationship between the initial cross-section, A_0 and the cross-section after extrusion, A_f is called the extrusion ratio and is expressed as:

$$R = \frac{A_0}{A_f} \tag{2.2}$$

Usually, for steel, the extrusion ratio is around 40:1, but for aluminium, it can be as high as 400:1.

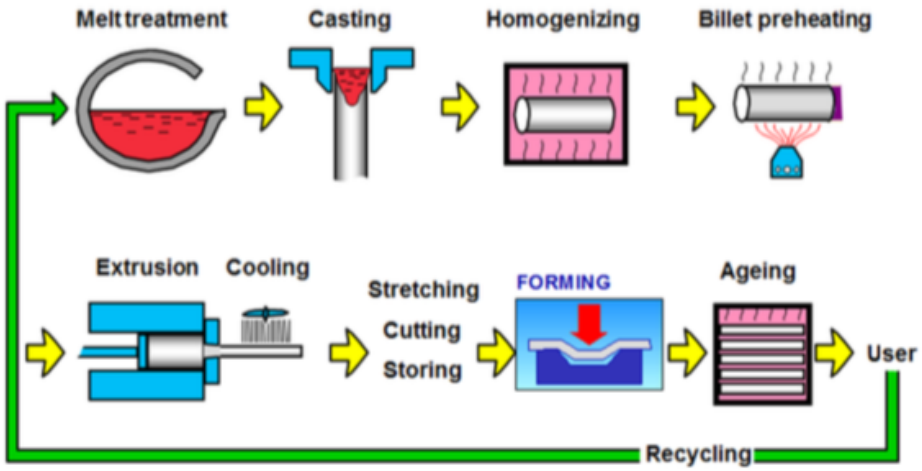

Figure 2.2.1: The entire route of aluminium from melting to a finished extrusion product, from reference [27].

The initial temperature of the billet can heavily influence the extrudability, the mechanical properties and the surface quality of the extrudate. By overheating the billet it is possible to obtain higher extrusion speeds, better mechanical properties and improved surface quality, [27]. Homogenisation is the heat treatment operation of cast feedstock material used to enhance the workability during deformation and to improve the properties of the final product, [14]. The predominant effects of the homogenisation process have on the microstructure is:

- Levelling out microsegregations and solutionise elements like Cu, Mg, Si and Zn.
- Eliminating low melting point eutectics in the metal (e.g. Al$-$$Mg_2Si$ in 6xxx alloys.
- Spheroidising insoluble phase particles (e.g. Fe rich phases).
- Transforming non-equilibrium phases to stable phases (e.g. acicular β-AlFeSi particles to more globular and spheroid α-AlFeSi particles in 6xxx alloys.
- Controlling the precipitation of dispersoid particles from dispersoid forming elements like Mn, Cr and Zr, [27].

The deformation is always greater in the surface layer which will in this region cause the metal to have a finer recrystallised grain size, [26]. The surface layer will cool down at a higher rate than the interior of the material. This means that the interior will stay at a higher temperature for a longer time than the surface which may result in grain growth in this area. The thickness of the recrystallisation layer in the extrudate at the surface will on a general basis increase with increasing ram speed and billet preheating temperature, [27]. The alloy content of Mg, Si and Cu has a minimal influence on the recrystallisation layer.

The Figures 2.2.1 and 2.2.2 gives a good illustrative overview of the whole metallurgical process from melting the aluminium to the finished extrusion product.

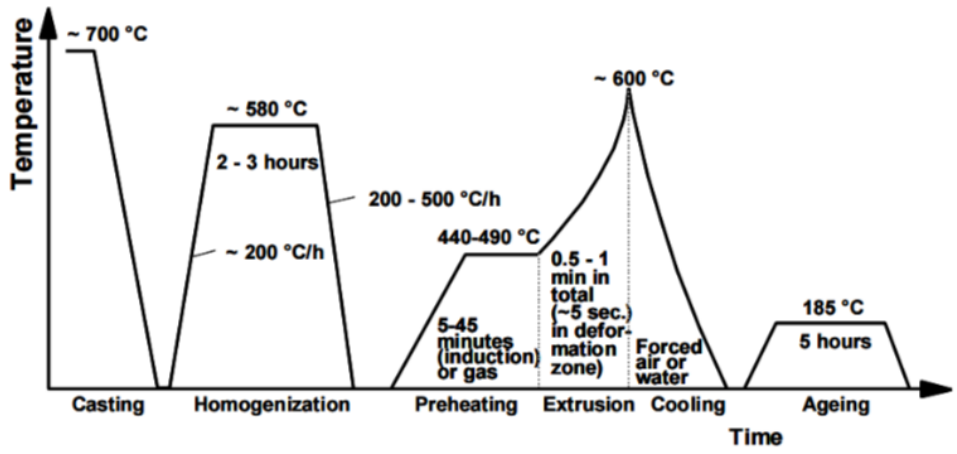

Figure 2.2.2: Common processing path for a thermomechanical process, from reference [27].

2.2.2 Screw extrusion

The joint effort between Hydro Aluminium and NTNU has brought forth a novel method of continuous extrusion of materials with high viscosity, [6]. This consolidation process was patented in 2008 under the name "Screw extruder for the continuous extrusion of materials with high viscosity". Look up reference [6] in the bibliography for the source of the patent. The concept of screw extrusion is widely used in the food and polymer industry.

Traditional extrusion is a batch process where when the whole billet has been pressed through the die it has to be reloaded with a new billet. Screw extrusion, on the other hand, can produce an extrusion profile continuously with a steady supply of feedstock material. Figure 2.2.3 show a schematic drawing from the original patent [6] where granulates are fed into the screw chamber and the build-up of solid material.

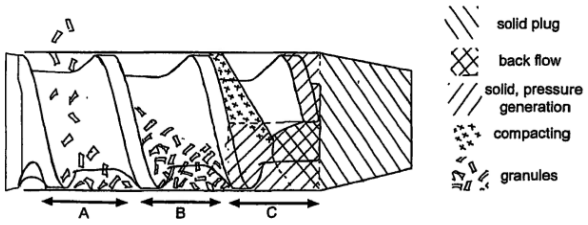

Figure 2.2.3: Patent sketch, from reference [6].

The whole screw extrusion process from assembly to disassembly is illustrated in Figure 2.2.4. The first step in this procedure is to assemble the chamber with the screw and the die. Then the whole chamber is heated up with a copper induction coil [6, 28]. When the chamber has reached the desired operation temperature, cleaned granulated raw material is fed to the end of the chamber. As the screw begins to rotate, the granulates will be transported forward in the chamber which will partially consolidate the granulates, as illustrated in step 3 in Figure 2.2.4. The screw transports the aluminium from the back of the chamber to the die and fills it up. Like most other metals, aluminium has a sticking friction at elevated temperature. The deformation and the friction forces from the consolidation of aluminium in the chamber will yield an additional heat generation as an outcome. To control the operation temperature compressed air can be applied in both the rear and frontal end of the chamber. As the aluminium in the extrusion chamber becomes more consolidated all the deformation will lead to the formation of metallic bonds of the aluminium and further to a solid metal plug, which is illustrated as step 4 in Figure 2.2.4. The deformation will also break down particles and secondary phases and reduce their size. When high enough pressure has been built up and the extrusion chamber is filled, the solid metal plug will be forced through the die into and into straight extrusion profile with a reduced cross-section. At this stage stable continuously extrusion is possible. The screw extruder can also be used for extrusion of other light metals, like Ti or Mg, or even mixtures of metallic composites, [6, 30]. After the end of the run and disassembly, necessary cleaning of equipment is required. The metal plug and big chunks of aluminium are removed with mechanical force and the equipment with aluminium

residue left on them are treated in a NaOH solution which will dissolve the aluminium but will not affect the steel in the tools.

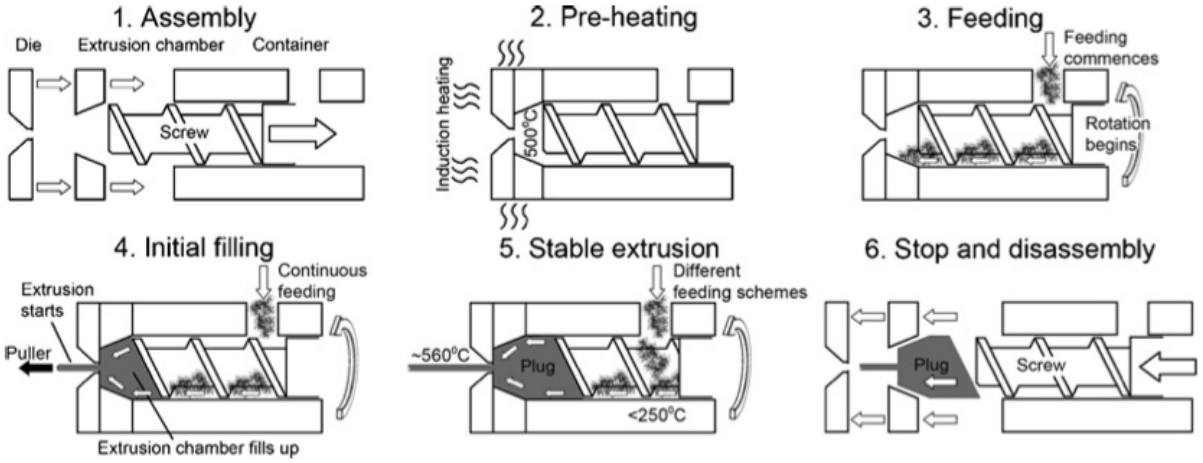

Figure 2.2.4: Experimental procedure in the screw chamber, from reference [28].

A recent study was done by Joost R. Duflou *et. al.* [7] of recycling aluminium through different processing routes, like e.g. remelting and extrusion have shown promising results for screw extrusion. The study implicates that this process is more energy and material efficient compared to other recycling routes, and in big-scale production, it has the potential of being the most environmentally friendly process route to recycle aluminium.

2.3 Microstructural evolution

During extrusion, and other thermomechanical manufacturing processes metals are subjected to severe plastic deformation in high-temperature conditions, which will result in microstructural alterations. These microstructural alterations will greatly influence the material properties. Several of the physical mechanisms that influence the strength of a metal is, as mentioned, strain hardening and the processes recovery, recrystallisation, and grain growth, [29]. The processes of recovery, recrystallisation and grain growth will be explained more in-depth in the consecutive section 2.3.1.

2.3.1 Recrystallisation

When a metal is subjected to deformation at lower temperatures ($T<0.5T_m$), energy is transferred and a portion of that energy will remain stored as dislocations, which is present as crystal defects in the microstructure, [13, 31]. This stored energy in the microstructure will be released upon annealing through three main processes, those of recovery, recrystallisation, and grain growth, [32].

When a deformed metal (Figure 2.3.1(a)) is exposed to high temperatures this may partially restore the metal's microstructure and properties to its original values, from before deformation (Figure 2.3.1(b)) by recovery, [13]. The high temperature activates processes like solid state diffusion that provides mechanisms in which dislocations are annihilated and rearranged in configurations with lower energy. Since the recovery doesn't completely remove the dislocation structure, a further restoration process is initiated which is termed recrystallisation. As an opposite to recovery, recrystallisation involves the formation of new dislocation-free grains within the deformed or recovered grains (Figure 2.3.1(c)). From partially recrystallised to fully recrystallised these new grains will continue to grow and consume the deformed and recovered grains until they all have been replaced by these new grains with low dislocation density (Figure 2.3.1(d)). Recrystallisation may be described as a discontinuous process since the nucleation and growth stages may occur heterogeneously throughout the material. During recrystallisation of alloys, solutes and second-phase particles may influence the recrystallisation kinetics where the size, morphology and chemical composition of these particles also are of importance. Since recrystallisation is a microstructural transformation, it is quantitatively measured through optical metallography. The driving force for the recrystallisation process is the energy difference between the deformed state and the dislocation-free state, [29].

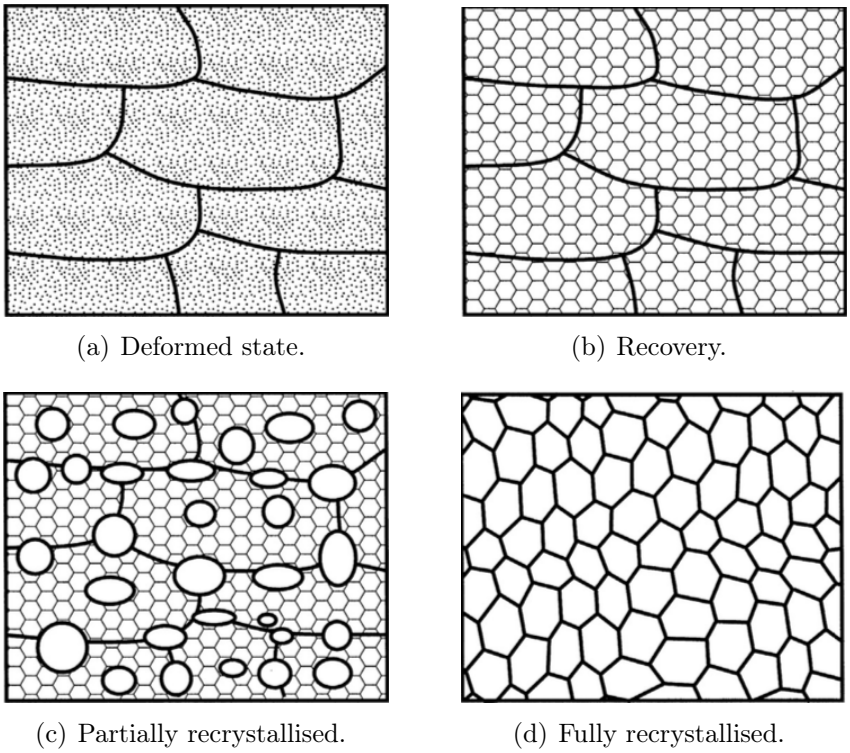

(a) Deformed state. (b) Recovery.

(c) Partially recrystallised. (d) Fully recrystallised.

Figure 2.3.1: An illustration of the recrystallization sequence, from reference [13]

Upon further exposure to elevated temperatures, this may result in grain growth where the large grains will eliminate the small grains and continue to grow, [13]. Controlling the grain size is important for numerous reasons. The Hall-Petch effect is a great example of why.

$$\sigma_y = \sigma_0 + k_y * d^{-\frac{1}{2}} \tag{2.3}$$

Where:
σ_y Yield stress
σ_0 Material constant for starting stress for dislocation movement
k_y Strengthening coefficient
d Average grain diameter

The Hall-Petch Equation (2.3) states that a small grain size will give an increase in strength of the metal as opposed to coarse grains, [11]. This is due to the fact that a fine-grained material has a greater total area of grain boundary to restrict the dislocation mobility.

2.4 Mechanical tests

2.4.1 Tensile strength

Valuable information of a metals mechanical properties can be obtained from a tension test, [26]. In a tension test, a machined specimen will be subjected to increasing axial load until it eventually fractures. The load applied and the elongation of the specimen is continuously measured by an extensometer during the test. The obtained data is usually presented in a plotted stress-strain curve, similar to Figure 2.4.1 which depict a stress-strain curve of a ductile metal. To minimise the geometrical factors from the specimen, the load and elongation are normalised to the respective parameters of engineering stress and engineering strain, [11]. Engineering stress σ is defined as the ratio of the instantaneous load, F applied perpendicular to the initial cross-section, A_0 ($\sigma = \frac{F}{A_0}$). Engineering strain ϵ is defined as the ratio of the deformation elongation, Δl and the initial length before deformation, l_0 ($\epsilon = \frac{\Delta l}{l_0}$).

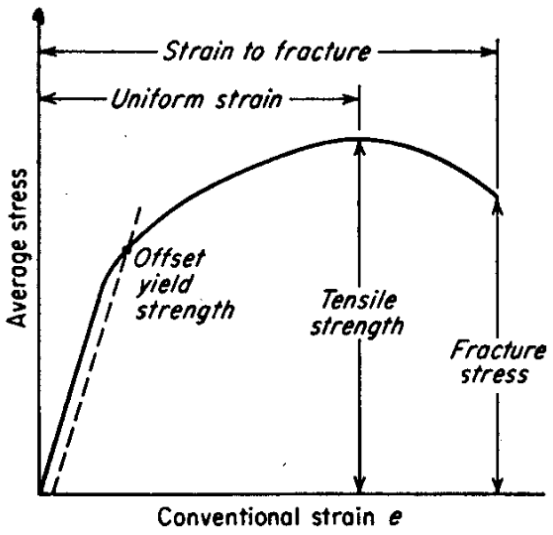

Figure 2.4.1: Typical stress-strain curve, from reference [26].

Important parameters which can be retrieved from the stress-strain curve are the ultimate tensile strength, σ_{UTS}, yield strength, σ_y, and the strain at fracture, ϵ.

The Portevin-Le Chatelier effect

The Portevin-Le Chatelier, (PLC) effect is caused by dynamic strain-ageing behaviour and yields serrations on the stress-strain curve [26, 33]. During deformation of tensile specimens, solute atoms in the alloy are able to diffuse at a faster rate than the speed of the dislocations so as to catch and lock them [26]. according, the load has to increase, and when the dislocations are ripped away from the solute atoms it will yield a load drop. After multiple recurrences, this will lead to serrations in the stress-strain curve. Mg in solid solution is known to initiate PLC [33]. Since PLC reduces the formability of the materials and can cause undesired markings at shaped product surfaces it is important to keep this in mind.

2.4.2 Hardness

Mainly, hardness is a measure which describes the resistance to deformation, and for metals, it indicates the metal's resistance against permanent or plastic deformation, [26]. Hardness is a poorly defined term which has different meanings depending on the person who measures and/or use it. For an engineer, the hardness is a simply measured and specified quantity which indicate the metal's strength and heat treatment. Vickers hardness (HV) method is used to measure the hardness of a material through indentation by an indenter, [11, 34]. A small diamond with square based-pyramidal geometry is forced into a surface of the specimen with a specific force, P, and the resulting indentation is measured under a microscope. The two diagonal lengths of the indentation are measured in the microscope and converted to a HV number with Equation 2.4 and 2.5. Preparations in form of grinding and polishing are needed to obtain a smooth even surface.

$$HV = \frac{2000Psin\frac{\theta}{2}}{d^2} = \frac{1854.4P}{d^2} \tag{2.4}$$

$$d = \frac{d_1 + d_2}{2} \tag{2.5}$$

Where:

HV	Vickers hardness number
P	Fixed force [kgf]
θ	Angle between opposite faces of the pyramid. Usually 136°
d	Average diagonal length
d_1 and d_2	Measured diagonal lengths

This test can provide a continuous scale of hardness, for a given load, from very soft metals with a HV of 5 to extremely hard materials with a HV of 1500, [26].

2.4.3 Coefficient of linear thermal expansion

The coefficient of linear thermal expansion (CTE) is a measure of reversible change of length to a material as a reaction to temperature difference [4, 35]. The CTE (α) value is given in $\frac{\mu m}{m^{\circ}C}$ and describes how many μm an object of x meters will expand or contract as a reaction to increasing or decreasing the temperature, respectively. The content of alloying elements and the volume fraction of intermetallic phases will control the behaviour of thermal expansion in aluminium alloys [36]. Different elements will either increase or decrease the CTE with different degrees. Table 2.1 shows that the addition of Al_2O_3, Cu, Fe, Ni and Si reduces the CTE while the addition of Mg and Zn increases it. The change of CTE as a result of an addition of per wt.% alloying is showed in approximately a linear manner and is given in Figure 2.4.2

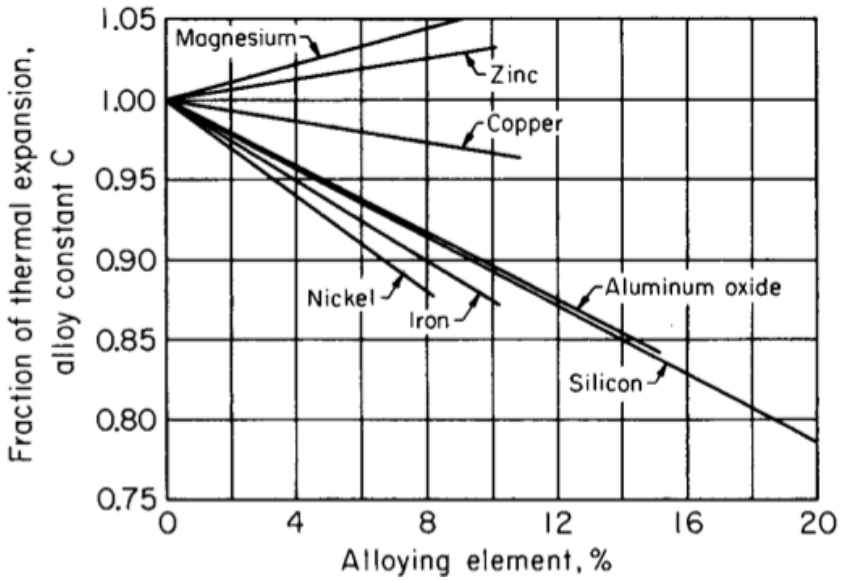

Figure 2.4.2: The effect of alloying elements on the thermal expansion of pure aluminium. Fraction is based of 1.0000 for pure aluminium, from reference [35].

For pure aluminium, the alloy constant is 1.0000 and Table 2.1 shows how much power per input wt.% of each alloy element to the pure aluminium will have. From Table 2.2, the CTE for pure aluminium is given as $23.6\frac{\mu m}{m°C}$ in the temperature range 20-100°C. If 12 wt.% of Si is added to the aluminium, the new alloy constant will be 0.8716 which will give a new CTE of $20.6\frac{\mu m}{m°C}$.

Table 2.1: The change of thermal expansion by adding alloying elements at annealed temper. Fraction 1.0000 is based on pure aluminium, from reference [35].

Alloying element	The change in alloy constant of pure Al per wt.% addition
Al_2O_3	-0.0105
Cu	-0.0033
Fe	-0.0125
Mg	+0.0055
Ni	-0.0150
Si	-0.0107
Zn	+0.0032

Elements in solid solution may combine into phases with low solubilities, like Mg_2Si. In annealed state, these phases will be diluted out from solid solution [35]. The formation of this insoluble phases will remove the alloying elements from the solid solution. From limited data, observations have shown that alloys containing phases like Mg_2Si will have a lower coefficient of thermal expansion than expected from calculations based on solely individual element addition. The heat treatment of an alloy will have an impact on the thermal expansion. Alloys heat treated in T4 and T6 tempers have been measured of having on average 0.0150 higher thermal expansion than for those alloys in annealed condition [35].

Table 2.2 provides the values of average coefficient of linear thermal expansion to some aluminium alloys and materials used in concrete constructions at different temperature ranges.

Table 2.2: Average coefficient of linear thermal expansion of some selected materials, from reference [37].

	Coefficient of thermal expansion (CTE) $[\frac{\mu m}{m°C}]$			
Material	-50-20°C	20-100°C	20-200°C	20-300°C
AA1xxx	21.8	23.6	24.5	25.5
AA2xxx	20.8	22.5	23.4	24.4
AA3xxx	21.5	23.2	24.1	25.1
AA365 (7.0% Si,0.3%Si)	-	21.5	22.5	23.5
AA336 (12.0%Si,2.5%Ni, 1.0%Mg, 1.0%Cu)	-	21.5	22.5	23.5
AA4032 (12.2%Si)	18.0	19.5	20.2	21.0
AA4043 (5.2%Si)	-	22.0	-	-
AA5083 (4.4% Mg,0.7%Mn)	22.3	24.2	25.0	26.0
AA5454 (2.7%Mg, 0.8%Mn)	21.9	23.7	24.6	25.6
AA6061 (1.0% Mg, 0.6%Si)	-	23.6	-	-
AA6063 (0.7% Mg,0.4%Si)	21.8	23.4	24.5	25.6
AA7xxx	21.4	23.1	24.0	25.0
AA8xxx	-	23.0	-	-
Carbon steel rebar	-	11.8	-	-
Glass fibre reinforced polyester	-	25	-	-
Concrete	6 - 14		-	-

2.5 Concrete

Concrete is a composite material consisting of a mixture of:

- Aggregates
  Aggregate is the common name for sand- and rock materials used in concrete and occupy usually 65% to 75% of the volume fraction in concrete, [1]. Sand aggregates are particles with a diameter between 0-8mm while coarse aggregates have a diameter of 8mm or greater. Since the aggregates occupy approximately 70% of concrete it is as anticipated that their properties will affect the concrete's own properties and quality. The different aggregate parameters will influence the fresh -, hardening and hardened concrete properties like e.g. the particles' shape will affect the properties of fresh concrete while the aggregate's mechanical and thermal properties are important parameters for hardened concrete.

- Cement
  Cement is a binder which after hydration chemically reacts by curing and creating adhesion between the aggregates, [1]. When cement is mixed with water it is called a cement paste and its properties are mainly dependent of the water and cement mass ratio, the w/c ratio. Cement and its chemistry are more thoroughly elaborated in the consecutive section.

- Admixtures
  An admixture for concrete is defined by the European Standard EN 934-2:2001 as:

  > "Material added during the mixing process of concrete in a quantity not more than 5% by mass of the cement content of the concrete, to modify the properties of the mix in the fresh or hardened state, [1]."

  These chemical admixtures are meant to make good concrete even better and its effect may depend on the time when adding admixture, temperature, amount of admixture and several other factors. Examples of typical admixtures used in the industry are plasticisers, air entraining, accelerating and retarding admixtures.

- Additives
  One method to enhance the mechanical properties and chemical durability of concrete is to supply it with active mineral additions, and these are usually added in larger quantities, [38]. By saying active additions suggest that these they are chemical reactive either alone or in combination with cement and/or it's products after hydration, [1]. Additives may also be chemically inert, and these are commonly referred to as fillers. They may, however, accelerate the cement hydration by providing surfaces for precipitation of hydration products, [1]. Pozzolans are alumina- and silica-containing materials which do not form materials with binder properties by themselves, but if they are in the presence of water they will form products with binder properties by reacting with calcium hydroxide.

Concrete is one of the most frequently used material today used in building projects due to its high strength and durability, convenience to use and is cheap, [39]. Concrete is used in industry, offshore, dams, tunnels, civil and military buildings, roads and etc.

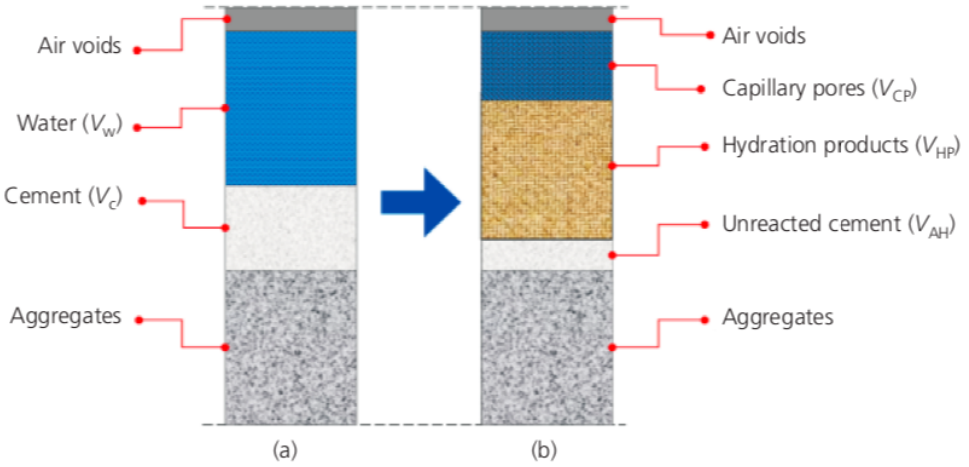

Figure 2.5.1: Schematic illustration of the volumetric proportions (not to scale) of the main constituents of concrete: (a) initial set time and (b) at time t after setting, from reference [40].

Cement chemistry

Cement, the basic component of concrete, is a hydraulic mineral binding material, [39]. When mixed with water it will turn into a paste that after a series of chemical and physical reactions will turn into a solid cement block and bind different materials together as illustrated in Figure 2.5.1. Cements are named based on their main hydraulic minerals like e.g. Portland cement and aluminate-cement, where Portland type is the most common one.

The most important constituent for manufacturing Portland clinker is limestone ($CaCO_{3(s)}$), which constitutes over 90% of the raw mix, [1]. To obtain the right composition of oxides the limestone is mixed with minor elements as for instance bauxite, quartz, gypsum or industrial waste products before it is finely ground to a raw meal.

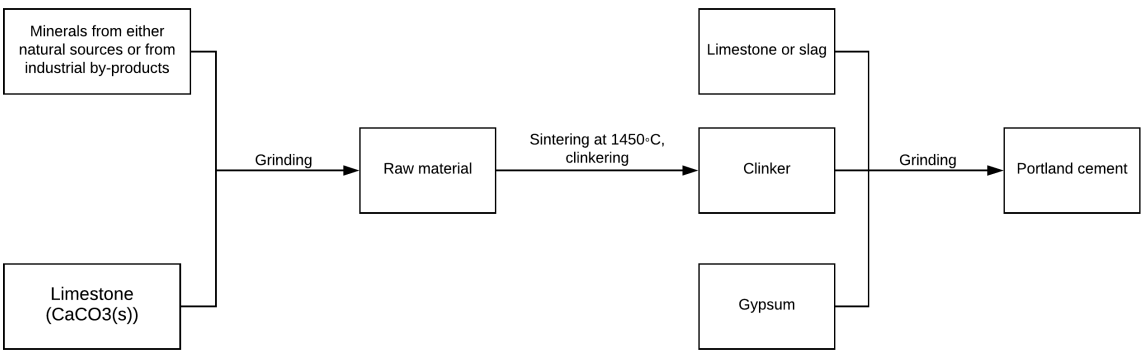

Figure 2.5.2: Simplified schematic overview of the Portland cement clinker production process, redrawn based on [39].

The process to produce Portland cement starts with heating up the raw material up to 1300°C, [1]. At approximately this temperature several reactions will happen, of which the most important ones are firstly the decomposition of calcite.

$$CaCO_{3(s)} \rightarrow CaO_{(s)} + CO_{2(g)} \tag{2.6}$$

The other reactions happening at this temperature is the decomposition of minor constituents and the reaction between lime ($CaO_{(s)}$), quartz and other minerals which yields belite, aluminate and ferrite, [1]. The homogeneous mixture of raw material is further heated up to 1450°C where it is sintered into nodules or lumps, usually 3-20 mm in diameter. This stage of the process is called clinkering and gives the Portland cement clinker, which after being mixed with a few percents of gypsum ($CaSO_4 \cdot 2\,H_2O_{(s)}$) and ground can be used in concrete as cement. In addition to releasing a vast amount of $CO_{2(g)}$ from the decomposition reaction is the whole manufacturing process highly energy demanding which is unfortunate in terms of environmentally challenges. Modern-day cement plants, like the Norcem Breivik plant, uses heat exchangers to preserve the energy from the hot gasses in the kiln and utilises in great parts alternative fossil fuels and CO_2 neutral biomass as their source of energy to replace primary fuels, which greatly reduces the overall CO_2 emissions.

Table 2.3: The Portland cement clinker's four major phases, from reference [1].

Major phase	Mineralogical term	Chemical notation	Abbreviated chemical notation
Tricalcium silicate	Alite	$3\,CaO \cdot SiO_2$	C_3S
Dicalcium Silicate	Belite	$2\,CaO \cdot SiO_2$	C_2S
Tricalcium aluminate	Aluminate	$3\,CaO \cdot Al_2O_3$	C_3A
Tetracalcium aluminoferrite	Ferrite	$4\,CaO \cdot Al_2O_3 \cdot Fe_2O_3$	C_4AF

In cement chemistry, the chemical compositions are often expressed as sums of oxides, and for simplicity, they are abbreviated to single letters, i.e. CaO=C, SiO_2=S, H_2O=H, etc.. The major phases of Portland cement and their compositions and abbreviations are present in Table 2.3. In addition to these major phases, the cement also contains minor components derived from the raw material or fuel like CaO, MgO, K_2O, Na_2O and chlorides. The major phases of Portland clinker presented in Table 2.3 are all reactive towards the water where the reaction products have very low solubility in water, [1]. When the dry cement is mixed with a fixed amount of water the cement paste produce will have a plasticity which will be lost as a function of time, [39]. This is called the initial

setting time where no strength is produced. During the final setting time is the moment where the cement will have strength. The process from the initial setting of cement to the final setting is known as condensation/setting and the strength of the compressive strength of the cement is measured 2, 7 and 28 days after hydration, [1]. The compressive strength of the cement will continue to increase over time and depending on the content of each of the various major phases will contribute to the increase in strength and/or the heat evolution from hydration. The strength will stop when there is no more water left in the concrete to react. After the setting and hardening reaction, the structure of the hydrated cement will be of a heterogeneous character and consist of different calcium oxide hydrates, gel, unreacted cement, free water and pores with different sizes as illustrated in Figure 2.5.3, [39].

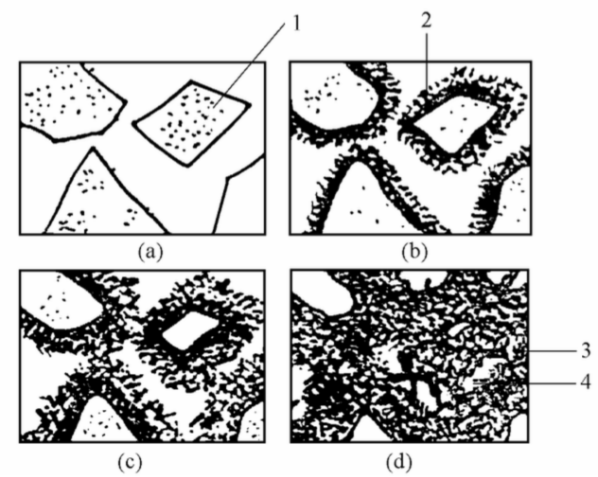

Figure 2.5.3: Schematic illustration of the setting and hardening process of cement where illustrated is: 1. Unhydrated cement granules; 2. Formation of cement gel; 3. $Ca(OH)_2$ and crystals of calcium-aluminate-hydrate ; 4. Capillary pore, from reference [39].

Cement, after being hydrated is highly alkaline due to the high concentration of $OH^-_{(aq)}$ formed in the pore solution, [1]. Here represented by the hydration reaction 2.7 of tricalcium silicate.

$$2 \cdot (3\,CaO \cdot SiO_{2(s)}) + 6\,H_2O_{(l)} \longrightarrow 3\,CaO \cdot 2\,SiO_2 \cdot 3\,H_2O_{(s)} + Ca(OH)_{2(aq)} \qquad (2.7)$$

The amount of $Na_2O_{(aq)}$ and $K_2O_{(aq)}$ in the cement is crucial for the pH since they can dissolute and provide additional $OH^-_{(aq)}$ formation to the pore solution, [1]. For ordinary Portland cement the pH is usually between 12.5 and 13, [41]. The high pH of the pore solution is highly sought after since it causes reinforcement steel to be in a passive condition and thereby preventing corrosion, [1]. The pH in the concrete however may be decreased due to deterioration mechanisms such as chloride ingress and carbonation where chloride ingress may form hydrochloric acid, [41]. The main reason to the reduction of pH in concrete is due to carbonation where calcium hydroxide in concrete is transformed into calcium carbonate.

$$CO_{2(aq)} + 2\,OH^-_{(aq)} \longrightarrow {CO_3}^{2-}{}_{(aq)} + H_2O_{(aq)} \tag{2.8}$$

$$Ca^{2+}_{(aq)} + {CO_3}^{2-}{}_{(aq)} \longrightarrow CaCO_{3(s)} \tag{2.9}$$

Compared to it's compressive strength is the tensile strength of concrete quite low, [1]. To correct this issue the concrete is usually reinforced, where the conventional type of reinforcement material is steel. Steel as reinforcement material in concrete is in theory a perfect match because of they both are inexpensive and are available in an abundance, have approximately similar CTE and the high alkalinity of concrete causes the steel to be in a passive condition in terms of corrosion. The steel surface is commonly patterned to obtain a better adhesion to the concrete. In addition to adding strength to the concrete structure, reinforcement are used in to restrain growth of large concentrated cracks, and ensure a more evenly distributed crack development along the entire structure, [42].

The carbonation can reduce the pH of the concrete down to values of 9, [41]. Depending of the chloride concentration corrosion of embedded steel rebars in concrete can already initiate at pH values of 11. Factors influencing rate of carbonation is the porosity and composition of the concrete and the amount of moisture, [1]. The reduction in pH of the concrete from carbonation and the presence of chlorides renders the steel highly susceptible to corrosion attacks.

Concrete is a material that is continuously changing and is mainly divided into three main phases with respect of it's "life cycle": fresh phase, hardening phase and service phase, [1]. In the fresh paste, which involves mixing, transport and casting the hydration takes place slowly. When the the concrete begin to gain measurable mechanical properties in the hardening phase it will generate a substantial amount of heat from the exothermic hydration reactions. In massive structures the temperature may raise to more than 40°C, but according to the standard specifications formulated by the Norwegian Public Roads Administration's "Prosesskode 2" dictates that the maximum temperature shall at no time exceed 65°C and that the temperature difference over the cross-section shall not exceed 20°C, [1]. After 1-2 days the maximum concrete temperature is usually reached and the the heat generation will gradually become more moderate and the heat loss to the environment will eventually dominate.

Concrete, like most other materials will during temperature variations experience thermal dilatation. $10\frac{\mu m}{m°C}$ is often used as the standard value of coefficient of thermal expansion (CTE) for concrete, but the CTE may however vary significantly since it is dependent of the moisture state of the binder phase and the type of aggregates is in the concrete, [1]. There are large variations in CTE of minerals where calcite has a low CTE of α = 4-6.5$\frac{\mu m}{m°C}$ and quartz has a high CTE of α = 10.6-15$\frac{\mu m}{m°C}$, and since the aggregates account for 65-70% of the volume of concrete, it is natural that it will have a major impact on CTE. The binder phase's moisture state will also have an impact on the CTE where a semi-dry binder will have almost a twice as high CTE than a water-saturated binder phase.

2.6 Corrosion of aluminium in alkaline media

The good corrosion resistance of aluminium and aluminium alloys stem from their highly protective, tightly adherent and invisible oxide film, [4]. If this oxide layer is subjected to any mechanical damage it will instantly reseal itself, and unlike rust, the aluminium oxide film is a stable and largely insoluble layer in the pH range 4 to 9, [43]. If the oxide layer is exposed to environments outside this pH range in strongly alkaline or acidic environments, this will result in disintegration of this oxide layer and thereby leaving the aluminium further exposed to corrosion. Figure 2.6.1 illustrates how the corrosion rate of aluminium and some other metals rapidly increase by increasing or decreasing the pH by just a little outside their passive area.

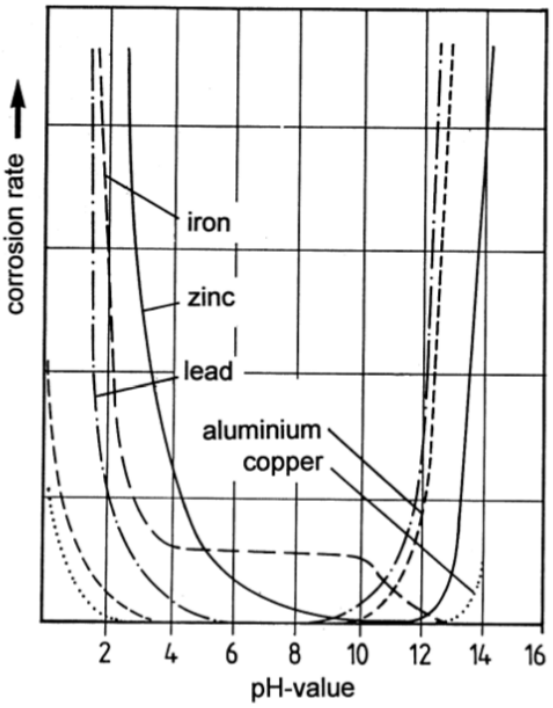

Figure 2.6.1: The corrosion rate of some selected metals as a function of pH, from reference [43].

The corrosion behaviour to aluminium is significantly affected by the composition of other elements in solid solution and second phase particles, [4, 44]. Elements like Mg in solid solution can diffuse into the $Al_2O_{3(s)}$ oxide layer make a thicker and more stable protective layer. Other elements like Cu and heavy metals like Pb will decrease the corrosion resistance with increasing amounts and make the aluminium susceptible to different types of corrosion. Some of the types of corrosion in which aluminium are exposed to are intergranular corrosion, stress cracking corrosion, pitting corrosion, and filiform corrosion.

Corrosion of aluminium in contact with concrete

Ordinary Portland cements (OPC) produce a highly alkaline environment in hardened state, which offer great corrosion protection with increasingly pH for steels as shown in Figure 2.6.1, but offers a corrosive environment in contact with aluminium, [43, 45]. In this alkaline environment the aluminium oxide layer will become unstable and the corrosion attack of the metal starts with dissolving the oxide layer according to the simplified reaction:

$$\mathrm{Al_2O_{3(s)}} + 2\,\mathrm{OH^-_{(aq)}} + \mathrm{H_2O_{(l)}} \longrightarrow 2\,\mathrm{Al(OH)_2O^-_{(aq)}} \tag{2.10}$$

This leaves the aluminium metal surface exposed for corrosion attack and reacts into aluminate $\mathrm{Al(OH)_2O^-}$ ions and hydrogen gas according to the reaction:

$$\begin{aligned} &\mathrm{Al_{(s)}} + 4\,\mathrm{OH^-_{(aq)}} \longrightarrow \mathrm{Al(OH)_2O^-_{(aq)}} + \mathrm{H_2O_{(l)}} + 3\,\mathrm{e^-} \\ &2\,\mathrm{H_2O_{(aq)}} + 2\,\mathrm{e^-} \longrightarrow 2\,\mathrm{OH^-_{(aq)}} + \mathrm{H_{2(g)}} \\ &\hline \\ &2\,\mathrm{Al_{(s)}} + 4\,\mathrm{H_2O_{(l)}} + 2\,\mathrm{OH^-_{(aq)}} \longrightarrow 2\,\mathrm{Al(OH)_2O^-_{(aq)}} + 3\,\mathrm{H_{2(g)}} \end{aligned} \tag{2.11}$$

The corrosion type which aluminium and its alloys is subjected to in alkaline environments is mainly uniform corrosion. Uniform corrosion will, as the name implies, cause an uniform and continuous decrease in the thickness over the entire surface area where the dissolution rate of the oxide layer will surpass the rate of formation, [43, 44]. The rate of uniform corrosion can easily be determined through measurement of total loss of mass or through quantitative measurement of hydrogen evolution.

The main concern with aluminium when used as a structural component in concrete is the formation of corrosion products which may cause the concrete to develop weaknesses like cracking or spalling, [43, 44]. The gas formation may contribute to making the concrete more porous and thereby increasing the risk of transportation of corrosive substances into the concrete and reinforcement material.

The study conducted by Setiadi *et. al.* [45] aluminium samples (99.999% Al and 99.5% Al 0.25% Fe) were immersed in various cement-based media and after 28 days a ring of white corrosion products were observed between the aluminium and cement interface. Through analysis in XRD the corrosion products of aluminium in OPC were identified to consist of aluminium hydroxide ($Al(OH)_3(s)$) and strätlingite ($2\,CaO \cdot Al_2O_3 \cdot SiO_2 \cdot 8\,H_2O\,(s)$) as the major components. Setiadi *et. al.* [45] suggest the corrosion of aluminium in concrete happens in three stages according to the schematically illustration in Figure 2.6.2. The first stage involves, as previously discussed, the dissolution of the oxide film and the formation of aluminate ions and hydrogen gas according to Equation 2.10 and 2.11, respectively, and the formation of the porous region between the cement and aluminium interfaces. The following stage involves the reaction between aluminate ions, silicates and $Ca(OH)_2$ into strätlingite. The mechanism behind the formation of strätlingite is still not fully understood, but the direct reaction of the aluminate ions with the silica hydrate in the cement paste seems like the most likely pathway for the strätlingite formation. In the last stage the area closest to the aluminium interface becomes depleted of OH^- ions due to the corrosion reaction and reduced diffusion rate as the cement hardens. This will cause the hydroxy aluminate ions to decompose, releasing OH^-, which will lead to further corrosion, and precipitate as an aluminium hydroxide phase at the aluminium surface.

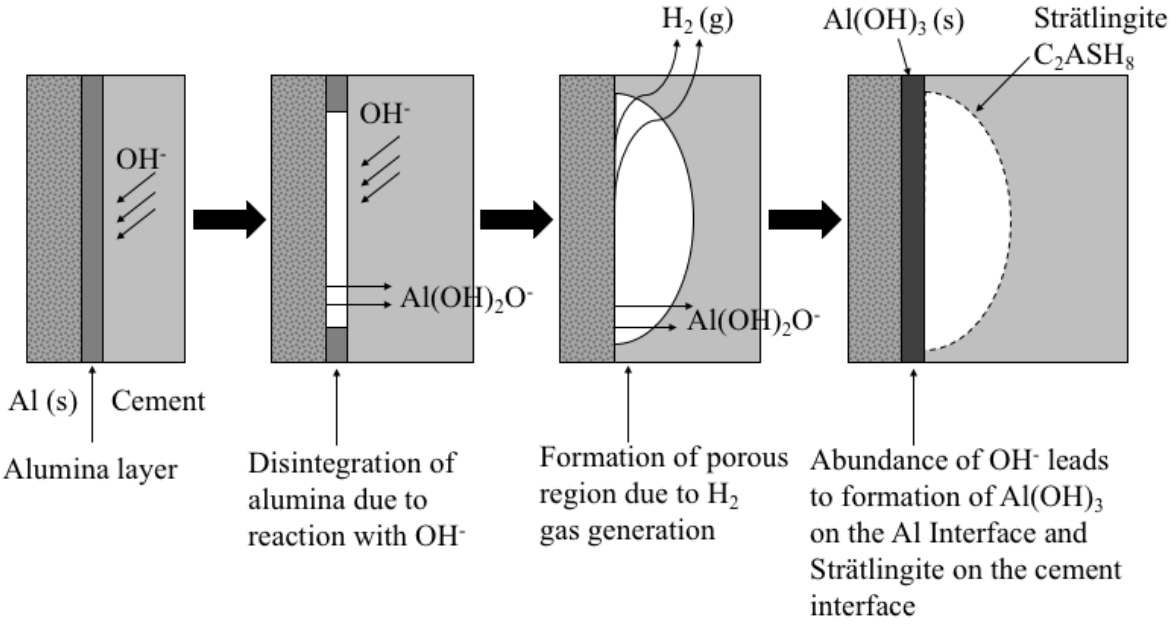

Figure 2.6.2: Schematic illustration of the corrosion sequence of Al in cement, redrawn based on [45].

The technique of anodising the aluminium in order to obtain a thicker and hence a more protective oxide layer is commonly used and also to obtain better adhesion to coating systems. This do not improve the resistance of corrosion to aluminium in contact with concrete since the layer will dissolve in the setting process of the concrete, [44].

Corrosion can on the other hand be limited by the choice of binder material in the concrete, [43]. As the Figure 2.6.3 illustrates, by selecting a different binder, e.g. cements with SCMs instead of OPC, the pH may be reduced and hence create an environment in the concrete where the aluminium better can withstand corrosion. After a while, the combination of a series of chemical reactions in the concrete and the formation of a protective layer of corrosion products on the aluminium surface will cause the corrosion rate to aluminium to stagnate, as shown after approximately 6 months in the Figure 2.6.3.

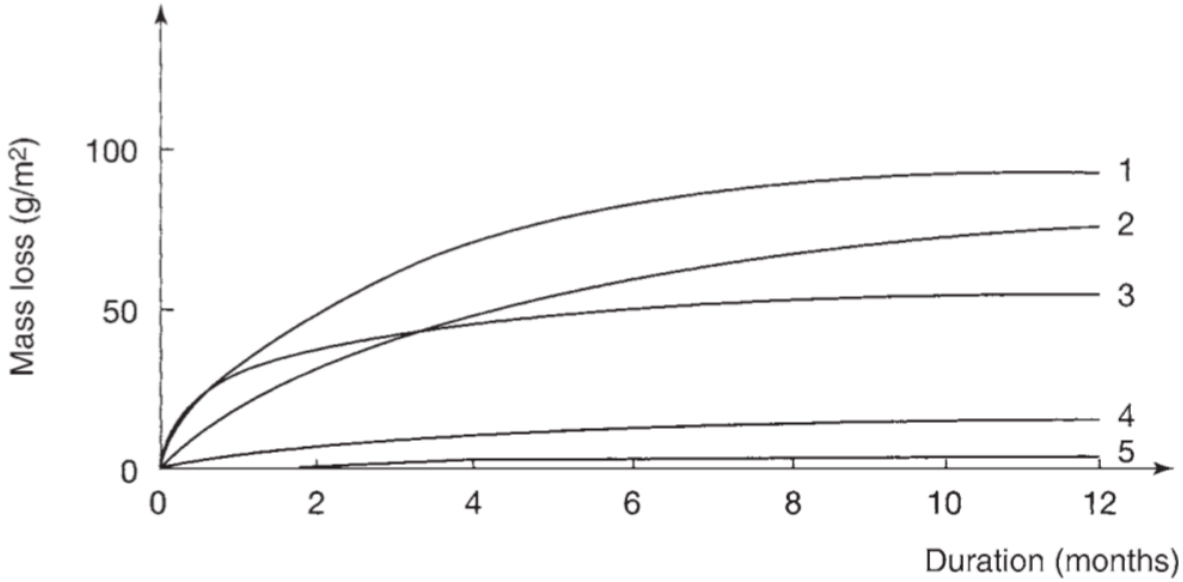

Figure 2.6.3: Mass loss of unprotected aluminium embedded in different types of media over a prolonged time, where 1 Hydraulic limestone, 2 ordinary Portland cement, 3 Blast furnace cement, 4 Alumina cement and 5 Plaster, from reference [44].

Inhibitor effect

Inhibitors are substances that will cancel or reduce corrosion attacks towards a metal when added in a low concentration to an environment or on the metal, [44, 46]. The mechanism of inhibitors has been hypothesised on many occasions, but is still today poorly understood. Inhibition is hypothesised to be a sequence of more and less identified processes and not one simple phenomenon. The inhibitors may act on a metal by altering the surface state, altering the anodic or cathodic reactions or even both simultaneously. The efficiency of the inhibitors are dependent of:

- Temperature, where the adsorption will decrease with increasing temperature
- pH
- The surface/volume ratio
- The concentration of the inhibitor

3 Experimental procedure

In the following sections 3.1.1 - 3.1.5 are the materials which were used and examined in this thesis presented.

3.1 Materials

In total, 5 different alloys of different compositions were examined during the experimental work of this thesis. The alloys were selected on the basis of their composition and what they bring along with regard to microstructural and mechanical properties. The alloys and their compositions are presented in this section.

3.1.1 Al-1Mg

This material was delivered as a billet from Hydro, as shown in Figure 3.1.1. The analysis of the alloys chemical composition was conducted by Hydro and is presented in Table 3.1. This material will henceforth be named 'Al-1Mg'.

This alloy was chosen to investigate how a smaller amount of Mg in solid solution would perform in terms of corrosion resistance with the inhibitor system in concrete, compared to Al-5Mg.

Table 3.1: Chemical composition of the Al−1 Mg alloy.

Alloying element	Weight percent [wt.%]	Alloying element	Weight percent [wt.%]
Mg	0.9701	Si	0.0468
Fe	0.0617	Mn	0.0010
Zn	0.0031	Ti	0.0145
Cr	0.0006	Ni	0.0023
Pb	0.0013	Sn	0.0006
B	0.0024	Bi	0.0002
Zr	0.0016	V	0.0016
Be	0.0056	Co	0.0002
Ga	0.0115	P	0.0003
Ag	0.0002	Cu	0.0008
Al	98.9		

3.1.2 Al-5Mg

This material was delivered as a billet from Hydro, as shown in Figure 3.1.1. The analysis of the alloys chemical composition was conducted by Hydro and is presented in Table 3.2. This material will henceforth be named 'Al-5Mg'.

An important point to call attention to is the high purity of this alloy and to the Al-1Mg alloy, where there are very few traces of other alloying elements other than the principle alloy element Mg. This alloy was chosen due to the alloys high content of Mg makes it highly resistant against chloride attacks and corrosion in sea water. It also showed exceptional corrosion resistance in concrete, which is more thoroughly described in section 3.7.

Table 3.2: Chemical composition of the Al−5 Mg alloy.

Alloying element	Weight percent [wt.%]	Alloying element	Weight percent [wt.%]
Mg	4.9209	Si	0.0525
Fe	0.0595	Mn	0.0010
Zn	0.0036	Ti	0.0314
Cr	0.0004	Ni	0.0023
Pb	0.0019	Sn	0.0005
B	0.0058	Ca	0.0001
Zr	0.0020	V	0.0048
Be	0.0019	Co	0.0002
Ga	0.0090	Cu	0.0007
Al	94.9		

Figure 3.1.1: Picture of the Al-Mg billets before homogenisation and extrusion.

3.1.3 Al-7Si-0.3Mg

This material was delivered as a billet from Hydro, as shown in Figure 3.1.2. The analysis of the alloy's chemical composition was conducted by Hydro and is presented in Table 3.3. This material will henceforth be named 'Al-7Si-0.3Mg'.

This alloy was chosen for the same reasons as the Al-12.7Si alloy. This material was investigated as an alloy in concrete to see how the decreased amount of Si and increased amount of Mg affected the corrosion properties.

Table 3.3: Chemical composition of the Al−7 Si−0.3 Mg alloy.

Alloying element	Weight percent [wt.%]	Alloying element	Weight percent [wt.%]
Si	6.9800	Fe	0.1004
Cu	0.0013	Mn	0.0019
Mg	0.2800	Cr	0.0003
Ni	0.0042	Zn	0.0023
B	0.0001	Ca	0.0004
Ga	0.0113	Na	0.0005
P	0.0002	Pb	0.0008
Sr	0.0247	Ti	0.0954
V	0.0104	Zr	0.0028
Al	92.52		

3.1.4 Al-12.7Si

This material was delivered as a cast from Hydro as shown in Figure 3.1.2. The analysis of the alloy's chemical composition was conducted by Hydro and is presented in Table 3.4. This material will henceforth be named 'Al-12.7Si'.

This Al-Si alloy was chosen due to its high Si content and the similarity in chemical composition to the alloy presented in section 3.1.5. The alloys high Si content will provide low coefficient of thermal expansion, and good wear resistance. It was mainly chosen to determine the impact of high Si content on corrosion properties in concrete.

Table 3.4: Chemical composition of the Al−12.7 Si alloy.

Alloying element	Weight percent [wt.%]	Alloying element	Weight percent [wt.%]
Si	12.680	Fe	0.0946
Cu	0.0009	Mn	0.0010
Mg	0.0130	Cr	0.0003
Ni	0.0046	Zn	0.0018
B	0.0001	Ca	0.0001
Ga	0.0101	P	0.0002
Pb	0.0006	Ti	0.0112
V	0.0113	Zr	0.0025
Co	0.0001	Sr	0.0001
Al	87.2		

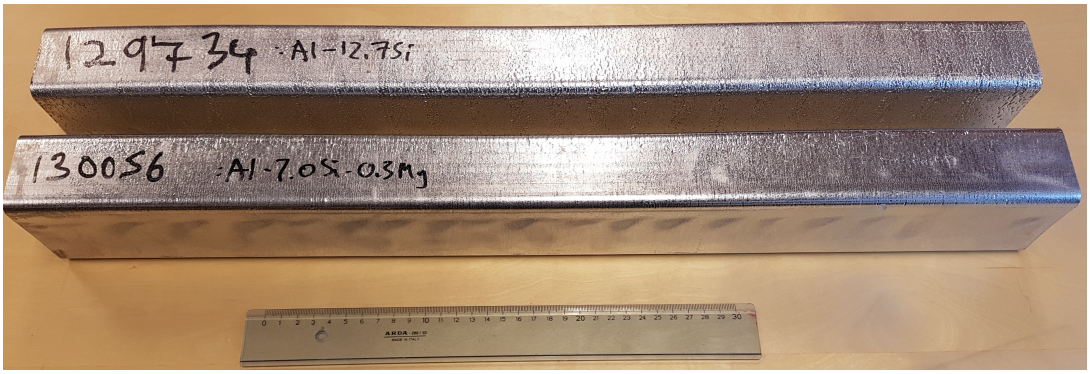

Figure 3.1.2: Picture of both the Al-7Si-0.3Mg and the Al-12.7Si billets.

3.1.5 Engine block

The car engine used in this thesis was a Suzuki H27 V6 2,7 L petrol engine, which earlier stood in a Suzuki Grand Vitara XL7. The car engine was given away for free and was previously located outdoors on a field, for an uncertain amount of time in Verdal municipal, Trøndelag county. Due to the immense amount of rust it was easy to separate the steel components from the aluminium components.

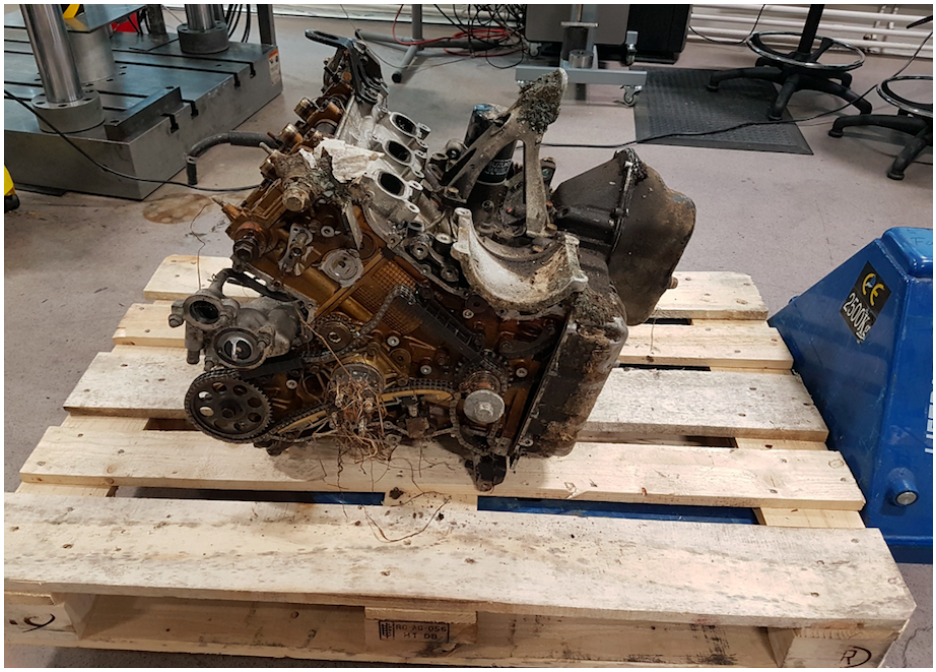

(a) Car engine as received

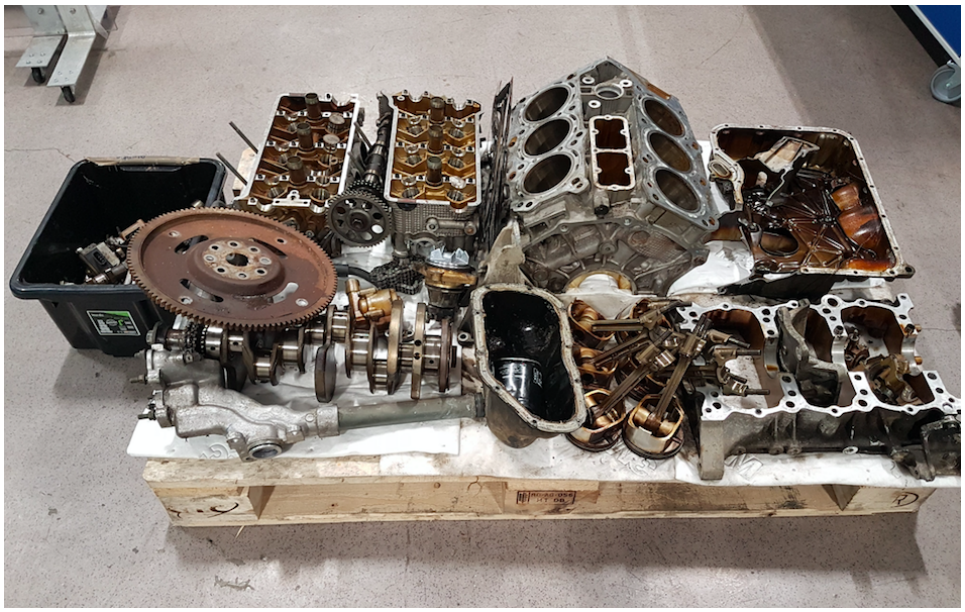

(b) Disassembled car engine

Figure 3.1.3: Pictures of the car engine.

Figures 3.1.3(a) and 3.1.3(b) show, respectively, how the car engine looked when it was received and how it looked after it was disassembled. At a closer inspection of picture 3.1.3(b) one may observe the pistons at right bottom, the crankshaft at the left bottom and the sump between these two.

The engine block is the largest single piece of metal in a car. It contains all of the engine components, which is why this engine component was chosen, [47]. These are usually made of secondary grade aluminium with many elemental contaminants and are cast by sand cast. The engine block is where the energy from combustion is converted into mechanical energy that causes the car to run.

Figure 3.1.4: Picture of the engine block used as feedstock material in this thesis.

The analysis of the engine blocks chemical composition was conducted by Hydro and is presented in Table 3.5. This material will henceforth be referred to as 'engine block'.

Table 3.5: Chemical composition of the material from the engine block.

Alloying element	Weight percent [wt.%]	Alloying element	Weight percent [wt.%]
Si	9.5690	Fe	0.5324
Cu	1,7313	Mn	0.1152
Mg	0.2101	Zn	0.1953
Ti	0.0199	Cr	0.0179
Ni	0.0227	Pb	0.0164
Sn	0.0091	Na	0.0027
Ca	0.0033	Zr	0.0035
V	0.0073	Be	0.0007
P	0.0011	Ga	0.0091
Cd	0.0007	Bi	0.0003
B	0.0005	Sb	0.0128
Al	87.52		

3.2 Grain structure characterisation

Samples were cut into suitable sizes with a Struers Lobotom-5 using a 20A25 cut-off wheel, designed for use on non-ferrous soft metals with HV80-400. The samples were then placed into small moulds (2.5cm in diameter) before they were casted into a epoxy mix. The epoxy mix used was EpoFix resin and EpoFix hardener in the ratio 25:3 which has a hardening time of 8-12 hours. The samples were then ground in a Struers Rotopol-31 and polished in a Sturers TegraForce-5 according to the process presented in Table 3.6.

Table 3.6: Grinding and polishing procedure.

Process	Grit size	Grind/polish material	Time [s]	Cleaning procedure
Grinding	#FEPA320	SiC	60	Water
Grinding	#FEPA500	SiC	60	Water
Grinding	#FEPA800	SiC	60	Water
Grinding	#FEPA1200	SiC	120	Water
Polishing	3 μm	DiaPro NAP B1	180	Water, cotton swab with soap and then ethanol
Polishing	1 μm	DiaPro NAP B1	240	Water, cotton swab with soap and then ethanol
Polishing	$\frac{1}{4}$ μm	DiaPro NAP B1	180	Water, cotton swab with soap and then ethanol

Further, the polished samples were prepared in a Buehler VibroMet for 8 hours with an amplitude of 70% to obtain a even and scratch-free surface finish.

In order to take micrographs of the grain structure in polarised light, the surface-polished samples had to be anodised. The anodising process started by first submerging the samples in a steel container, which also functioned as a counter electrode, with 5% tetrafluorobotic acid (HBF_4) covering the sample surface. A platina rod connected to the current output was used to apply a voltage of 20V to the sample surfaces for 90 seconds to obtain an oxide layer. Anodising the aluminium surface through electrochemical oxidation will generate an amorphous oxide layer which enables the study of the microstructure and the grain structure in cross polarised light, [48]. By additional applying a λ-plate the grains will obtain different colours due to the optical anisotropy of aluminium and the oxide layer's rotation. When the wave direction from the oxide layer from the grain is 45° to the polariser and analyser the grains will be imaged as either blue or yellow. If the wave direction is parallel the grains will become purple.

3.2.1 Light optical microscopy (LOM)

The examination of microstructures was conducted in a Leica MeF4 Light Optical Microscope (OM) as shown in Figure 3.2.1(a). Both the transverse cross-section and the longitudinal cross-section, parallel to the extrusion direction were examined. The polished samples were imaged with bright field illumination, while the anodised samples were imaged by inserting a polariser and analyser in crossed position. To obtain more colours and to make it easier to separate grains a λ-plate was inserted with an incline of 7°.

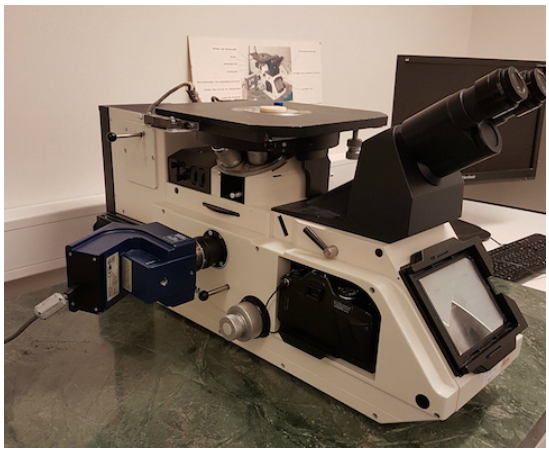

(a) Picture of the Leica MeF4 Light Optical Microscope.

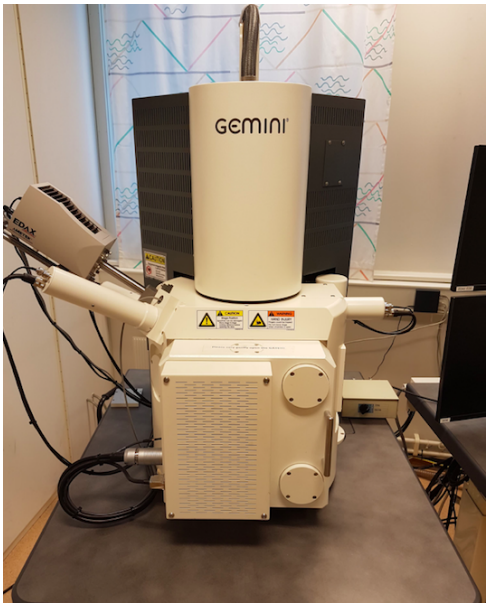

(b) Picture of the LV-Fe Zeiss Supra 55 VP scanning electron microscope with the attached EDS on the left side marked EDAX.

Figure 3.2.1: Photography of both the LOM and the SEM used in this thesis

3.2.2 Scanning electron microscopy (SEM)

A LV-Fe Zeiss Supra 55 VP scanning electron microscope (SEM), as shown in Figure 3.2.1(b), was used to examine the microstructure and morphology of the samples before and after extrusion. An acceleration voltage of 10kV with secondary electrons (SE) was used, while the working distance was usually set to 10mm and the aperture set to 160μm. To examine the particles and second phases of the alloy Energy Dispersive X-ray Spectroscopy (EDS) was used. During EDS was the aperture set to 160μm, and TEAM software for microanalysis were used to evaluate the results.

The sample's chemical composition is obtained through energy dispersive x-ray spectrography (EDS) where the atoms in the sample are bombarded with high-energy electrons, [49]. The electrons in the atoms at rest lay on discrete energy levels or electron shells (K-, L-, M-shell). When the high-energy electrons from the SEM's electron cannon hit these electron they may be excited to an outer electron shell and thereby ionise the atom. The excited electron wants to return to its original energy shell and during this return it will emit X-rays, photons or Auger electrons to maintain the energy balance. The energy difference between between the two electron shells released from the excited electron is specific for atoms of a certain atomic number and can be measured with EDS.

3.3 Mechanical property measurements

3.3.1 Hardness

All samples were ground with the grind procedure presented in Table 3.6 from #FEPA 320 to 3μm polish to ensure an even and scratch-free surface which would yield consistent measurements. The hardness measurements were conducted on a Matsuzawa DVK-1S hardness tester instrument with the settings 0.5 kilogram force (kgf) and 15 seconds load time. The hardness measurements of the alloys were performed both before and after extrusion, where a total of 6 measurements were performed to obtain a good statistical assessment basis. The measurements were taken at random points on the billets, while on the extruded profiles the measurements were aquired from the transverse cross-section where measurements were taken from both the centre of the profile and from the edge, as illustrated in Figure 3.3.2.

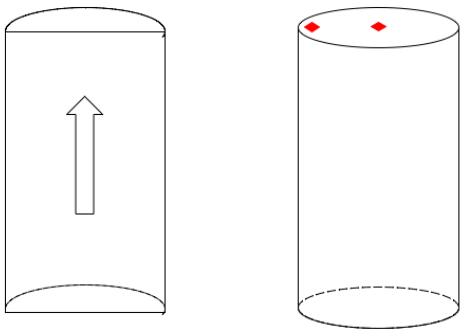

Figure 3.3.1: Indentation positions for hardness measurement indicated at the red squares and illustration of the respective the longitudinal and transverse cross-section used for microstructure characterisation. The arrow on the transverse specimen display the extrusion direction in the micrographs taken of the specimen.

3.3.2 Tension test

The round tensile specimens were machined to the preferred dimensions, presented in Figure 3.3.2 at the Finmekanisk Verksted at Realfagsbygget NTNU, Trondheim. The tensile specimens were tested in a MTS810 servo-hydraulic universal testing machine with 2 $\frac{mm}{min}$ strain rate and with a 25 mm extensometer. The tensile specimen was mounted by their ends in the testing apparatus and the apparatus applied an increasing load at a constant rate. The applied load was measured with a load cell and the elongation was measured with the extensometer.

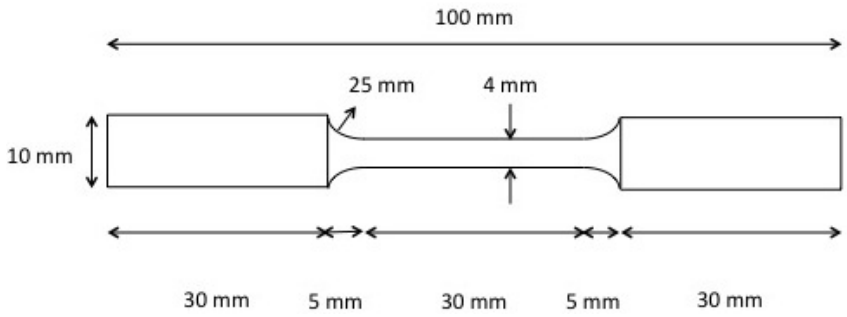

Figure 3.3.2: The dimensions of a round tensile specimen.

3.4 Techniques for measuring the coefficient of linear thermal expansion

Two different methods were used in the attempt of measuring the CTE of the alloys. The method presented in the following section 3.4 is based on the author's earlier work [8].

Thermodilatometry

The coefficient of linear thermal expansion (CTE) of solid objects can be measured through the thermomechanical method of dilatometery [50]. The CTE of samples in this project was measured in a Netzsch 402C push-rod dilatometer. A constant heating rate was chosen at a specified temperature range. The length difference upon both heating and cooling is measured electronically, by the push-rod, as $\frac{\Delta l}{l_0}$ as a function of temperature similar as to figure 3.4.1(b). The alumina calibration sample and the aluminium alloy samples dimension are described in Figure 3.4.1(a). The method is more thoroughly described in the ASTM standard method for push-rod dilatometry [50].

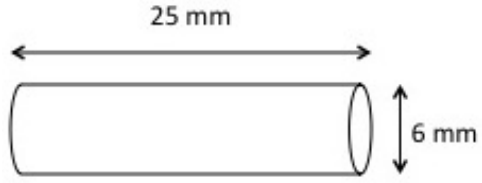

(a) The dimensions of the speciemen measured in the Netzsch 402C push-rod dilatometer.

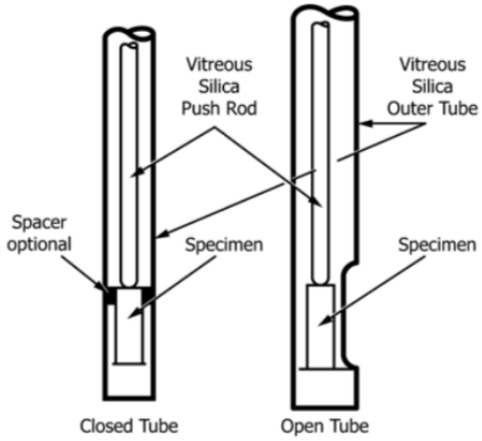

(b) A common form of the specimen holder for push-rod dilatometry, from reference [50].

Figure 3.4.1: Schematically figures of the dimensions of the dilatometer specimens and the form of the specimen holder.

The specimens were measured at room temperature to the closest 1x10^{-2} mm before they were installed in the dilatometer. The dilatometer chamber was flushed with Ar gas for 5 minutes to ensure inert atmosphere. The Ar gas and the maximum temperature were chosen to avoid oxidation of the samples. An alumina sample was used for calibration at the desired temperature program before the samples could be analysed. The temperature programs are given in Table 3.7. The constant heating rate were set to $2\frac{^\circ C}{min}$. The ASTM [50] states that the normal start temperature is usually 20°C, but due to the high room temperature in the laboratory the start temperature was set to 30°C.

Table 3.7: This table presents the different temperature programs of the dilatometer runs. After reaching max temperature the specimen was held there for a certain period of time before the cooling step commenced.

Temperature program	Heating step [°C]	Hold temperature at max T and duration [°C, min]	Cooling step [°C]
1	30 - 250	250, 30	250 - 30
2	30 - 100	110, 10	110 - 30
3	30 - 70	70, 10	70 - 30

The results from the thermodilatometery measurements are presented graphically as the expansion ($\frac{\Delta l}{l_0}$) as a function of the temperature (T). CTE was determined by measuring the slope of both the heating and cooling curve in different temperature ranges in the graph, as shown in Equation 3.1. The results showed that the samples were not heated at a steady rate which resulted in nonlinear parts in both the heating and cooling curve. Therefore were CTE measured at temperature intervals in the graphs were the curves were linear. The ΔT was usually chosen to be between 20-60°C

$$\alpha = \frac{1}{\mathrm{l_0}}(\frac{\Delta \mathrm{l}}{\Delta \mathrm{T}}) \tag{3.1}$$

α	Coefficient of linear thermal expansion [$\frac{\mu m}{m°C}$]
l_0	Initial sample length at room temperature [μm]
Δl	The length difference of the specimen between any two temperatures [μm]
ΔT	Change in temperature [°C]

Extensometer

In an additional experiment the CTE was obtained by measuring the elongation of the samples with an extensometer during exposure to a temperature difference. An extensometer (25mm) was coupled to a round sample with a length of approximately 100mm mounted in an oven with adjustable temperature setting. The oven was heated up in temperature segments of 5 and 10 °C and the elongation was measured after 5 to 10 minutes when the whole sample had reached the same temperature as the oven. Same procedure for the cooling step. As with the dilatometery in section 3.4, the elongation was measured as a function of temperature and the CTE was obtained from the slope of the curve withing a linear area.

3.5 Extrusion

For the attempt to use aluminium as reinforcement material in concrete, it was decided that the profiles would be produced through RAM extrusion. The original idea was to manufacture the rods through screw extruded recycled aluminium, but as a result of a variety of reasons this became a difficult and time-consuming route to produce such a large amount of reinforcement material at this point. The main focus of the DARE2C project was to produce aluminium reinforcement rods that can operate in concrete, and therefore it has to be a future goal to use screw-extruded aluminium reinforcement rods until the procedures for implementing aluminium in concrete are in place.

In order to meet the need for the amount of reinforcement material which was required for the tests, 3 bolts of the Al-5Mg alloy with the lengths of <20cm long and 1 bolt of the Al-1Mg alloy with the length of approximately 10 cm were cut. It was decided to produce both smooth reinforcement rods with ø10mm of both the alloys and reverse T profiles of the Al-5Mg alloy as shown in Figure 3.5.1.

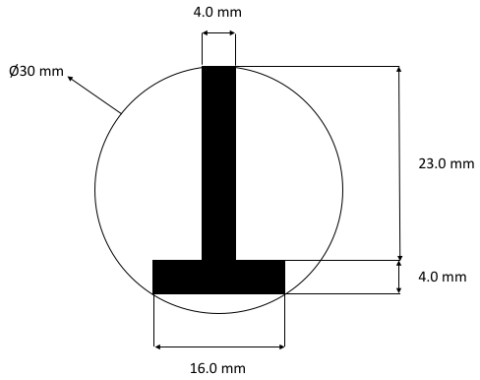

Figure 3.5.1: The dimensions of the extruded T profile, redrawn based on [42].

As established in Section 2.2.1, a suitable homogenisation cycle would greatly improve the extrudability of the billets and their mechanical and surface properties. Both the Al-5Mg billets and the Al-1Mg billet were subjected to the same homogenisation route in order to produce a state of supersaturation/precipitation. All the billets were heated simultaneously in a circulating air furnace with precise temperature control. The billets were heated to a temperature of 430°C, which is just below the Al-Mg eutectic temperature, and held there for 3 hours before they all were directly water quenched in order to freeze the state of supersaturation/precipitation. In addition, the billets were preheated to 430°C before the extrusion commenced.

The extrusion took place in at the SINTEF lab in Verkstedhallen and were done under the direction of HYDRO with the help of SINTEF and NTNU. The extrusion process was done with a vertical extrusion press. The advantages of vertical extrusion presses is that they have a higher rate of production, and are more floor efficient than horizontal presses. They also have easier alignment between the press ram and the tools, [26]. The press was installed in the first floor, so to be able to produce extrudants of desired lengths a floor pit was installed in the basement floor right under. The floor pit was approximately 6

meters deep and filled with water to be able to quench the aluminium rod as observed in Figure 3.5.2. The distance between the die and the floor pit was around 2 meters. When the profiles acquired a manageable temperature, they were pulled out of the pit.

Table 3.8: Extrusion parameters

Alloy	Temperature [°C]	Initial cross-section [mm^2]	Final cross-section [mm^2]	Ram speed [mm/s]	Ram force [kN]
Al-1Mg	430	7088	79	1	4000
Al-5Mg	430	7088	79 & 156 (T-profile)	1	7000

The extrusion log for Al-1Mg and Al-5Mg is presented in Appendix B. It is important to emphasise that the temperature of the profiles from when they exited the die after extrusion and before quenching was not measured. The energy from the deformation adds a lot of heat to the system, so it is fair to assume that the profiles, when exiting the die would have a higher temperature than 430°C.

(a) The extruder at the first floor.

(b) The basement right under the extruder.

Figure 3.5.2: Photographs of the extrusion process with here Prof. II Oddvin Reiso in picture (b) who is standing in the basement and directing the profile from the extruder at the first floor straight into the water pit.

3.6 Screw extrusion

The Al-7Si-0.3Mg and Al-12.7Si alloys were produced in the autumn of 2017 by Amundsen, [8]. Before the screw extrusion process could commence it was of importance that the feedstock material was free from contamination. The Al-Si alloys were machined by using ethanol as coolant and did thereby not need to be cleaned. As for the engine block, its surface where it was supposed to be machined was wiped with acetone, and no coolant was used during the machining into granulates, as shown in Figure 3.6.1.

Figure 3.6.1: Machined granulates of the engine block. The granulates of the two Al-Si alloys were nearly identical.

The screw extrusion process requires continuous surveillance to ensure optimum run parameters. After the assembling procedure of the machine, presented in Figure 2.2.4, the die was heated up to ca. 300°C to make the material more plastic. The temperature was not risen to operation temperature since the deformation of the material in the die released large amounts of heat. When this temperature was reached, feeding could proceed, and a slow screw rotation velocity was applied. The screw would transport the material across the chamber and into the die where it would be compacted into a solid mass. When the desired run temperature was reached, one could observe that the extrusion process would initiate when the momentum of the screw increased as a result of high enough pressure build-up in the chamber. In Figure 3.6.2 illustrates the screw extruder during the operation of processing one of the Al-Si alloys with descriptive arrows. Arrow 1 show the die, the heat source and the continuous production of profile. Arrow 2 show the chamber where the screw is transporting the granulates from arrow 3 into the die. The blue component in the back which arrow 4 indicates is the gear and transmission from the electric motor atop.

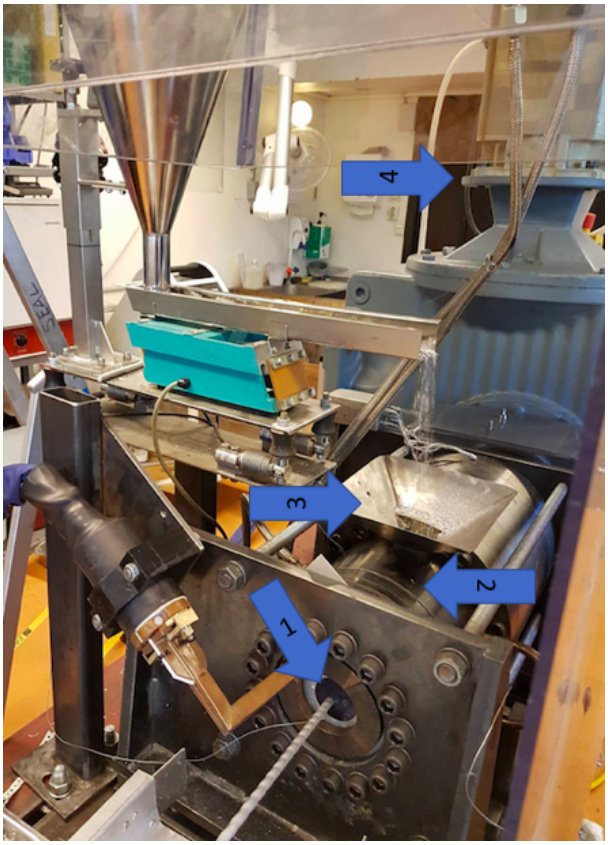

Figure 3.6.2: Picture of the screw extruder during operation.

The pressure build-up depends on four parameters; the geometry of the screw, frictional conditions, size of the die opening, and the material characteristics. At this stage a right balance between temperature, feeding rate and screw velocity would result in a stable production of profile out of the die. The temperature of the back line, (almost at the start of the chamber) was thoroughly observed. As too high temperatures here would significantly decrease or even stop the profile production. In principle at this stage it is possible to produce profile continuously as long the temperature is controlled and the feeding rate is stable. The run parameters during screw extrusion of each of the alloy can be observed in Table 3.9.

Table 3.9: Screw extrusion parameters.

Alloy	Die diameter[mm]	Die temperature [°C]	Screw velocity [RPM]	Quenching
Al-7Si-0.3Mg	10	530	6	No
Al-12.7Si	10	530	6	No
Engine block	10	500	3-4	No

3.7 Hydrogen evolution measurement

In order to obtain a less alkaline concrete with the goal to limit and/or cancel the corrosion reaction of aluminium, 55% of the ordinary Portland clinker was replaced with calcined clay as a SCM and the aluminium samples were submerged in an inhibitor solution. Since the DARE2C project is still ongoing and the inhibitor is in the process of becoming patented, the identity of the inhibitor will not be revealed and will hence be named 'inhibitor'. The calcined clay, which mainly consist of silicates, function as other SCM by consuming unreacted cement $Ca(OH)_2$ and producing more binder material, [51].

At an early stage of the thesis work, measurements were carried out together with Prof. Dr.Harald Justnes, where the aluminium samples were submerged in the inhibitor solution for 18 hours. The results were unanimous and showed that all the alloys tested developed so much gas that they filled the measuring cylinder within a short time with the exception of the Al-5Mg alloy. Prof. Dr.Harald Justnes had on a earlier stage of the DARE2C project done the same measurement where the Al-5Mg in the inhibitor solution showed no sign of gas formation at all over a period of several days in the same cement mix, presented later in this section. On this basis, it was decided to carry out the experiment presented in the next section 3.8 with the choice of this alloy as reinforcement material.

From the corrosion reaction of aluminium, shown in Equation 2.11 it can be seen that the formation of hydrogen is on of the end products, which thereby makes it fair to assume that the gas captured in this experiment is hydrogen. At some point in the future of the DARE2C project, it is planned to conduct gas chromatography measurements to determine the final composition of this gas.

The process of evaluating hydrogen evolution from embedded aluminium samples in concrete started by initially weighing out 300 grams of solids where 55% of the Portland clinker was replaced with calcined marl. Then 210 grams of water was separately weighed and then added with ice cubes in order to control temperature, and a certain amount of Mg salt. The identity and the quantity of the Mg salt will not be revealed since it is also a part of the corrosion protection system. What which can be revealed of some of the function the addition of the salt, which will hence be named MgX_2, gives is done in order to decrease the pH. According to the reaction presented in Equation 3.2, the MgX_2 will react the alkalies in the concrete into $Mg(OH)_2$ which has a pH of 10.5 and into NaX which is a neutral salt, and further contribute to a lower pH of the cement.

$$MgX_{2(s)}) + 2\,NaOH_{(aq)} \longrightarrow Mg(OH)_{2(s)} + 2\,NaX_{(aq)} \tag{3.2}$$

(a) Before mixing the cement and blending it in a blender.

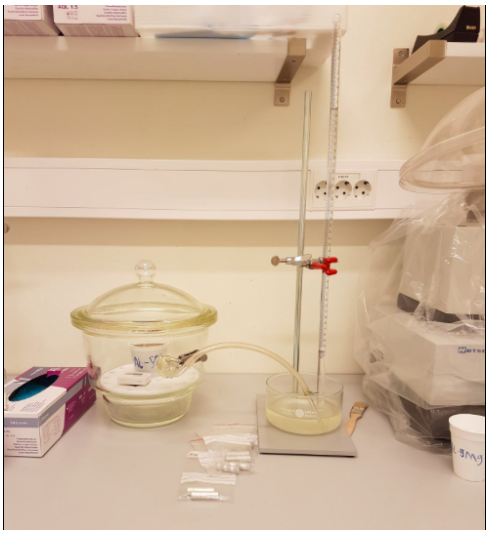

(b) The set-up for measuring hydrogen evolution.

Figure 3.7.1: Photographs of the hydrogen evolution measurement set-up.

The solids were then poured into the container containing water, ice cubes and the salt and mixed together by using a standard Bosch hand blender. To ensure homogeneity of the cement paste it was first mixed quite vigorously for 1 minute, then set for 5 minutes to rest before being mixed one last time for 1 additional minute. The cement paste was then after the mixing procedure poured into white plastic containers. The experimental set-up is depicted in Figure 3.7.1(a). The aluminium samples, with the dimension of ø10mm and 40mm length, were then taken out of the inhibitor solution and placed in the cement cup in a up standing position. The cup was immediately placed into the desiccator after the insertion of aluminium.

The corrosion rate of aluminium in cement was measured qualitatively by looking at the amount of gas developed through the reaction. As depicted in Figure 3.7.1(b), an airtight desiccator was coupled up to a tube which was lead into a water beaker. From there the tube was lead into a measuring cylinder filled to the end with water. Since it was submerged into the water beaker, all the gas evolved from the reaction could be captured and then measured in the cylinder. The gas pressure had to be built up to be able to escape into the measuring cylinder, so instead of a continuous gas supply, the gas came in batches as bubbles with different gas volumes at different time intervals.

The pH of of all the cement batches were taken by collecting the free water at the surface with a pipette, and then measure it by applying the water on standard pH test strips for alkaline solutions.

3.8 Casting and testing the aluminium reinforced concrete beams

It should be pointed out that the author was responsible for producing the aluminium reinforcement rods to the beams, but was only participant in some of the work of casting and testing the concrete beams and had no responsibility for this process. This study was executed under the management of the three civil engineering students with the supervision and cooperation with the Department of Structural Engineering at NTNU and the research institution SINTEF. The author does not take any credit for the work that was done in this experiment. This section is included to give the reader an insight in the work which was done in this multidisciplinary cooperation, administered by the DARE2C project and what results this collaboration gave. The photographs used in this section were taken by the author himself, but the Figures 3.8.2(a-c) and 3.8.3-3.8.5 are redrawn based on the figures used in the civil engineering students master thesis together with the theory of the various failure mechanisms which is based on their work, [42].

Manufacturing the reinforced concrete beams

(a) Picture from the mixing of the concrete. At the picture it can be observed water being added into the blender with the aggregate and cement mixture.

(b) Picture of the fresh concrete mix being poured into into the formwork with corrosion protected reinforcement bars

Figure 3.8.1: Pictures taken from the concrete manufacturing and beam production.

A total of six reinforced concrete beams were produced in this experiment. The positions of the embedded reinforcement rods are presented in the Figures 3.8.2(a-c). One beam was embedded with commercial ø10 mm ribbed steel reinforcement to served the purpose by being a benchmark for the aluminium reinforcement. Three beams were embedded with ø10 mm circular reinforcement rods and two were embedded with upside-down-turned T-profiles.

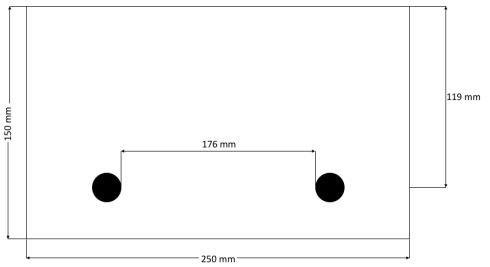

(a) The position of the two ribbed steel reinforcement rods in one of the concrete beams.

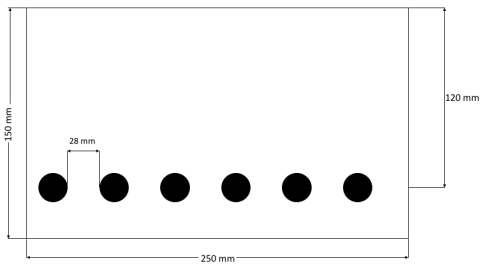

(b) The position of the six ø10 mm aluminium reinforcement rods in three of the concrete beams.

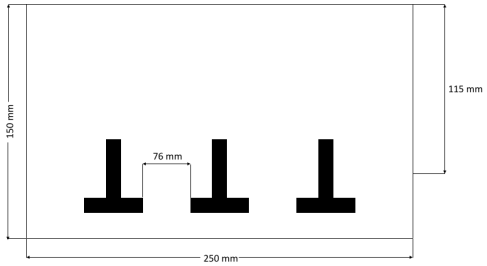

(c) The position of the three upside-down-turned T-profile reinforcements of aluminium in two of the concrete beams.

Figure 3.8.2: The cross-section dimensions of the beams and the placements of the rebars in the formwork, and eventually the beams (not to scale), redrawn based on [42].

After the Al-5Mg profiles were extruded, they were cut into the calculated lengths of 1.05 m and additional round ø10 mm rods of 0.20 m were cut out for anchoring, and prepared in the inhibitor solution for 16 hours. The anchoring to the reinforcement were bound transversely to the reinforcement rods according in Figure 3.8.1. Usually the anchoring are weld to the reinforcement rods to secure them into position and to avoiding slipping during the pouring of the fresh concrete into the formwork, but due to HSE reasons it was not possible to weld the anchoring rods onto the reinforcement.

The same concrete prescription was used as that described in section 3.7, with the addition of aggregates of various grain sizes, ranging from fine 0-8 mm to coarse 8 - 16 mm. In addition was a suerplactiziser added in as admixture which would make the concrete more workable without affecting the w/c ratio. After the mixing procedure, the concrete mix was transferred into the formwork with reinforcement system according to Figure 3.8.1. The beams were stored away to fully harden before they be tested. The civil engineering students performed a series of tests of both the concrete in fresh state, e.g. air content and density and in hardened state e.g. compression strength to obtain vital data and properties of the concrete for their master thesis.

The 4-point bend testing of the concrete beams

All of the six beams were subjected to the same 4-point bending test where they were placed in a loading cylinder where the load was applied in multiple consecutive steps until failure, [42]. To better observe the crack development, the beams were painted white. The three failure types that could occur to the beams during this test were:

Moment failure

The application of external load to the beam which results in vertical crack throughout the longitudinal section of the beam and breaking it in the middle, [42].

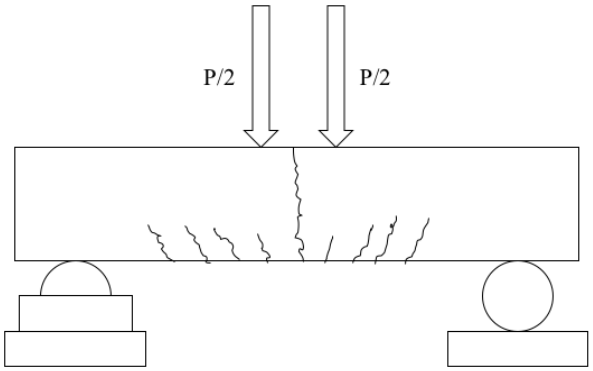

Figure 3.8.3: Bend moment failure of a reinforced concrete beam under applied load, redrawn based on [42].

Shear failure

The cracks development from the load application point which will transverse crosswise to the closest support point, as shown in Figure 3.8.4, [42].

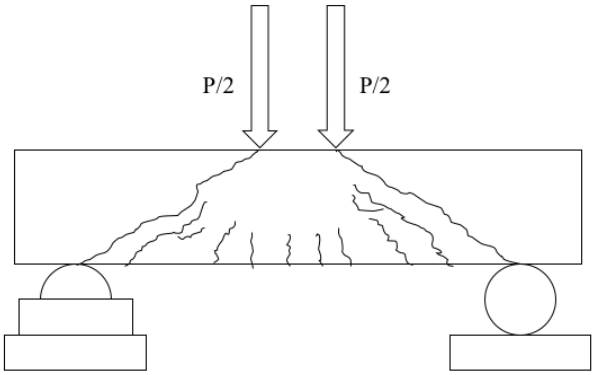

Figure 3.8.4: Shear failure of a reinforced concrete beam under applied load, redrawn based on [42].

Anchorage failure

Anchorage failure occur due to poor adhesion which will make the reinforcement to slip at into the centre of the beam, [1, 42]. This results in development of large concentrated cracks in the centre of the beam, where the load is applied instead of the more favourable scenario where smaller cracks are evenly distributed across the beam, as shown in Figure 3.8.5.

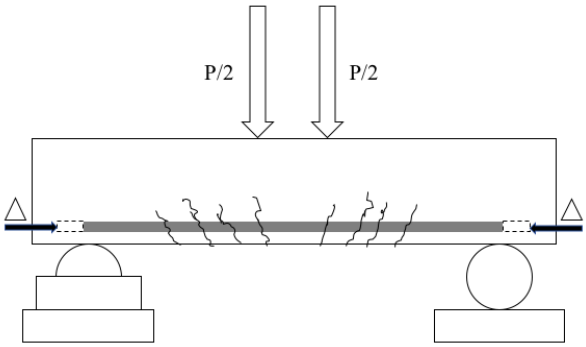

Figure 3.8.5: Anchorage failure of a reinforced concrete beam under applied load, redrawn based on [42]. The Δ symbols in the figure indicates the displacement of the reinforcement towards the centre of the beam.

4 Results

The results from the various experiments are presented in this section. In appendix A a schematic flow chart representation of the experimental work done in this thesis is presented which can give an overview of the what results were obtained in the different processes and experiments.

4.1 Hardness

This section presents the hardness which was measured for each of the alloys from both before and after extrusion. From the billets and the engine block a sample from the middle of the material was cut out and then 6 measurements were made at random points. As for the extruded products, the hardness measurements where only collected from the transverse cross-sections. Due to the differences that occur in the microstructure after thermomechanical processing, the hardness was measured at both the centre of the sample and the edge as shown in Figure 3.3.1. In both of the measuring areas, 6 measurements were also taken, with a certain distance from each other to avoid incorrect measurements.

Al-Mg alloys

The measurements clearly show that the extrusion had no major impact on the hardness of the Al-Mg alloys. As expected, the Al-Mg alloy with the most wt.% Mg in solid solution has the highest hardness, while the Al-1Mg alloy has a hardness that is relatively similar to pure aluminium. The hardness of the Al-5Mg alloy is found to be relatively similar throughout the structure, with standard deviations taken into account. On the other hand, the hardness of the Al-1Mg alloy shows lower values in the centre of the profile compared to the edge.

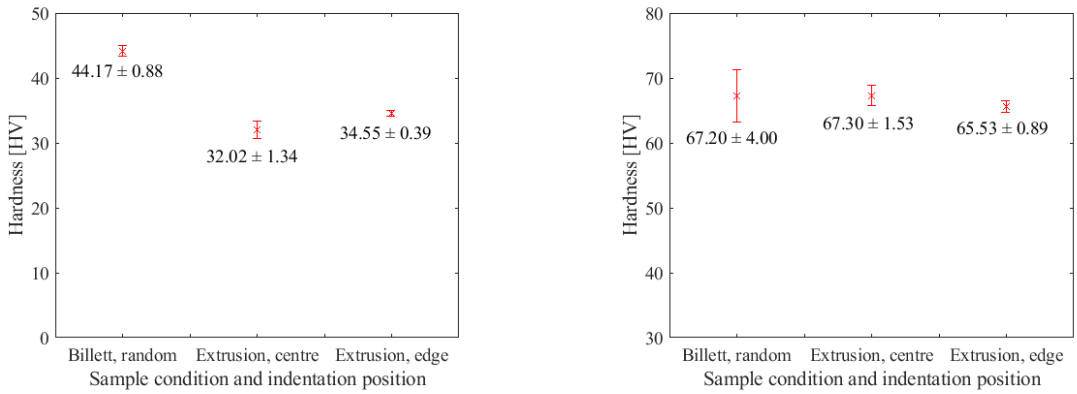

(a) Al-1Mg

(b) Al-5Mg

Figure 4.1.1: The vickers hardness values of both the Al-Mg alloys from before and after extrusion, with given standard deviation.

Al-Si alloys

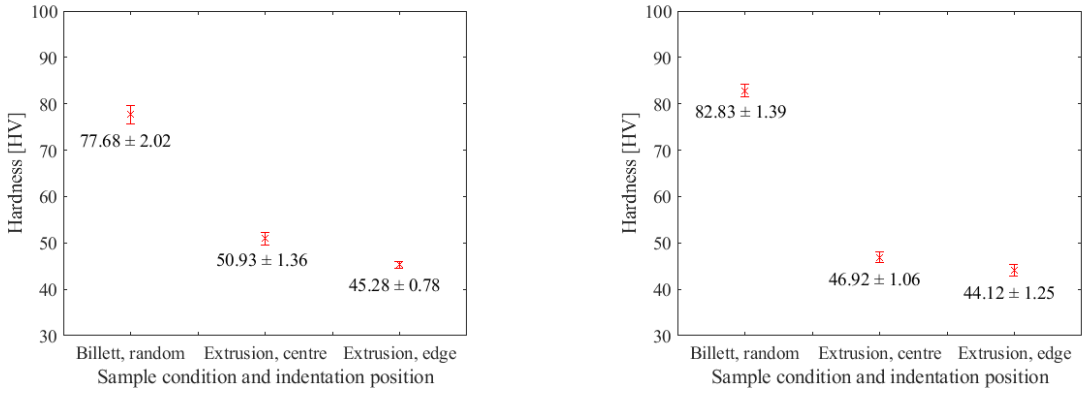

(a) Al-7Si-0.3Mg (b) Al-12.7Si

Figure 4.1.2: The vickers hardness values of both the Al-Si alloys from before and after extrusion, with given standard deviation.

The hardness measurements show that the strength of the Al-Si alloys is affected by extrusion. For both the alloys the hardness values drops approximately 35-40 HV. Both alloys show the same tendency that the hardness of the centre of the profile is greater than compared to the edge, after screw extrusion.

The engine block

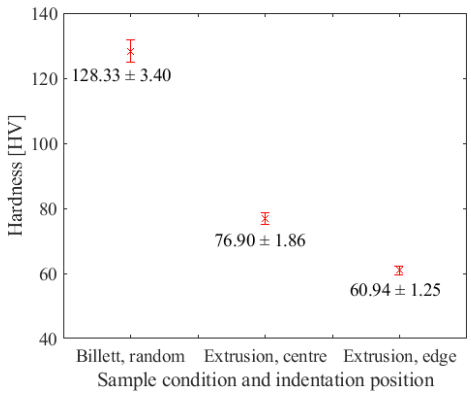

Figure 4.1.3: The vickers hardness values of the engine block from before and after extrusion, with given standard deviation.

The engine block before screw extrusion has the highest hardness value of all of the alloys in this thesis. This is as expected regarding its chemical composition and the fact that it is a cast alloy. The measurements taken from the extruded profile indicates that the screw

extrusion process has a major impact on the hardness of this alloy, where the hardness values drop with approximately 50-70 HV after the process. In resemblance with the two Al-Si alloys, the engine block alloy possesses the same tendency that the hardness values are greater in the centre of the profile than at the edge.

4.2 Tensile strength

This section summarises the tensile test results where the values are given in engineering stress-stress to minimise the geometrical factors. Three tensile samples of each alloy were made to rule out random sources of error and establish an acceptable statistical basis. The ductility values are not included since the standard deviations were so high that they could not be determined with good enough accuracy.

The Al-Mg alloys

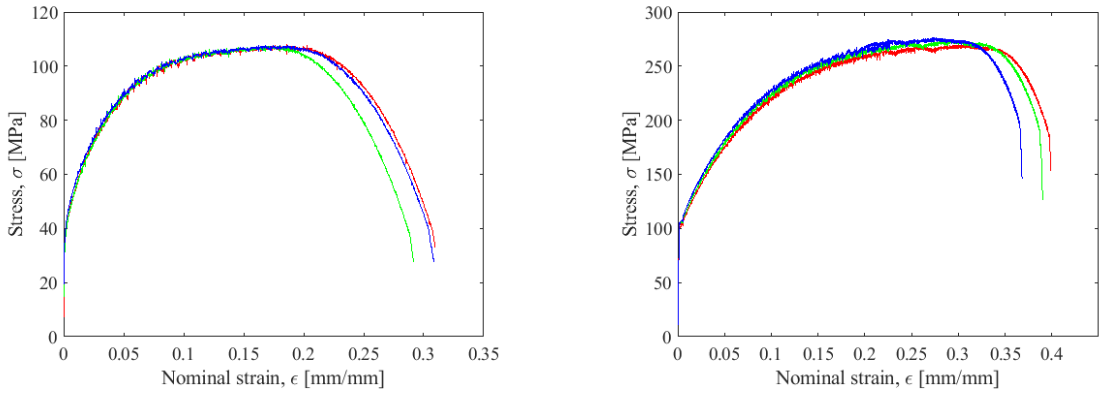

(a) Al-1Mg (b) Al-5Mg

Figure 4.2.1: Tensile strength of the Al-Mg alloys after extrusion.

The tensile strength of the Al-Mg alloys in the as-cast state was not examined since their prior strength before extrusion was established as irrelevant for further experiments in this thesis.

The Al-1Mg alloy displayed a quite ductile behaviour where a large strain at fracture. However, the Al-5Mg alloy showed a much higher strength compared to Al-1Mg and portrayed identical similar ductile behaviour. With ductile behaviour, it is implied that after reaching UTS, a reduction in the cross-section was observed at the fracture point, which is known as necking. Serration on the stress-strain curves to both of the alloys was observed, which indicates PLC.

The Al-Si alloys

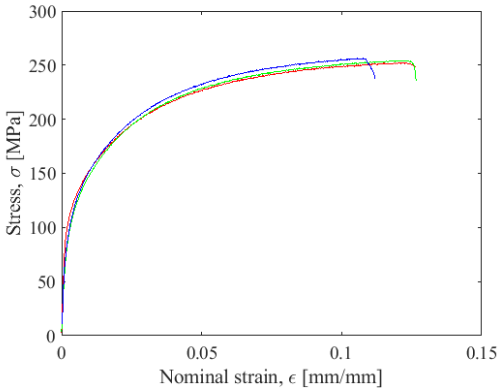

(a) Al-7Si-0.3Mg as billet.

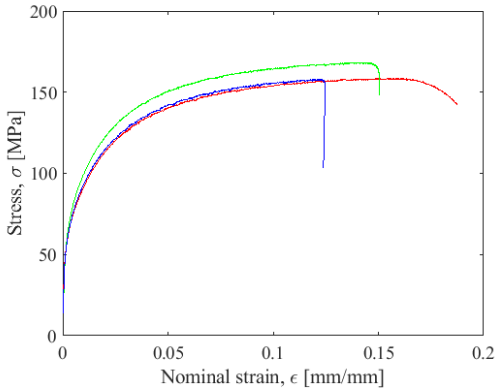

(b) Al-7Si-0.3Mg after extrusion.

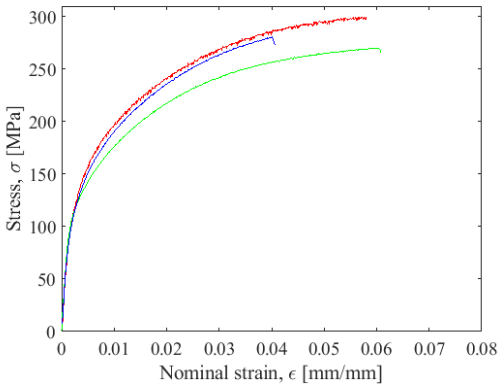

(c) Al-12.7Si as billet.

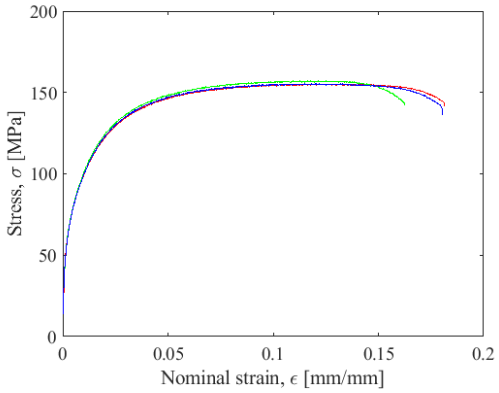

(d) Al-12.7Si after extrusion.

Figure 4.2.2: Tensile strength of the Al-Si alloys before and after screw extrusion.

The Al-Si alloys in the as-cast state displayed the typical characteristics for brittle materials which include high strength and low ductility. With brittle behaviour, it is implied that the samples fractures after reaching UTS without the reduction in the cross-section of the sample. One of the samples to the as-cast Al-7Si-0.3Mg alloys snapped at UTS during the tensile testing, which can be observed in the blue curve in figure 4.2.2(b), but was taken into account for.

For both the AL-Si alloys, the strength was significantly reduced after being processed through screw extrusion. They both obtained a ductile behaviour as-extruded, but the strain at fracture was not remarkably higher. Some minor serrations are observed for the Al-Si alloys in both as-cast and as-extruded state at their curves, but nothing in comparison to the Al-Mg alloys. It almost seems that the two Al-Si alloys obtain the same yield and ultimate tensile strength after screw extrusion.

The measured parameters from the tensile testings are summarised and presented in Table 4.1.

Table 4.1: Tensile strength results given in average value ± standard deviation

	Tensile strength results		
Aluminium alloy	[Before/after] extrusion	Offset yield strength (σ_y) [MPa]	Ultimate tensile strength (σ_{UTS}) [MPa]
Al-1Mg	After	65.43 ± 3.66	107.8 ± 0.26
Al-5Mg	After	144.5 ± 1.14	273.97 ± 3.59
Al-7Si-0.3Mg	Before	140.3 ± 3.6	254.2 ± 2.2
	After	93.8 ± 3.8	161.7 ± 5.8
Al-12.7Si	Before	166.1 ± 13.3	283.6 ± 15.1
	After	96.0 ± 1.8	156.0 ± 1.1

4.3 Coefficient of linear thermal expansion

Data retrieved from thermodilatometry

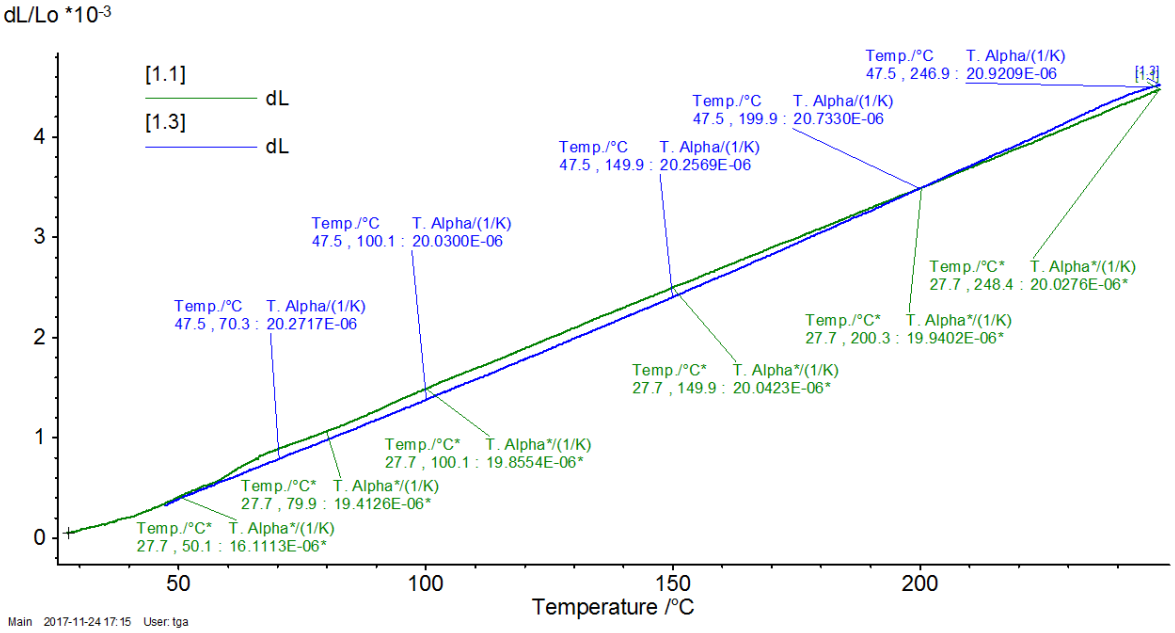

Figure 4.3.1: CTE of screw extruded Al-12.7Si from 30-250°C where the green curve represents the heating step and the blue consequently represents the cooling step. The CTE is defined as "T.Alpha" in the graphs in addition to the temperature range it was measured in.

In this experiment were only the Al-12.7Si and Al-7Si-0.3Mg alloys examined. The graphical representations from the thermodilatometry trials of Al-12.7Si in the 30-110°C and 30-70°C temperature intervals and the AL-7Si-0.3Mg in all three temperature intervals can be found in appendix E. The results are based on the author's previous work, [8]

The Tables 4.2, 4.3 and 4.4 summarises the results of the CTE obtained from the thermodilatometry measurements. The CTE values were extracted from the slope of the curves where the curve had little curvature, i.e. were at its most linear. Measuring CTE from areas where the curve has a high curvature does not give accurate measurement since the high curvature is probably a result of an error source. The ASTM E228 [50] suggests to measure the CTE from a 100°C interval, but since that accounted for inaccurate measure points from high curvature areas, the CTE was rather measured from smaller temperature intervals. The CTE was examined at both the heating step and the cooling step. The values marked with "*" indicates that the value is either far above or far below the value the literature indicates it should be.

Table 4.2: Coefficient of linear thermal expansion measured with push-rod dilatometry.

Coefficient of linear thermal expansion 30-250°C [$\frac{\mu m}{m°C}$]						
	The heating curve			The cooling curve		
Material	30-50°C	30-150°C	30-250°C	60-100°C	100-150°C	150-250°C
Billet						
Al-7.0Si -0.3Mg	16.7*	24.8	28.9*	24.1	24.5	24.4
Al-12.7Si	17.4	21.2	23.2	22.2	22.4	23.2
Profile after screw extrusion						
Al-7.0Si -0.3Mg	19.5	23.2	24.6	23.8	23.3	24.1
Al-12.7Si	16.2	19.9	20.22	19.7	20.4	21.8

The results in Table 4.2 indicated that with higher amounts of alloying elements like Si yields an equal reduction in CTE. On the heating curve, there is a trend that the CTE increases at higher temperatures for all of the alloys. Another trend indicated that the as-extruded samples had a smaller CTE than the as-cast samples. The Al-7Si-0.3Mg yielded some unusual readings for the CTE where the curve had some sections with big curvatures which indicate inaccurate CTE values.

Table 4.3: Coefficient of linear thermal expansion measured with push-rod dilatometry.

Coefficient of linear thermal expansion 30-110°C [$\frac{\mu m}{m°C}$]						
	The heating curve			The cooling curve		
Material	30-60°C	60-110°C	30-110°C	50-80°C	80-110°C	50-110°C
Billet						
Al-7.0Si -0.3Mg	22.0	25.4	24.3	25.5	24.7	25
Al-12.7Si	19.7	20.5	21.3	22.9	24.0	22.5
Profile after screw extrusion						
Al-7.0Si -0.3Mg	15.6*	23.2	21.8	24.1	22.7	23.3
Al-12.7Si	15.1*	20.4	19.8	23.3	20.9	21.9

The measurements conducted on the temperature program 30 110°C showed the same trends regarding the reduction of CTE as a function of the amount of alloying elements and the effect of thermomechanical processing. Compared to the values presented in the theory the trend should be that the CTE got higher in with higher temperature and lower

with decreasing temperature, which is not always the case with these results. The quite low measurement of CTE of Al-12.7Si after being screw extruded is rather inaccurate since the curve has a quite big curvature. The measurements of the CTE in the 30-110°C column in Table 4.3 in both the heating and cooling step, is presented to visualise how the measurement would have been if the slope was calculated from the entire curve.

Table 4.4: Coefficient of linear thermal expansion measured with push-rod dilatometry.

Coefficient of linear thermal expansion 30-70°C $[\frac{\mu m}{m°C}]$				
	The heating curve		The cooling curve	
Material	30-50°C	30-70°C	50-60°C	50-70°C
Billet				
Al-7.0Si -0.3Mg	21.6	23.3	24.9	24.2
Al-12.7Si	18.7	20.3	23.4	23.0
Profile after screw extrusion				
Al-7.0Si -0.3Mg	18.6	21.5	24.1	23.4
Al-12.7Si	19.2	20.5	20.9	20.6

The results of the CTE measurements at the 30-70°C set-up gave values that are quite similar to the values given in the theory section about CTE. Since the slope is measured over quite small temperature intervals this may lead to some uncertainty. The curvature of the slopes was to a certain extent small which again removes some of the uncertainty.

Data retrieved from manually measuring with extensometer

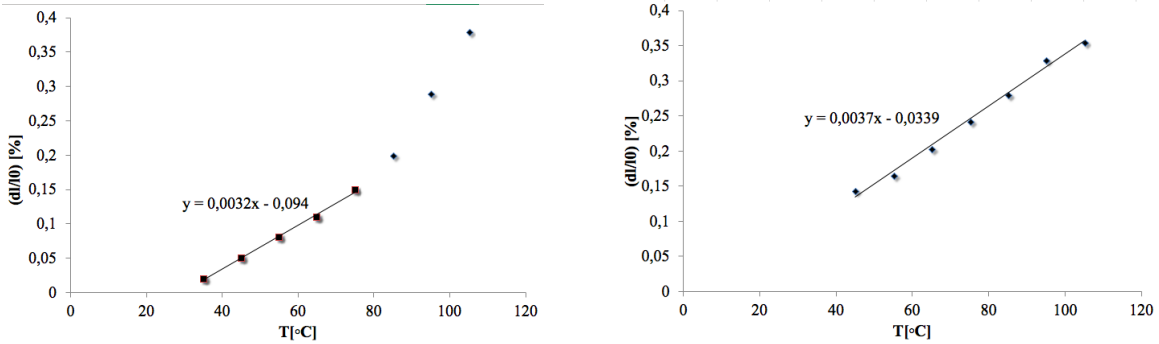

(a) Data collected from heating up the sample.

(b) Data obtained from cooling the sample down from the max temperature.

Figure 4.3.2: Hardness of the Al-Mg alloys before and after extrusion.

In this experiment, the Al-12.7Si, Al-7Si-0.3Mg and Al-5Mg alloys were examined. The plots and the rest of the raw data from the manual measurement with extensometer the of the Al-5Mg and Al-7Si-0.3Mg alloys can be found in appendix E.

The oven was manually controlled with the purpose of holding the sample at the desired temperature until it was assured that the whole specimen had reached the same temperature and then measured. In Figure 4.3.2(a) it can be observed that the slope was placed in the small curvature area and this was done for all three samples. The Al-7Si-0.3Mg and Al-5Mg alloys are observed to attain curves with smaller curvature than Al-12.7Si. From Table 4.5 it is observed that the CTE values of all the three alloys are remarkably higher than both the values obtained from thermodilatometry measurements and the literature values presented in Table 2.2.

Table 4.5: Summary of the results obtained from manually measuring the CTE from an extensometer.

Alloy	The heating curve	The cooling curve
Al-5Mg	31	44
Al-7Si-0.3Mg	31	-
Al-12.7Si	32	37

4.4 Observations made during screw extrusion trials

Ethanol was used as a coolant when the Al-Si alloys were machined into granulates. It was of uttermost importance that oil or other organic compound were not used in the machining process or would contaminate the material before the screw extrusion process commenced. The high temperature evolved during the process would make these contaminants react and evaporate them into smoke. As for the engine block, no coolants were used during machining into granulates. Since the surface was cleaned with acetone before machining and under a visual inspection no traces of contaminant could be observed was it decided that the granulates were clean. For neither of the Al-Si alloys, there was no observation of smoke development during the screw extrusion process. For the engine block, however, there was a significant smoke development during the extrusion test

Compared to preliminary screw extrusion attempts with other aluminium alloys like Al-Fe and Al-Mg-Si, both the Al-Si alloys and the engine block granulates had a significantly slower extrusion speed. The produced profiles of the Al-Si profiles had an uneven surface geometry, while the surface to the engine block, in addition, was quite damaged, as seen in Figures 4.4.1(a-b).

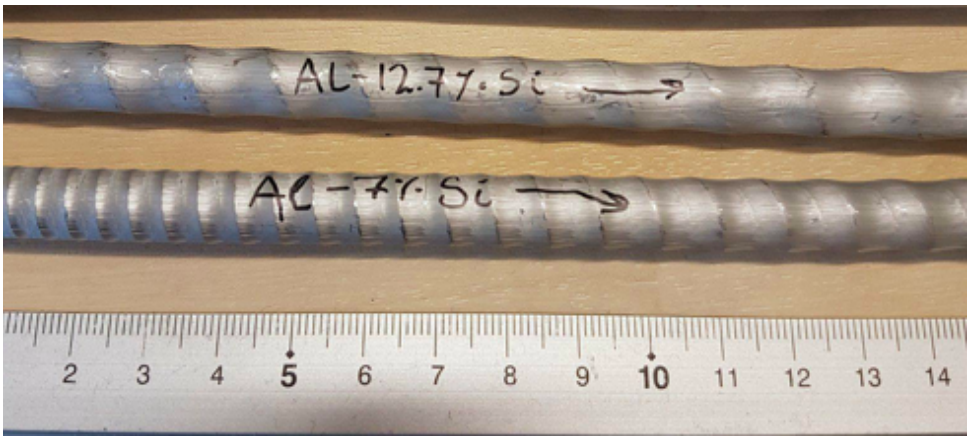

(a) The profiles of the two Al-Si alloys. The extrusion direction is to the right according to the arrows in this picture.

(b) The profile of the engine block material. The extrusion direction is to the left in this picture.

Figure 4.4.1: Photographs of the profiles produced through screw extrusion.

4.5 Grain structure characterisation by LOM

Al-1Mg

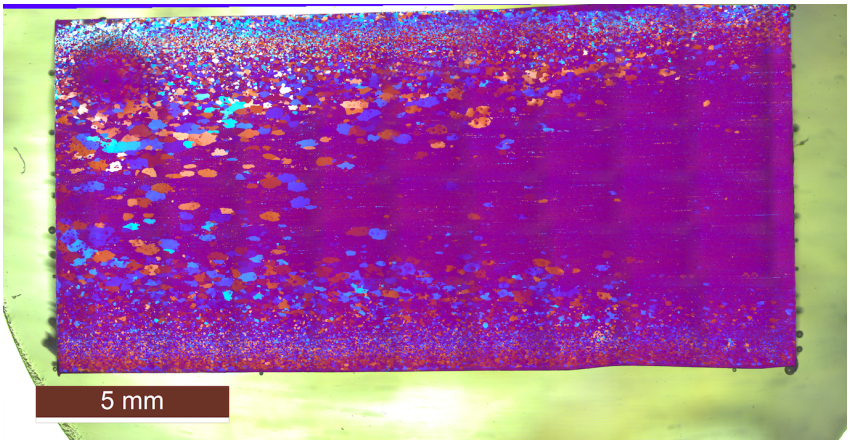

(a) Polarised light illumination and 50x magnification of the whole longitudinal cross-section.

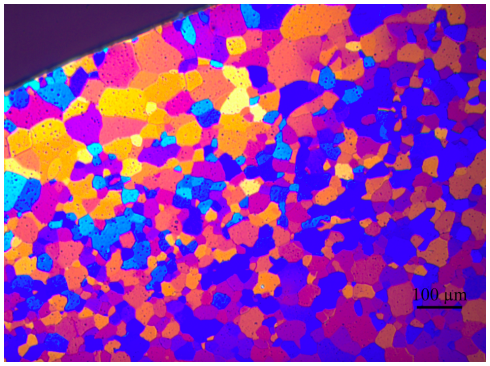

(b) Polarised light illumination and 10x magnification of the edge of the transverse cross-section.

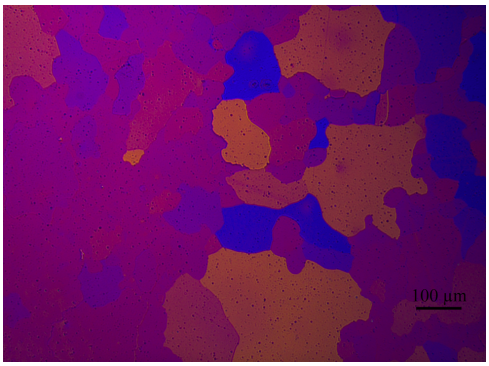

(c) Polarised light illumination and 10x magnification of the centre of the transverse cross-section.

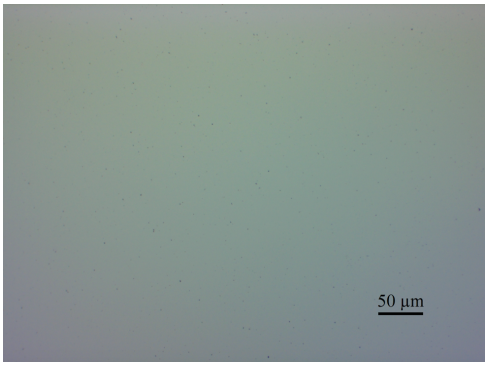

(d) Bright-field illumination and 20x magnification.

Figure 4.5.1: LOM micrographs of the Al-1Mg alloy after extrusion.

Figures 4.5.1(a-d) displays the microstructure of the Al-1Mg alloy as-extruded. The micrograph sample is taken from approximately 0.5 m from the start of the extrusion profile. In the anodised micrographs 4.5.1(a-c) it can be observed that the edges are fully recrystallised while the centre of the profile mainly contains a deformed structure with elongated grains and some few partially recrystallised grains. The surface grains (4.5.1(b)) shows random reflection which indicates random crystallographic orientation while the interior grains (4.5.1(c)) show uniform reflection, which indicates high degree of preferred crystallographic orientation. The distinctive spot which is observed in the upper-left corner in micrograph 4.5.1(a) is the contact area from the platinum electrode during the anodising process. From the bright field illumination micrograph in 4.5.1(d) only a few fine, insoluble, black and dispersed particles are observed.

Al-5Mg

The micrograph of the anodised samples in the Figures 4.5.2(a-c), compared to the ones for Al-1Mg, show a homogeneous and a fully recrystallised structure throughout the whole profile with new equiaxed grains. The micrograph sample is taken from approximately 2 meters from the extrusion starting end of the profile, and as with the Al-1Mg, the spot which can be observed in Figure 4.5.2 (a) is also from the anodising process. The same particle structure in the bright field illumination micrograph of this alloy can be observed in 4.5.2(a), as in with the Al-1Mg. From the micrograph of the entire longitudinal cross-section of the anodised sample, as shown in Figure C.0.3 it may be observed, as with the Al-1Mg that the interior grains of the profile centre show a more uniform reflection than the grains close to the surface, which also here indicates high degree of preferred crystallographic orientation.

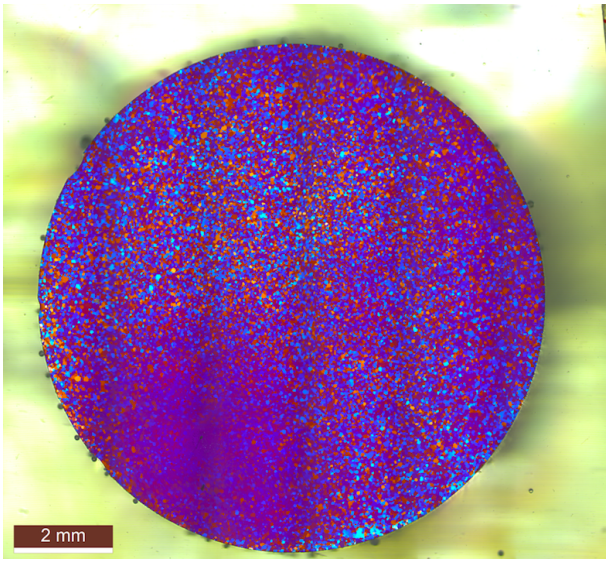

(a) Polarised light illumination and 50x magnification of the whole transverse cross-section.

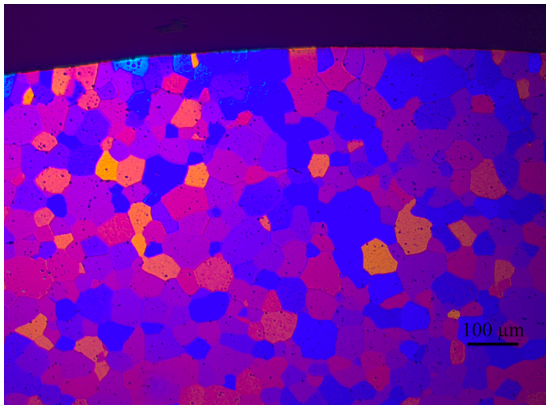

(b) Polarised light illumination and 10x magnification of the edge of the transverse cross-section.

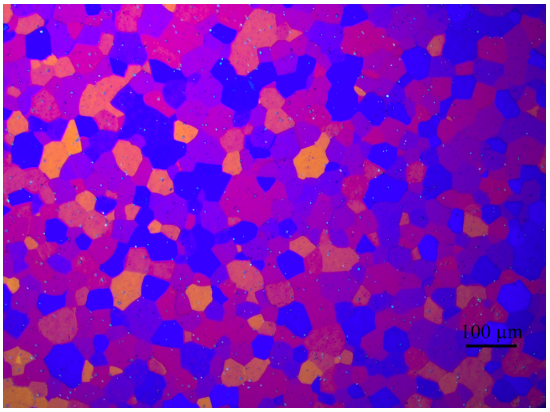

(c) Polarised light illumination and 10x magnification of the centre of the transverse cross-section.

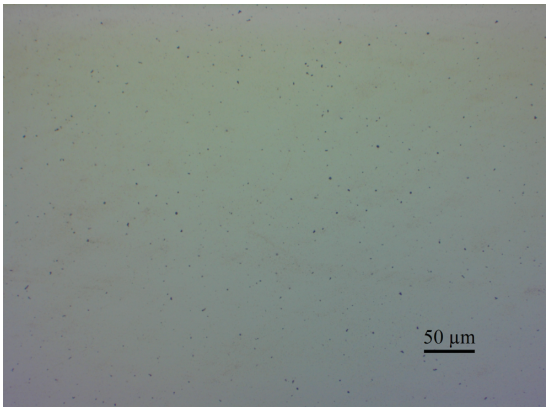

(d) Bright-field illumination and 20x magnification.

Figure 4.5.2: LOM micrographs of the Al-5Mg alloy after extrusion.

Al-7Si-0.3Mg

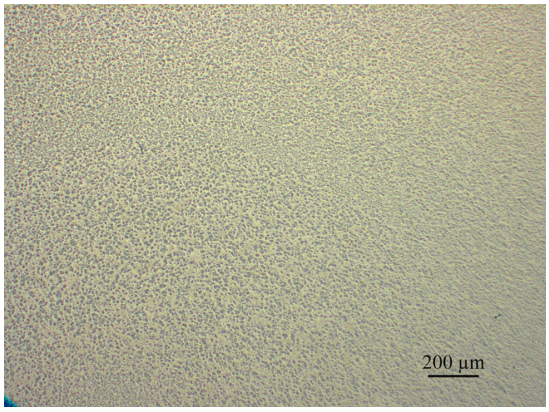

(a) Bright-field illumination and 5x magnification of the transverse cross-section..

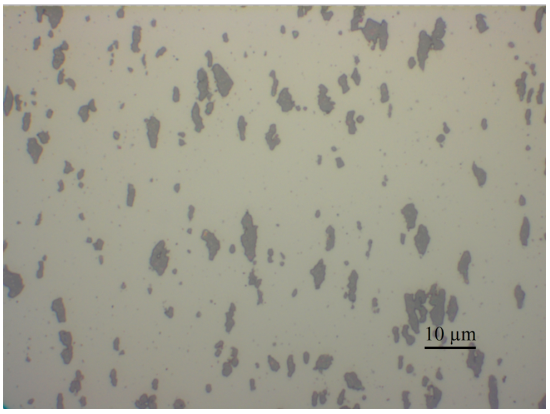

(b) Bright-field illumination and 100x magnification of the longitudinal cross-section..

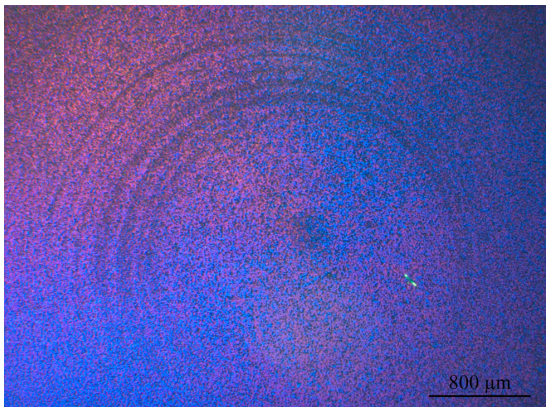

(c) Polarised light illumination and 2.5x magnification of the transverse cross-section.

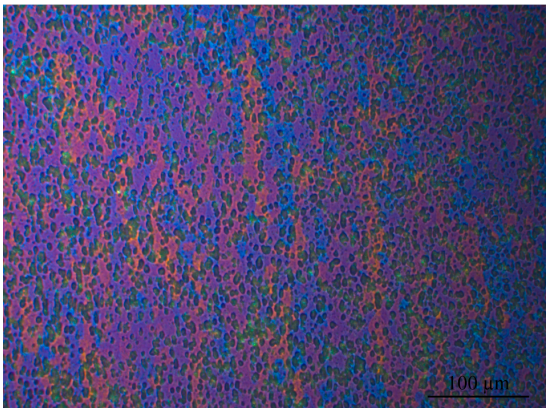

(d) Polarised light illumination and 5x magnification of the longitudinal cross-section.

Figure 4.5.3: LOM micrographs of the Al-7Si-0.3Mg alloy after screw extrusion.

The micrographs in Figures 4.5.3(a-d) presents micrographs of the microstructure of the Al-7Si-0.3Mg alloy after the screw extrusion process. The bright field illumination micrographs in Figures 4.5.1(a-b) presents a coarse and well-distributed particle-structure in the Al matrix. The anodised micrograph of the transverse cross-section in Figure 4.5.3(c) reveals a spiral-like structure which stems from the rotational motion of the screw which simultaneously takes place while the material is being forced out of the die. The grain structure presented in the micrograph of the anodised transverse cross-section in Figure 4.5.3(d) has the characteristics of a fibrous deformation structure.

Al-12.7Si

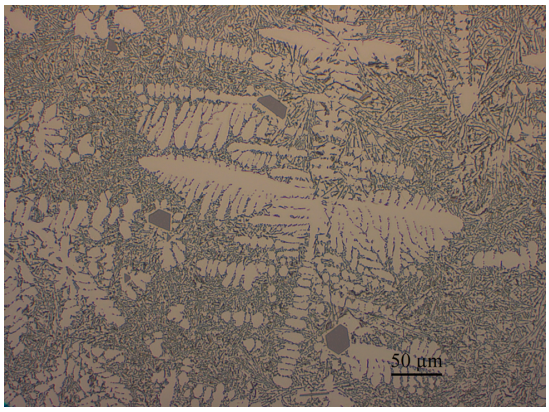

(a) Bright-field illumination and 20x magnification.

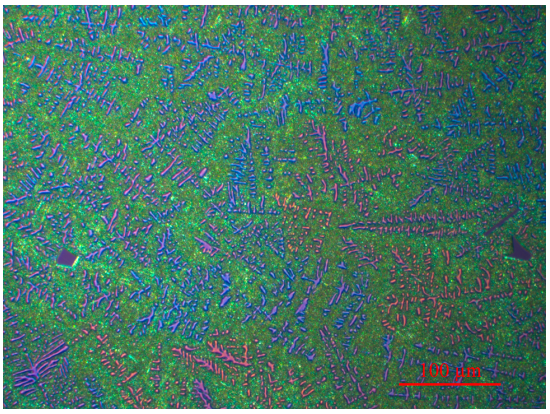

(b) Polarised light illumination and 20x magnification.

Figure 4.5.4: LOM micrographs of the Al-12.7Si billet before extrusion.

To better understand the effect of the microstructural changes that come with the screw extrusion process, it may be useful to examine the microstructure of the material in the as-cast state prior to this process. The microstructure of the Al-12.7Si alloy in the as-cast state is presented in the bright-field illumination micrograph in Figure D.0.5(a). The micrograph displays a typical interdendritic eutectic Al-Si microstructure of a modified cast alloy. The aluminium is present as white dendritic cells, while the Si is present as eutectic Si with flaky and angular morphology. The high concentration of Si leads to the formation of coarse and blocky primary Si crystals in the microstructure.

The deformation introduced to the material at temperatures under the melting point to this alloy leads to that the eutectic Si structure has been dispersed and been evenly distributed in the microstructure as coarse and deformed Si particles in the microstructure, which can be seen in the bright-field illumination micrographs in the Figures 4.5.5(a-b). Compared to the Al-7Si-0.3Mg is there a greater volume fraction of Si present in the microstructure of Al-12.7Si. Apart from that does the Al-12.7Si microstructure possess the same spiral-like pattern and the deformed fibrous Al grains as the Al-7Si-0.3Mg microstructure.

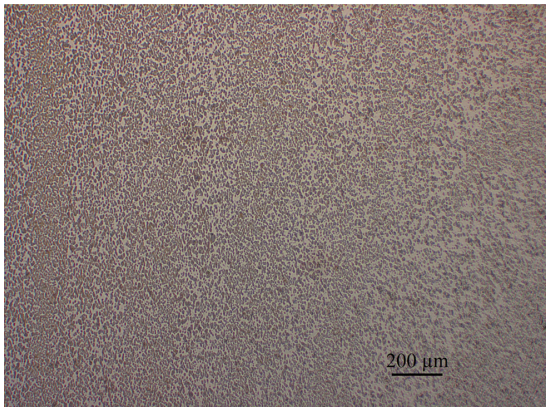

(a) Bright-field illumination and 5x magnification of the longitudinal cross-section..

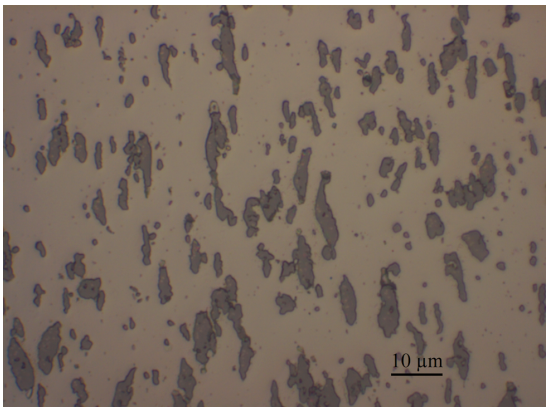

(b) Bright-field illumination and 100x magnification of the longitudinal cross-section..

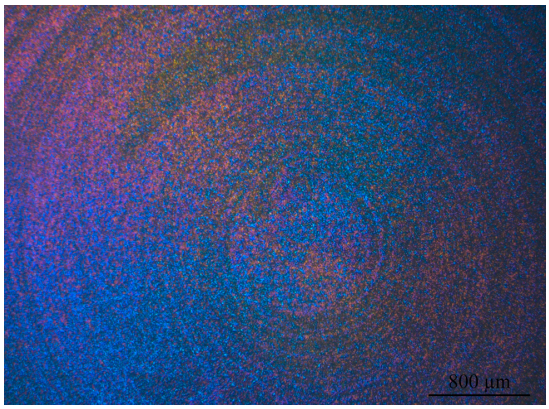

(c) Polarised light illumination and 2.5x magnification of the transverse cross-section.

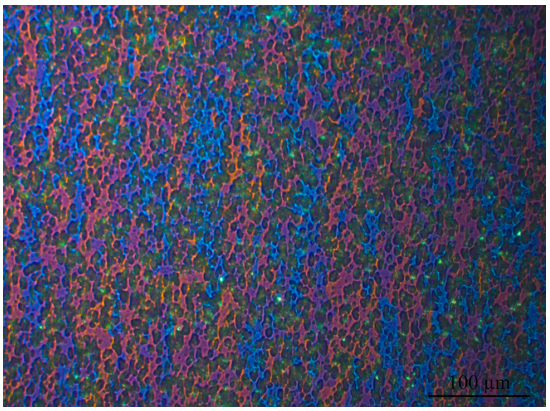

(d) Polarised light illumination and 20x magnification of the longitudinal cross-section.

Figure 4.5.5: LOM micrographs of the Al-12.7Si alloy after screw extrusion.

Engine block

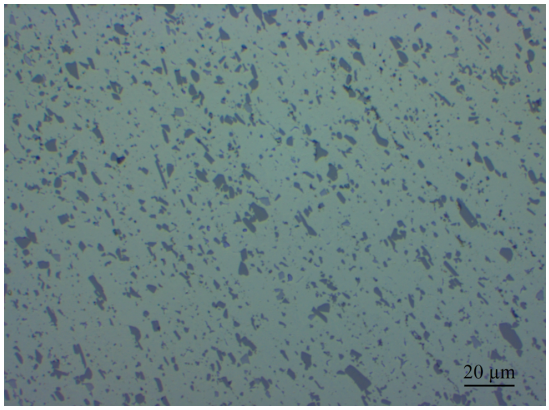

(a) Bright-field illumination and 50x magnification of the transverse cross-section.

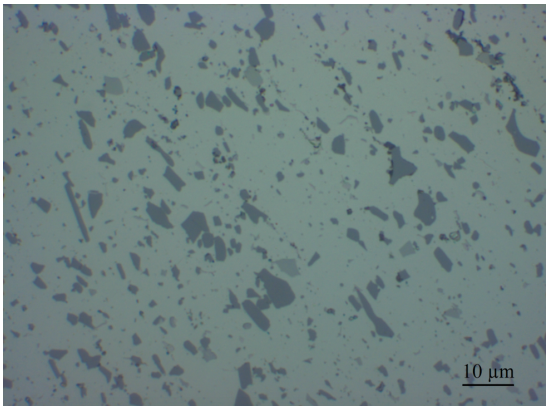

(b) Bright-field illumination and 100x magnification of the transverse cross-section..

Figure 4.5.6: LOM micrographs of the particles in the car engine microstructure after screw extrusion.

The engine block proves to possess the same characteristic microstructural features as the Al-Si alloys have after screw extrusion. Since the material contains a certain amount of other elements such as Cu, Fe and other impurities, these in addition to Si will be present in the deformed particle morphology of the microstructure and will be further assessed in the EDS measurements. The polarised light illumination micrographs of the anodised sample are presented in the Figures 4.5.7(a-e). In the micrograph of the longitudinal cross-section of Figure 4.5.7 (c), it is possible to observe extended grains in the centre of the sample while approaching the surface of the transverse cross-section of Figure 4.5.7 (d), there may seem to have been a partial to full recrystallisation of the grains. The microstructure of the as-cast material is highly dependent on where on the engine block the micrograph sample is collected from. The material in the different positions in the engine block is firstly affected by the different cooling rate during casting and secondly the temperature impact where the engine is in use.

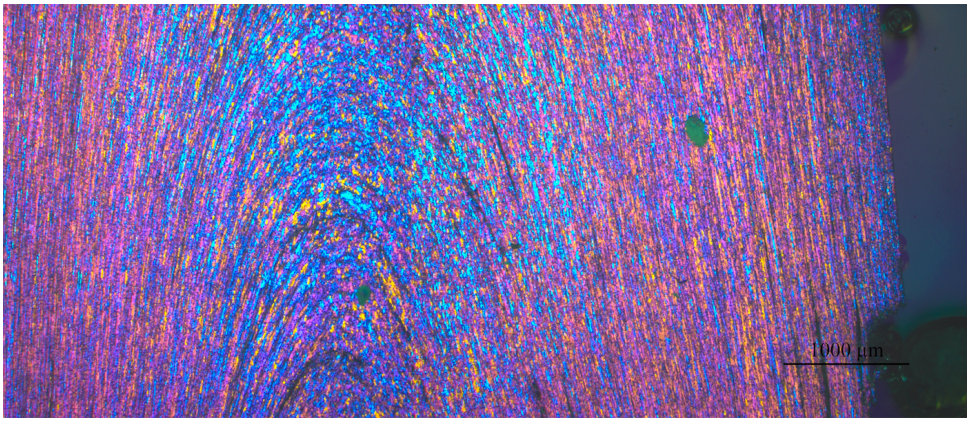

(a) Polarised light illumination and 2.5x magnification of the longitudinal cross-section.

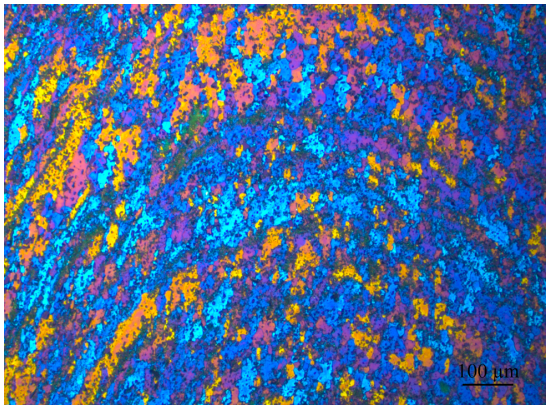

(b) Polarised light illumination and 10x magnification of the centre of the longitudinal cross-section.

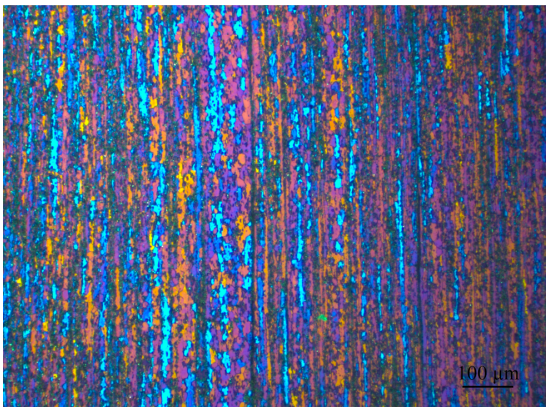

(c) Polarised light illumination and 10x magnification of the edge of longitudinal cross-section.

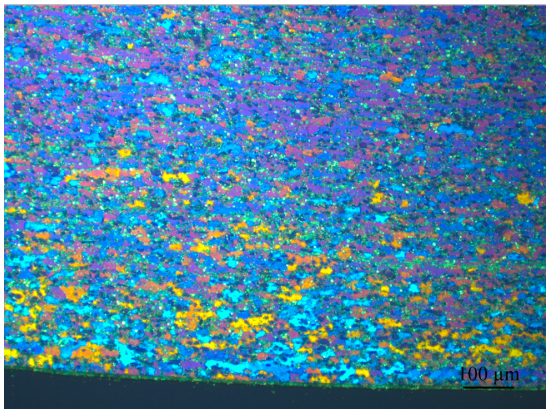

(d) Polarised light illumination and 20x magnification of the edge of transverse cross-section.

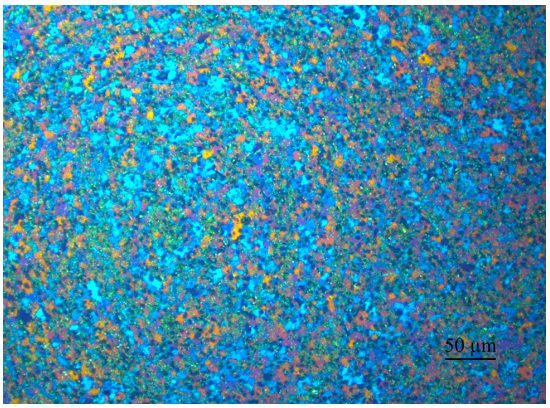

(e) Bright-field illumination and 20x magnification of the centre of transverse cross-section..

Figure 4.5.7: LOM micrographs of the engine block microstructure after screw extrusion.

Table 4.6: The average grain sizes of the Al-Mg samples before and after extrusion.

Sample	[Before/after] extrusion	Measure position	Grain size [μm]
Al-1Mg	Before	Random	50
	After	Centre	76
		Edge	33
Al-5Mg	Before	Random	73
	After	Centre	27
		Edge	41

The grain sizes were determined by using the linear interception of grain-boundaries procedure, as in accordance with the ASTM Standard E112,"Standard Test Methods for Determining Average Grain Size", [52].

Table 4.7: The average grain sizes of the Al-Si samples and the engine block before and after screw extrusion.

Sample	[Before/after] extrusion	Measure position	Grain size [μm]
Al-7Si-0.3Mg	Before	Random	216
	After	Centre	19
		Edge	14
Al-12.7Si	Before	Random	162
	After	Centre	18
		Edge	11
Engine block	Before	Random	111
	After	Centre	27
		Edge	17

To accurate establish the grain size of as-cast Al-7Si-0.3Mg and Al-12.7Si alloys were difficult due to their dendritic microstructure, so for the numbers presented in Table 4.7 they can just be interpreted to be average grain sizes for as-cast Al-Si alloys. The interior Al-grains of the screw extruded samples with longitudinal cross-section had an elongated morphology so it was difficult to establish statistically accurate measurements of the average grain sizes.

A repetitive trend observed for the screw extruded samples was that the grain at the surface of the profile had on average lower grain size than those in the centre.

4.6 Particle characterisation by SEM

The surfaces of the Al-1Mg and Al-5Mg alloys and the engine block after extrusion were examined in SEM and EDS characterisation, and are presented in this section.

Heavier elements will appear brighter than the lighter elements in the micrographs. The second phases constituents appear in the microstructure due to their content exceeds the solid solubility limit.

Al-1Mg

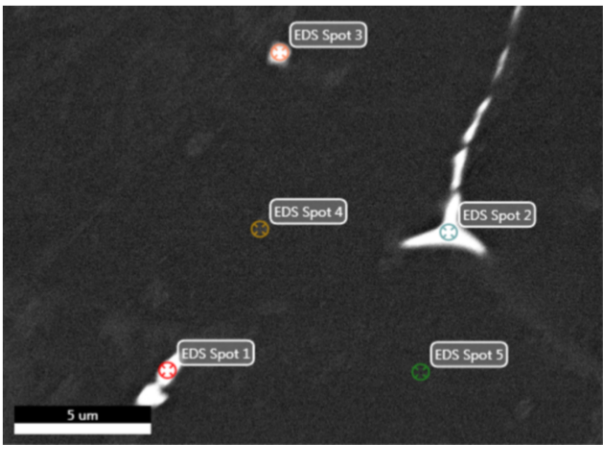

Figure 4.6.1: SEM micrographs of the Al-1Mg alloy billet 5000x magnification. Points indicate where analysis with EDS where taken.

In the Al-1Mg microstructure, only a few Al-Fe containing particles were observed mainly along the grain boundaries. EDS point measure of the confirms that approximately 1 wt.% Mg are present in solid solution in the Al matrix.

Table 4.8: EDS spectrum of the Al-1Mg extrusion profile.

Element	Content [wt.%]	Error [wt.%]
EDS spot 1		
Fe	18.89	2.48
Mg	1.10	7.28
Al	80.01	3.28
EDS spot 2		
Fe	22.71	2.40
Al	77.29	3.41
EDS spot 3		
Fe	12.32	2.66
Al	87.68	2.86
EDS spot 4		
Mg	2.35	3.96
Al	97.65	2.33

Al-5Mg

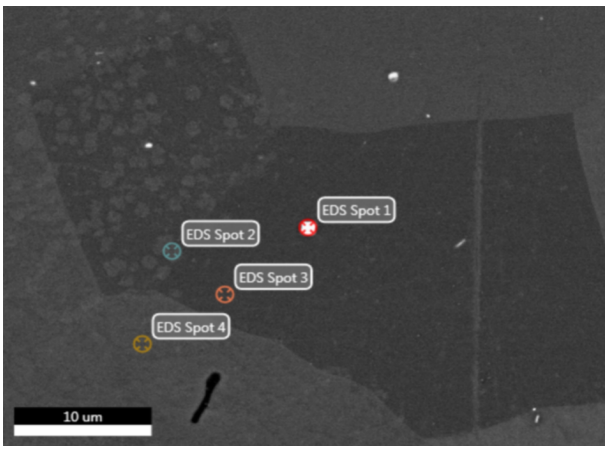

Figure 4.6.2: SEM micrograph of the Al-5Mg alloy extrusion profile 2500x magnification. Points indicate where analysis with EDS where taken.

Table 4.9: EDS spectrum of the Al-5Mg extrusion profile.

Element	Content [wt.%]	Error [wt.%]
EDS spot 1		
Fe	19.99	2.21
Mg	1.92	4.66
Al	78.08	3.29
EDS spot 2		
Mg	6.13	2.63
Al	93.87	2.51
EDS spot 3		
Mg	5.77	2.64
Al	94.23	2.49
EDS spot 4		
Mg	5.76	2.64
Al	94.24	2.49

As with the Al-1Mg alloy, only a few Al-Fe containing particles were observed mainly along the grain boundaries. EDS point measure of the confirms that approximately 5 wt.% Mg are present in solid solution in the Al matrix.

Engine block

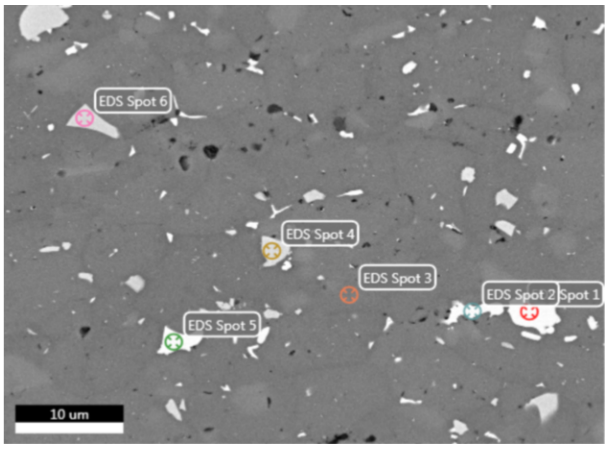

Figure 4.6.3: SEM micrograph of the engine block extrusion profile 2000x magnification. Points indicate where analysis with EDS where taken.

The engine block material contains large coarse grains in the Al matrix. The composition of these particles is mainly Al-Cu, Al-(Fe, Mn)-Cu-Si and Si. EDS point measurements

indicate that the Cu and Si are majorly present in particle structure and not in solid solution. Pb containing particles were also observed.

Table 4.10: EDS spectrum of the engine block extrusion profile.

Element	Content [wt.%]	Error [wt.%]
EDS spot 1		
Ni	2.84	6.25
Cu	51.19	2.47
Al	45.97	5.46
EDS spot 2		
Ni	2.94	5.95
Cu	49.71	2.47
Al	47.35	5.39
EDS spot 3		
Cu	2.85	5.26
Al	97.15	2.39
EDS spot 4		
Fe	13.28	3.41
Cu	8.91	4.27
Al	61.74	3.82
Si	10.35	6.29
Cu	51.19	2.47
Mn	5.71	17.69
EDS spot 5		
Ni	2.63	6.32
Cu	48.05	2.57
Al	49.32	5.30
EDS spot 6		
Fe	13.03	3.63
Cu	7.33	4.48
Al	62.35	3.76
Si	10.14	6.23
Mn	7.14	12.71

4.7 Hydrogen-evolution of aluminium alloys in cement paste

All the aluminium samples were tested in the same cement prescription as presented in section 3.7. The data collected were the amount of generated gas from the corrosion reaction of aluminium in the alkaline environment and the pH. The pH was measured to approximately 11.5 for all of the cement paste samples. The results of the Al-5Mg tests revealed no hydrogen formation and is thereby not graphically presented. All the tested aluminium samples were treated in the inhibitor solution for 7 days except the Al-7Si-0.3Mg alloy which was treated in 72 hours. In Figures, 4.7.1(a-e) is the experimental result retrieved from the hydrogen measurement trials of aluminium samples in cement paste. They are graphically presented to where the observations of interests are the rate of evolution and the total amount of developed gas before the cement hardened. The gas entered the measuring cylinder in the form of bubbles, due to the pressure had to be built up to be able to leave the tube from the desiccator. This is the reason to why the gas evolution is presented in a step-wise manner as a function of the time in the Figures 4.7.1(a-e). Due to the deformed surface of the screw extruded engine block profile, a test of this material in cement would not have been representative. The deformed surface provides poor corrosion resistance. This test is intended to examine the corrosion resistance of the alloy type and the effect of the inhibitor on it, rather than the profiles performance.

The main difference that distinguishes these results from previous trials, where the samples were treated in the inhibitor solution for 18 hours is the total amount of gas developed. Both the Al-Si alloys, the engine block and the Al-1Mg produced more than 50 mL of gas before the cement had fully cured. When the aluminium samples were treated in the solution for a longer period of time, there was a clear trend that a smaller total amount of gas was developed. Of the samples presented, the Al-7Si-0.3Mg treated in 72 hours in inhibitor solution produced approximately 50 mL gas in total where the other samples, treated for 7 days only produced approximately 40 mL of gas after the cement had cured. The high Si-containing alloys Al-12.7Si and the engine block seemed to quickly,i.e. within the first 5 minutes, to produce approximately 20 - 30 mL of gas before the reaction rate significantly stagnated. For those alloys with lower Si content, Al-7Si-0.3Mg and Al-1Mg, no gas was developed until after 20-30 minutes. The gas development afterwards was less frequent was a remarkable observation was that the Al-1Mg alloy ceased to develop gas after a total of 40 minutes, similar to Al-12.7Si and the engine block while Al-7Si-0.3Mg developed gas for additional 40 minutes.

A cement paste sample without an aluminium sample was examined in the desiccator as a benchmark sample. The trial showed a fast initial gas development with a high rate which ceased after approximately 40 minutes, where it had produced a total of 23 mL of gas.

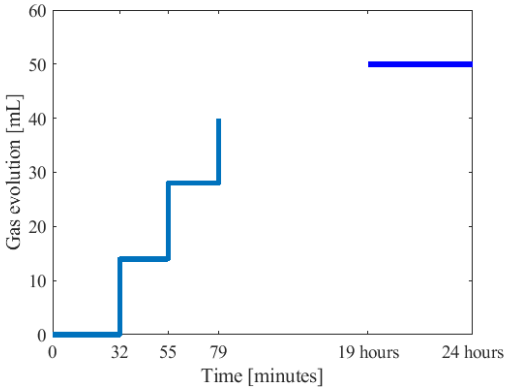

(a) Al-7Si-0.3Mg treated in inhibitor solution for 72 hours.

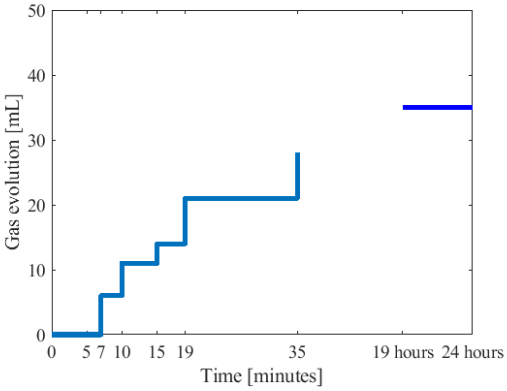

(b) Al-12.7Si treated in inhibitor solution for 7 days

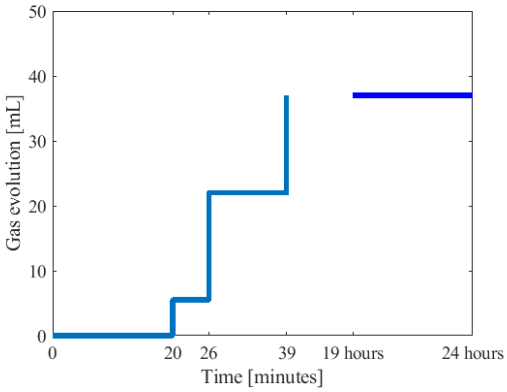

(c) Al-1Mg treated in inhibitor solution for 7 days

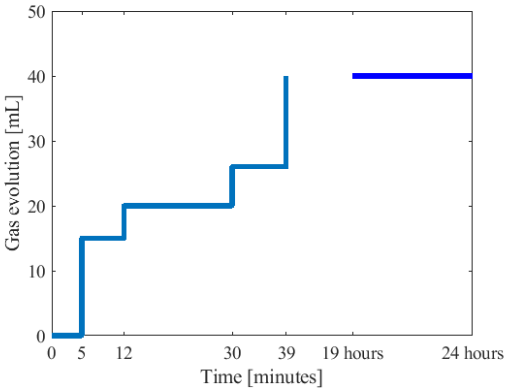

(d) Engine block treated in inhibitor solution for 7 days

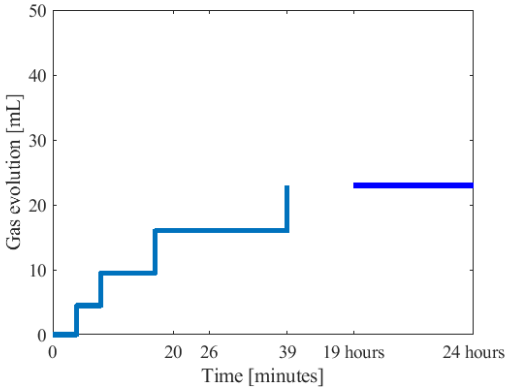

(e) Cement paste without an aluminium sample.

Figure 4.7.1: Gas evolution measurements

4.8 The 4-point bending test of the concrete beams results

The six reinforced concrete beams were tested after approximately 50 days with hardening. The desired failure mechanism for the concrete beams was shear failure.

Table 4.11: Failure types of the reinforced concrete beams in the 4-point bend tests.

Reinforcement material and geometry in concrete beams	Failure type
Ribbed steel bars	Shear
Aluminium T-profile #1	Anchorage
Aluminium T-profile #2	Anchorage
Aluminium circular ø10 mm rod #1	Anchorage
Aluminium circular ø10 mm rod #2	Anchorage
Aluminium circular ø10 mm rod #3	Anchorage

The steel reinforced beam acquired shear failure, while the aluminium reinforced beams acquired anchorage failure due to poor adhesion between the concrete and the reinforcement surface. As for the aluminium reinforced beams, this resulted in large concentrated cracks at the bottom of the beam. After the 4-point bend tests, the beams were split in half to inspect the reinforcement beams surfaces after corrosion. The inspection revealed that there were no visible observations of corrosion products on the Al-5Mg reinforcement rods.

Figure 4.8.1: Picture from the 4-point bend testing of one of the ø10mm aluminium reinforced concrete beams.

5 Discussion

5.1 The effects of chemical composition and thermomechanical processing on the mechanical properties

5.1.1 Hardness

The hardness measurements indicate that the hardness is more affected by the particles and solid solution strengthening than grain structure. The two Al-Mg alloys which were extruded confirms this statement. The EDS measurements revealed that both alloys contain only small volumes fractions of Al-Fe particles which will not affect the hardness greatly, but the real difference lies in the Mg content. Al-5Mg has a higher Mg content than Al-1Mg and thereby a higher hardness. The degree that the grain size affects the hardness is well presented in the measurements of Al-1Mg after extrusion. It revealed that the larger grains in the centre of the profile lead to a lower hardness than compared to the edge with small recrystallised grains. Since the alloy in as-cast state was not heat treated, and the microstructure contained a small amount of second phase constitutes, lead to the conclusion that the thermomechanical treatment had little to no effect on the hardness. This applies for both the Al-Mg alloys.

The hardness results of the Al-Si alloys show that the hardness is greatly affected by the silicon particles morphology and volume fraction, solid solution and the thermomechanical processing. The typical billet structure of Al-Si alloys, which is shown in Figure D.0.5(a) shows the the microstructure contains of soft aluminium equiaxed dendrites and relatively fine eutectic Si phase. The chemical composition does not reveal other element which in solid solution which noticeably increases the hardness, so the hardness here mainly stems from the Si. When the indentation from the vickers measurement is taken, a large volume fraction of this eutectic Si phase will contribute to high hardness values. With finer lamellae eutectic comes higher values of hardness. When the Al-Si alloys are processed through screw extrusion these second phase particles will undergo big changes in both morphology and distribution in the Al matrix.

After screw extrusion the microstructure obtains a deformation structure where the Si particles become more spheroidal, coarsened and dispersed while the dendritic Al structure disappears. A possible explanation to this microstructure may be the occurrence of partially melting of the material in the screw chamber. In Table 3.9 are the screw extrusion parameters presented, where one parameter is the die temperature. Although this is the area where the highest temperature is measured, it is not the area where the highest temperature occurs. The highest temperature will occur at the end of the screw due to heat generation from the deformation. Especially with the Al-Si alloys which where the die temperature was 530°C, then it is highly likely that the temperature may have risen to near the eutectic melting point of 577°C and caused partially melting. The spiral-like pattern in the microstructure seems to have some minor effect on the hardness where the hardness near the surface has a tendency to lower than the in the centre. This developed deformation structure seems to have a generally lower hardness than the as-cast structure.

As for the engine block which in addition to high Si content also contained Cu, had a remarkably higher hardness than the Al-Si alloys. The EDS micrographs revealed high fraction volumes of constituents like Al-Fe-Se, Al-Fe-Mn, Al-Cu-Mg have varying values of hardness (400 HV - 1000 HV). These in addition to Cu in solid solution seems to have a great impact on the hardness. The hardness dropped significantly after screw extrusion, which may be explained to follow the same mechanism with particle morphology and distribution as with the Al-Si alloys. A significantly high amount of pores were produced in the material due to the smoke development during the thermomechanical processing, which may explain the lower hardness at the edge than in the centre in addition of the spiral-like microstructure from the screw. Due to the Cu and Mg amount in the car engine, this alloy may be heat treated and may gain higher hardness thereby, where Cu will precipitate into $AlCu_2$ and Mg into Mg_2Si

5.1.2 Tensile strength

The strength contribution to the concrete from the reinforcement material is very important and has led to high demands on both stiffness and strength of reinforcement. Compared with steel, Al has three times as low E-module than steel. However, this can be corrected by extruding the aluminium into geometries which compensate for the low Young's modulus. The technology of extruding aluminium is highly advanced design of aluminium profiles is mostly limited by imagination. The strength of the aluminium can be improved by alloying with elements which makes the material responsive to heat treatments. If these in addition to being heat treated are strain hardened too, the strength can easily match the strength to ordinary carbon steel. Typical values of σ_{UTS} and density to ordinary carbon steel (1020) are respectively 410 MPa and 7.86 $\frac{g}{cm^3}$ which gives a strength-to-weight ratio of 52.16, [4]. 6061 is a typical precipitation-hardenable aluminium alloy which contains approximately 1.0 wt.% Mg and 0.6 wt.% Si as main alloying elements. This is a general purpose alloy which is one of the most popular alloys to extrude. When heat treated to peak strength, this alloy can achieve a σ_{UTS} of 310 MPa, and with the low density of 2.71 $\frac{g}{cm^3}$ which aluminium is known for, gives a relative strength-to-weight ratio of 114.4. This is twice the high as in comparison to the carbon steel. The strength can be further enhanced through strain hardening to values of 410 MPa, but this will severely compromise the ductility of the material. Alloys in the 7xxx-series can with proper heat treatment reach a σ_{UTS} of 600 MPa, which makes this alloy class a desirable material to be used in structural components of aircraft where the strength-to-weight ratio is important. Due to the principal alloying elements of Zn, Mg and Cu is this alloy series highly susceptible to corrosion and usually applied with coating or other corrosion protection system when used. To summarise, by allowing the use of other alloys in concrete which heat treated and by manufacturing these with desirable cross-section geometries, the lower mechanical properties of aluminium relative to steel can be compensated for.

The tensile strength trials of the Al-5Mg alloy were done in order to supply the civil engineering students with the necessary information about the mechanical properties of the reinforcement material. The results were primarily used for dimension the reinforcement

material, anchoring and the concrete beams and to simulate the behaviour of the reinforcement in a 4-point bend test. As presented in Table 4.1 the ultimate tensile strength, σ_{UTS} was measured to be 274.0±3.6 MPa and the yield strength, σ_y to be 144.5±1.2 MPa. The ductility measurements from this alloy and the others presented in this thesis were not included since the standard variation was so high and could not, therefore, be determined with certainty. In order to justify the statement that solid solution strengthening increase both the strength and hardness, tensile strength tests were also done on the Al-1Mg alloy. Here σ_{UTS} was measured to be 107.8±0.26 MPa and the yield strength, σ_y to be 65.43±3.7 MPa. The additional 4 wt.% Mg in the Al-5Mg seemed to has almost doubled the strength of this alloy compared to the Al-1Mg. If the Al-5Mg alloy was exposed to a strain hardening treatment, it could, in theory, achieve a σ_{UTS} 440 MPa, but as already mentioned at the expense on the ductility, [4]. As a basis for being used as a reinforcement material, higher ductility will be more important than great strength.

Since the Al-Si alloys should not be used as a reinforcement material, the results of the tensile tests have not been much emphasised. What can be interpreted from the results is that in the as-cast state the materials show to be quite brittle, and after they have been screw extruded, they achieve a lower strength but in return a slightly higher ductility. Si has a low solubility in Al, which means that the contribution from solid solution strengthening is quite low since there are no other major alloying phases which can give significantly strength contribution to the alloy. Al-7Si-0.3Mg has approximately 0.2 wt.% Mg more than Al-12.7Si which may explain its slightly higher strength. The Al-12.7Si in as-cast state gains its high strength from the eutectic Si structure, but when this structure is altered during screw extrusion leads to a less brittle behaviour and a lower strength.

Due to the considerable smoke development during the screw extrusion of the engine block, this lead to a deformed surface and a quite porous structure, which can be better observed in Figure 5.5.1. This combined would have yielded results that are not representative of the actual strength of the material. The mechanical properties were not the main priority either since the goal was just to investigate the possibility of recycling it through screw extrusion. It would probably have had similar results such as the Al-Si alloys with being brittle and having high strength in the as-cast state and being more ductile with lower strength after extrusion. Due to the other alloying elements, especially Cu, the material has consequently a higher strength.

5.2 Grain structure observations of the thermomechanical processed alloys through LOM and SEM examinations

The microstructural characteristics of an alloy greatly influences the physical properties, [11]. Properties like ductility, hardness, strength, toughness and wear to an alloy largely determines the applications to it. The formability of aluminium prior thermomechanical processes is greatly dependent on the grain size where e.g. large grains can lead to poor formability. Proper temperature control of the material right out of the die is also important. The results of poor temperature control i.e. insufficient quenching can lead to uncontrollable recrystallisation, grain growth and development of second-phase particles which might yield undesired microstructures and thereby inferior mechanical properties. As explained through the Hall-Patch relationship between yield strength and average grain size in Equation 2.3, an alloy with smaller average grain size will have a higher additional strength contribution than compared to the same alloy with higher average grain size.

Prior to the extrusion of the two Al-Mg alloys were they both prepared with a homogenisation treatment. This was mainly done to spheroidse the insoluble Fe containing particles, which were found in the EDS measurements of the billet micrographs of both alloys and to solutionise the Mg-containing particles found in Al-5Mg in Figure 4.6.2. These EDS measurements of the alloys before extrusion can be observed in appendix F. EDS measurements and light optical micrographs of the Al-Mg alloys after homogenisation were not examined since this is already a well know procedure and was not important for the implementation of aluminium reinforcement in concrete. Which can be observed in Figure D.0.2, the Al-5Mg billet had a typical cast structure before extrusion. The cast structure of the Al-1Mg alloy in Figure D.0.1 is not representative since the micrograph sample was taken from atop of the billet edge and not from the centre of the material. How the microstructure and the mechanical properties were in the as-cast state was not prioritised, since it was the extruded profiles which would be embedded as reinforcement in concrete. Therefore is the main focus from the LOM and SEM examinations based on the microstructural properties of the alloys after thermomechanical processing.

The cross-sections of the Al-Mg profiles presented in Figure 4.5.1(a) for Al-1Mg and 4.5.2(a) for Al-5Mg reveals that they were partly and fully recrystallised, respectively. both the condition of high temperature and high strains for recrystallisation were met. The extrusion ratios of the ø10 mm profiles and the T-profiles where respectively R=90 and R=45, which indicates that there were sufficient with strain present. The temperature of the profiles after extrusion was additionally higher than 430°C since the plastic deformation probably led to a rise in temperature. Even though the extruded profiles were quenched right after exiting the die, there was a sufficient distance between the die and the water pit where the Al-Mg alloys were exposed to a high temperature after deformation, which evidently allowed recrystallisation. The distance from the die to the water pit was approximately 2 meters, which can be observed in Figure 3.5.2(b). Calculations through mass conservation from the extrusion parameters presented in Table 3.5.2 states that the velocity of the ø10 mm profiles out of the die was 89.7 $\frac{mm}{s}$, which essentially means that the profiles were kept at high temperature for about 20 seconds before they

were quenched. The T-profiles with a bigger final cross-section were consequentially exposed to the high temperatures for a longer period. The Al-5Mg micrograph revealed a homogeneous and a fully recrystallised structure throughout the whole profile with new equiaxed grain, while in the Al-1Mg micrograph is it observed that the edges are fully recrystallised while the centre of the profile mainly contains a deformed structure with elongated grains and some few partially recrystallised grains. The deformation structure of the Al-1Mg alloy is essentially elongate grains from the billet structure, and it can be explained that there was only enough deformation to initiate recrystallisation at the edge of this ductile material and not in the centre.

The screw extrusion process had the same effect on all the three high Si-containing alloys with regards on the particle morphology and distribution, and the cross-section patterns. As can be seen in Figures D.0.5(a-b) and D.0.4(a-d) of Al-12.7Si and Al-7Si-0.3Mg and engine block in Figure 5.2.1, all these three alloys had a typical as-cast structure for their alloy class. As mentioned earlier, the particle structure after screw extruding becomes deformed with a coarser and more spheroidised morphology and is more widely distributed in the Al matrix. The dendritic Al structure in the two Al-Si alloys also disappears. The spiral-like pattern of these screw extruded materials, in the transverse cross-sections which may be observed in the Figures 4.5.3(c), 4.5.5(c) and 5.5.1 is mainly due to the material flow in the chamber generated from the screw motion. The patterns observed in the longitudinal cross-sections of the screw extruded engine block in Figure 4.5.7(a-c) reveals a flow-like pattern which arises from the pressure build-up from the screw. An observation made by all the screw extruded materials was that the transverse cross-sectional micrographs indicated that the material near the surface was fully recrystallised. The material in the centre of the profile has a deformed microstructure where elongated grain was layered in line with the direction of the material flow. A possible explanation that recrystallization occurs near the profile surface and to a minimal extent in the centre of the profile must come from the sticking friction of the material close to the chamber wall and induce enough deformation to induce recrystallisation. The screw extrusion process is still a fairly new process where some of the mechanisms still are not fully understood. This thesis has not focused on the mechanisms behind this process, but by obtaining more knowledge and a better understanding of this process through future studies will enable for better control, greater efficiency and more possibilities of this process.

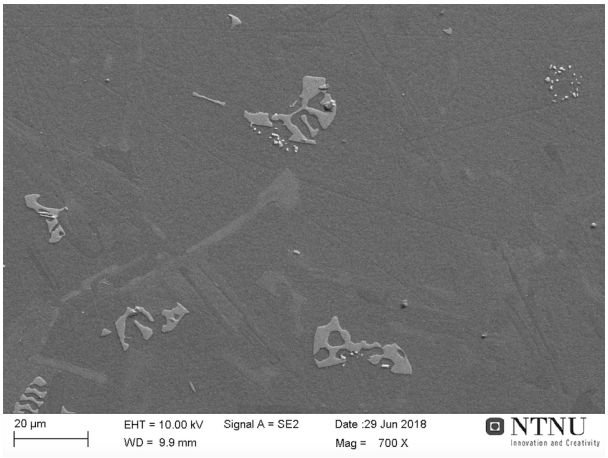

Figure 5.2.1: SEM micrograph of the engine block before screw extrusion. The SEM parameters are presented in the micrograph. In this micrograph particles with "Chinese script" morphology and light-grey Si phases with no distinctive particle contour may be observed.

In addition to formability during thermomechanical processing, the microstructure is also vital for the corrosion properties of the material. For the Al-Mg alloys, the presence of $\beta - Al_2Mg_3$ could potentially make these alloys susceptible to intergranular corrosion. This particle was observed in the EDS measurements of the Al-5Mg alloy before extrusion, but due to the homogenisation treatment, none could be found in the EDS examination of the as-extruded micrographs. Uniform corrosion is the main corrosion mechanism for aluminium alloys in concrete, so IGC not the main concerning corrosion mechanism. However the formation of $\beta - Al_2Mg_3$ depletes the Al-matrix of soluble Mg which consequentially reduces the corrosion resistance. It can therefore be concluded that the homogenisation heat treatment also helped to increase the corrosion resistance of the Al-Mg alloys in additions to improve the extrudability.

According to the analysis of the engine blocks chemical composition, it contained approximately 1.73 wt.% Cu. Although the addition of this alloying element greatly improves the mechanical properties of the material will the corrosion properties decrease according the addition. Engine blocks are usually manufactured as a secondary casting material, meaning will contain other impurities other than its principle alloying elements. In addition to the secondary phases composed of Al-Cu, Al-(Fe, Mn)-Cu-Si and Si, some particles containing Pb were found. The presence of heavy metals like Pb and other impurities has a major negative impact on the corrosion properties of the material.

By better understanding the mechanisms of the inhibitor and its effect on the protective oxide layer in the alkaline environment this may allow the use of other alloys. Particles and microstructures that reduce the corrosion resistance and makes the material susceptible to various corrosion types may, regardless of how the inhibitor works, lead to corrosion. These microstructural features however can be managed through proper alloying and thermomechanical processing.

5.3 The interpretation of the CTE data and its importance for reinforcement materials in concrete

One of the challenges by implementing aluminium as reinforcement in concrete is the thermal expansion coefficient, where pure aluminium has a twice as high CTE than concrete. Carbon steel, on the other hand, has a similar CTE as concrete, which is one of many arguments which is used when the good compatibility of steel as reinforcement material in concrete is discussed. To demonstrate the importance of this effect, this can be shown through an example by calculating how much the reinforcement rods and the concrete beams, used in the 4 point bending test were expanded during the cement hardening. Let's say the steel and aluminium rods and the entire concrete beams were all 1.0 m for simplicity. In this example, it is also assumed that the concrete curing reaction generated so much heat that the temperature rose to 50°C. The CTE values of the materials are concrete: $\alpha_{\text{concrete}} = 10\frac{\mu m}{m°\text{C}}$, carbon steel: $\alpha_{\text{steel}} = 12\frac{\mu m}{m°\text{C}}$ and Al-5Mg: $\alpha_{\text{Al-5Mg}} = 24\frac{\mu m}{m°\text{C}}$.

$$\begin{aligned}
&\text{Elongation of the concrete beams} && = 10\frac{\mu m}{m°\text{C}} * 1.0m * 50°\text{C} = 500\mu m = 0.5mm \\
&\text{Elongation of the steel rebars} && = 12\frac{\mu m}{m°\text{C}} * 1.0m * 50°\text{C} = 600\mu m = 0.6mm \\
&\text{Elongation of the aluminium rebars} && = 24\frac{\mu m}{m°\text{C}} * 1.0m * 50°\text{C} = 1200\mu m = 1.2mm
\end{aligned}$$

In this hypothetical experiment, one can see that the concrete beam with steel reinforcement both had a corresponding increase in length, while the concrete beam with aluminium reinforcement expanded the aluminium 0.7 mm more than the concrete. Such values create doubts about using aluminium as reinforcement in larger dimension designs, but would this really have so much to say in constructions under normal temperatures?

According to some of the members of the DARE2C project, their professional assessment was that the high CTE of aluminium in concrete would not be a problem under normal operating temperature and during the curing of concrete. An important point that supports this, focusing on curing was that none of the concrete beams with aluminium rebars used in the 4 point bend test that lost its adhesion to the concrete before the test itself. As stated in the theory, according to the standard specifications formulated by the Norwegian Public Roads Administration's "Prosesskode 2" dictates that the maximum temperature shall at no time exceed 65°C and that the temperature difference over the cross-section shall not exceed 20°C. This essentially means that the temperature will not be a limiting factor for the use of aluminium reinforcement. What can be a limiting factor, however, is the dimensions of the concrete structure. For example, if the aluminium rods and the concrete beam are both 10 meters long, this will lead to an expansion where the difference in length of these two materials will be 7 mm. The effects of expansion, however, can be taken into account by the construction engineers, and may thus not be a problem anymore.

The measurement of CTE involves two parameters: the change in length and the change in temperature. At first, it seemed appropriate to measure CTE with push-rod thermodilatometry according to ASTM E228, [50]. Only the two Al-Si alloys were examined

in this experiment with the goal to investigate the effects of the alloy content on the CTE. Both the results and the theory agreed on that higher amounts of Si reduced the CTE significantly compared to pure aluminium. Results also indicated that the CTE of the materials in the as-cast state were higher than as-extruded and that the CTE measurements of the cooling curve were a little higher than the heating curve. Highly accurate measurements would have been achieved if the curves were almost completely linear with smooth slopes that would have matched and given theoretical values. In almost all the measurements with the dilatometer and especially with the measurements with the extensometer was it all from one to several nonlinear areas on the curves, which can be observed in appendix E. The CTE is measured by measuring the slope of the expansion-temperature curve in a certain temperature interval. A low slope of the curve will give a low CTE, and correspondingly a high slope will yield a high CTE. If the slope is measured in a non-linear area, this will lead to false results. In appendix E, one can observe with the measurements of Al-12.7Si from 30-100°C in Figure E.0.1 and Al-7Si-0.3Mg from 30-70°C in Figure E.0.4 that these dilatometry trials gave inaccurate values with values down to 12 $\frac{\mu m}{m°C}$ due to the non-linearity of the curve.

The temperature program where the temperature went up to 250 was primarily chosen since a higher temperature gives a larger data range, which in turn gives a better statistic foundation. It was also chosen to be under this temperature and with Ar atmosphere, to ensure no reaction would occur with the oxide layer or microstructure. The other two temperature programs were chosen to see what the measurements at a lower temperature would give and to simulate the temperatures that the aluminium could possibly experience when the concrete hardened. What can be concluded with the results is that the CTE values obtained from Al-12.7Si and as extruded in the 30-250°C temperature range, listed in Table 4.2 are the most accurate results and those closest to the literature values. Even though the CTE value in the temperature range here of $16.2\frac{\mu m}{m°C}$ is lower than what the literature says, the trend for and the value else are approximately correct. Through manually controlling the oven temperature and reading of the expansion from an extensometer, it was possible to measure out the CTE from the expansion - temperature curve. By doing this it was at first believed that some of the mechanical errors which occurred with the thermodilatometry measurements would be avoided. The temperature could be elevated and hold there for a while until it was assured that the whole sample achieved that specific temperature. The oven regretfully had a slow cooling rate and therefore were no further samples measured than the samples presented. The data retrieved from measuring manually with an extensometer should have worked in theory, but it seems that this method is not sensitive enough and gave results, seen in Table 4.5 with too high values and trends that are not even close to the literature values.

The main reason of why the thermodilatometry gave results at lower temperature intervals which were inaccurate may stem from that the Netzsch 402C push-rod dilatometer which was is more applicable for ceramic materials than metals with low melting-point. The ASTM E228 even states that the method is general applicable to materials having absolute linear expansion coefficients exceeding $0.5\frac{\mu m}{m°C}$ for a 1000°C range, [50]. The ASTM E228 also list these following point for possible sources of error:

- Accuracy of the length and temperature measurements

- Deviation of the specimen mean temperature from that indicated by the sensor
- Deviation of linearity of the transducer
- Temperature gradient between the dilatometer tube and push-rod

The ASTM E228 also suggests that if the specimen length at the end of the trial differed from the initial measured length, a retest should be taken, [50]. This was not done in this thesis since it was believed that the low temperature would take into account and prevent any possible plastic deformation of the sample after a trial. The ASTM E228 states that the precision of this test is higher than of other push-rid dilatometry techniques and thermomechanical analysis as ASTM E831, but is significantly lower than of absolute methods like ASTM E289, [53, 54]. The ASTM E289 describes interferometric techniques for solids in the -150°C to 700°C temperature range by using either a Fizeau interferometer or a Michelson interferometer, [54]. Here is interference of monochromatic light reflected from the opposite surfaces which then creates fringes pattern. These changes as the specimen are heated up may be monitored, and yield a highly accurate CTE measurement with an accuracy approaching $\pm 0.04 \frac{\mu m}{m^{\circ}\mathrm{C}}$. The literature values, however, may vary from source to source since they may have been calculated from differently numerical formulas and may depend on whether the expansion relates to a temperature range or a single temperature, [55]. In the review article done by James J., D. *et. al.*, [55] it has been illustrated how much the difference of measured CTE may be with different definitions of CTE. If CTE is defined over a temperature range and it is measured by the curvature of the $\frac{\Delta l}{l_0}$ versus temperature plot, will this give a measured CTE which is lower than that defined at a single temperature. This difference will only become greater at higher temperatures, but the difference in CTE measured at specific temperatures are relatively low. This essentially means that in what way the CTE is defined may be important if CTE data, of a material, is to be used in potential engineering situations

In order to round off, there may be some recommendations for future measurements of CTE. If future measurements are to be made using thermodilatometry in accordance with ASTM standard E228, several parallels should be made to exclude systematic errors and CTE should be defined and calculated in several ways to provide an overview of its impact. Otherwise, is it highly recommended to measure CTE with high accuracy by interferometric techniques as described in ASTM standard E289. In order to take the thread with the high CTE of aluminium in combination with concrete, it is assumed that it will not have anything to say under normal temperature conditions. It is, however, recommended to investigate the effect of CTE in larger structures.

If it appears that in larger structures this may be a problem, this may be resolved by improving the inhibitor parameters which makes it possible to implement other aluminium alloys such as Al-Si with a low CTE. However, if the inhibitor parameters should enable the use of other alloys it should rather be focused on implementing aluminium alloys with higher strength and let the potential CTE challenges be resolved by changing the design on the construction.

5.4 The durability and performance of the aluminium alloys in concrete

What can be interpreted from the gas measurements of aluminium in cement is first and foremost that longer exposure in the inhibitor solution gives lower gas development. The lower alloyed Al-7Si-0.3Mg and Al-1Mg samples had a more delayed reaction and did not develop gas until a considerable amount of time after the higher alloyed Al-12.7Si and engine block. There was also a tendency in total amount of gas produced. Al-7Si-0.3Mg which was treated in 72 hours produced about 50 mL in total of gas during the cement hydration reaction, while the other alloys which were treated longer in the inhibitor produced approximately 40 mL of gas.

Without revealing too much about the inhibitor, it may appear that along with the reduced pH of the cement, a much more stable oxide layer on the aluminium surface is formed when the aluminium is exposed to the alkaline environment. It cannot be revealed whether the new oxide layer is formed in the inhibitor itself or during exposure to the alkaline environment, but it is reasonable to assume that the new oxide layer formed has such protective properties in terms of stability and/or thickness that it halts the corrosion reaction partly or completely. An explanation of why Al-5Mg does not corrode at all in the cement may be that together with the inhibitor, an oxide layer is formed which is more stable at high pH than Al_2O_3. According to Prof. Dr Justnes, H., this new oxide may have a spinel crystal structure with a possible chemical composition consisting of $MgAl_2O_4$. To more thoroughly determine the nature of this oxide layer, a new study should be conducted where this oxide layer should be examined in SEM, TEM, XRD and XPS both before and after concrete exposure, to characterise its chemical composition and structure.

A benchmark cement sample without an aluminium sample was also measured. A certain amount of approximately 23 ml of gas was collected in the measuring cylinder, which does not correspond with the theory. As far as the cement chemistry is concerned there should not be developed gas from the curing reaction of cement alone. The gas developed should only, in theory, happen from the hydrogen evolution from the corrosion reaction to aluminium exposed to an alkaline media. In a conversation with Prof. Dr Justnes H., he agreed with this statement. The only options that could make sense were that the air was mechanically captured in the mixture during mixing and released during curing, or maybe that over-pressure was formed when the lid of the desiccator was put on. The lid was slid onto the desiccator and therefore where this error source excluded. Water vapour was neither a plausible probability. However, the curing reaction from cement should not provide such measurements. In view of the measurements from the cement sample without aluminium, the assumption that only hydrogen gas is developed in the desiccator may not be entirely correct. In order to determine the type of gas developed in the cement sample and the concentration of hydrogen in the gas with aluminium in the cement, measurements of the gas through gas chromatography should be undertaken.

Measuring gas evolution in the desiccator setup is still a useful method for quantitatively estimating the degree of corrosion on the aluminium in contact with the concrete. It does not manage to accurately measure corrosion and the inhibitory effect, but until the gas and inhibitor mechanism is further determined is this method still relevant as an indicator of corrosion. A method that can determine the degree of corrosion of aluminium in concrete with great certainty is to simply split a sample in two after 8 months and visually inspect the aluminium surface. Prof. Dr Justnes H. had done similar tests earlier with inhibitor protected and not protected aluminium samples where the non protected sample developed significant amounts of corrosion products on the surface while the protected samples corrosion products could not be observed. As seen in Figure 5.4.1, the cement sample with the Al-7Si-0.3Mg alloy were same-wise split in half to observe the surface after 28 days of exposure. The surface is somewhat grey-ish but does not show any visible signs of corrosion. To get a better estimate on the corrosion, the sample should be embedded in the cement in 8 months before it should be inspected.

Figure 5.4.1: The figure shows a sample from one of the hydrogen evolution trials where the hardened cement sample is split in two after 14 days in order to observe the aluminium surface after corrosion.

As feared, was the mechanical adhesion between the smooth aluminium reinforcement bars and the concrete big enough which resulted in anchorage failure for all the concrete beams with reinforced aluminium. The T-profile shape was originally chosen due to the large surface area and was believed to be sufficient to provide better friction resistance to the concrete, but to no use. the ribbed steel reinforcement, on the other hand, did not slip

in the concrete since the geometry of the deformation pattern gave a better mechanical barrier against slipping. Ideally, the aluminium reinforcements should also have ridges on the surface similar to the ribbed steel reinforcements, to obtain the equally bonding to the concrete. This was not possible at this time for the aluminium profiles due to the limited time available for the participant in this project. On the other hand, two observations were made showing promising results for the project. First, it was observed that the reinforcement rods behaved mechanically identical to the steel reinforcement prior to the anchoring failure. Secondly, after the 4-point bend tests, the aluminium reinforcement in the beams was inspected and showed no signs of corrosion. Together, this forms the basis that from a purely chemical standpoint aluminium is compatible to be used in this type of concrete, but further trials must be made, where the aluminium bars have a deformation pattern to finally determine whether it can be used as reinforcement in concrete structures.

In a DARE2C meeting, the possibilities of this type of concrete were discussed. It was mentioned that it is a common procedure in the industry to weld on anchoring at the end of the reinforcement to avoid anchoring failures, which may be used as an additional measure in future trials with ribbed aluminium rods to further prevent this type of failure.

An important point raised during the meeting was the fire safety of this type of concrete. If aluminium would have been used as reinforcement in a concrete structure, this concrete construction might not have been safe in a fire like steel reinforced concrete, due to two reasons. First of all, Al-Mg alloys have a melting point of approximately over 600°C and will at lower temperatures than that lose some of its structural strength. A fire can easily reach temperatures way beyond this point the which basically means the structural support from the aluminium reinforcement in this scenario will be useless. In addition, will the CTE at lower temperatures cause the concrete to crack, which makes this scenario even worse. Hypothetically, it would only have been a matter of short time from when the fire would have occurred until the concrete becoming unstable during such heat development. In a more optimistic view, this should not be seen as a stopper for the entire project, but rather a motive to find other applications. A possible application where this new type of concrete has the potential to dominate, and even chance to replace ordinary steel reinforced concrete is used in marine environments. Marine environments with high levels of salt and moisture make this a field of application where great emphasis is placed on the concrete to protect steel reinforcement from corrosion. When the concrete is reinforced with aluminium, this is not an equally big problem, which allows designing the concrete with more strength and less deadweight. When this new material becomes commercially available this leaves it up to the imagination of construction engineers of new ways they can build bridges, quays and other marine constructions. The industry company Veidekke, was also quite interested in investigating the use of an aluminium reinforcement net inside concrete walls, where the structural strength requirement of the reinforcement is much lower.

As for the road ahead for the project the main priority should lie in investigating the mechanisms of the inhibitor and the oxide layer produced on the aluminium surface. This may enable the use of other aluminium alloys with precipitation systems and with much higher strength. Anodising the aluminium is a commonly used method in the industry

to increase the thickness of the oxide layer and thereby by itself making the aluminium more corrosion resistant against atmospheric corrosion. It is also used as a pretreatment to ensure good adhesion with applied protective coatings. This may in addition to the deformation pattern help the aluminium reinforcement to achieve even better adhesion to the concrete. The anodised layer by itself will not be able to withstand the alkaline environment in concrete since it itself will be dissolved, but it stops after the concrete has hardened and the pore water disappears and OH^- is consumed, [44]. This anodised layer contains pores which might together with the inhibitor, create this stable oxide layer much faster and maybe enabling the use of other alloys.

Calcined marl was the supplementary cementitious materials (SCM) used in these trials with both the hydrogen measurement and the concrete beam production. In addition to it being easily accessible, it has through recent studies shown promising properties which may be used in other fields in the concrete industry, [51]. SCMs are usually industrial by-products, where the ones widely used in Norway are silica fume, fly ash and blast-furnace slag, which obtain binding properties together with cement, [1]. The DARE2C project has as a secondary objective focused on the potential use of red mud as an SMC. "Red mud", or bauxite residue, is a highly alkaline waste product generated during alumina extraction from bauxite and is predominately composed of complex-alkaline minerals, [56]. The production of 1-ton alumina product will generate approximately 0.5 to 2 tons of bauxite residue. Today there are no economical alternatives instead of a landfill and therefore is the possibility to use bauxite residue as a replacement to cement in concrete highly sought after. The possibility of red mud as SCM has not examined in this study because of stability requirements i.e. pH. It is planned to execute experiments with red mud as SCM at a later stage in the DARE2C project, but improvements are needed to the corrosion protection system to enable aluminium as reinforcement. If the red mud shows a potential of being a good SCM, the high pH development from the use of it may still be used together with steel reinforcement where the high pH will give additional protection from corrosion to the steel. A concrete construction with the use of aluminium industrial waste as SCM and the use of recycled aluminium as reinforcement would have been a very environmentally friendly material and to some extent poetic.

5.5 Challenges and opportunities with recycling car engines through screw extrusion

The recycling of the engine block of the used car engine was primarily a feasibility study to investigate the possibility of processing this type of aluminium alloy through screw extrusion. The engine block is alloyed with a relatively high content of Si and Cu due to the mechanical and tribological requirements imposed on a motor block which makes this type of alloys quite hard. Screw extrusion of more ductile alloys such as pure Al and Al-Mg-Si was well established before the start of this project, but screw extrusion of Al-Si alloys and especially with Al-Si-Cu had never been tried until this point. It was feared that the material with the hard eutectic structure of Si along with the content of Cu would prove to be too tough to produce profiles with.

During the extrusion run, it turned out that the hard alloying elements made it difficult to get the extruded material. However, after fine-tuning the run parameters with regards to material feed, temperature control and screw velocity it proved possible to screw extrude these aluminium alloys. Despite being able to produce this alloys class through screw extrusion was the extrusion speed quite slow compared to screw extruding other alloys. Further work on processing Al-Si and Al-Si-Cu alloys through screw extrusion will firstly be in improving the run parameters to optimise the process. Some suggestions for improvements are to try other geometries and sizes of the granulate and experiment with the run temperature and screw velocity. Due to the hard nature of the alloy, perhaps a larger engine for the screw extruder and a larger screw could be an opportunity to maximise the efficiency of the process. The temperature control system could also be improved by implementing other cooling systems e.g. water or oil based systems.

Before the engine block was delivered to be granulated, the surface which was to be machined was wiped down with acetone to remove dirt and oil residue from the surface. During the machining, no coolant was used. If any coolant had been used it would have meant that the granules would have had to be purified in acetone and thermally cleansed to remove any traces of oil residues. Oil residue or traces of dirt on the granulates would have led to smoke development during the screw extrusion process due to the high temperatures. Based on this and by a visual inspection it was decided that cleaning the material was not necessary since no oil was used during machining. This however proved to be a mistake since a considerable amount of smoke was developed during the extrusion attempt. It is unclear where the impurities in the material originated, whether it was oil residues from when the engine still was in use or if it was introduced during a step in the material preparation process. In hindsight, the material should have been cleaned regardless of its current appearance. Considering its former area of application in the oil-rich environment was it an optimistic thought that it would be free from impurities. The granules should have been cleaned in accordance with the procedure developed by Cui J. *et. al.* [57]. In this procedure the granulates are first thoroughly cleaned in acetone and then dried for 24 hours at 100°C to prevent water vapour from forming during screw extrusion. Thereafter the material is thermally cleansed at 350°C at 30 minutes in order to evaporate any organic material and removing the last traces of impurities. The smoke development led to pore formation in the profile, which can be seen in the transverse

cross section of Figure 5.5.1.

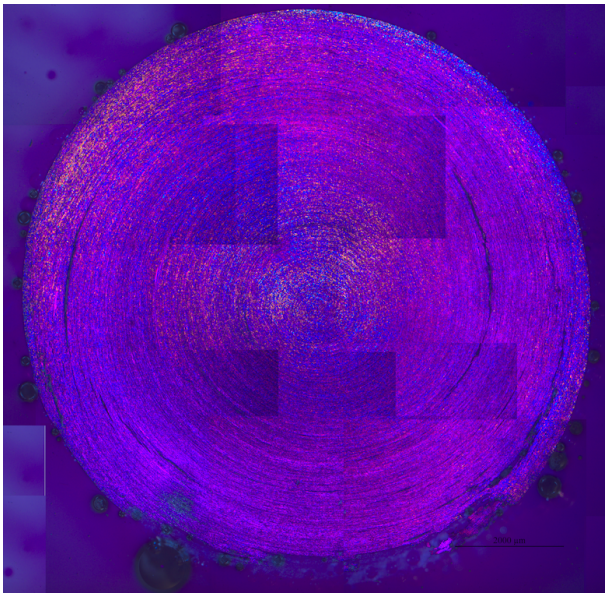

Figure 5.5.1: The transverse cross-section of the screw extruded car engine. The dark squares stem from the stitching process, where some images stitched together had less light during the microscopy.

The use of a single flight screw was chosen for the car engine and for the two Al-Si alloys. A single flight screw allows for better temperature control during the extrusion run due to the screw geometry, [12]. The screw geometry ensures that the majority of consolidation occurs at the end of the chamber, near the die rather than along the entire chamber. This helps to improve control of heat development from consolidation, with the current cooling system. The pressure generated from the screw tip was observed to lead to uneven flow, which may explain the surface geometry of the Al-Si alloys observed in Figure 4.4.1. With the use of a double flight, the screw may produce a more symmetrical profile at the expense of feeding rate. For the engine block profile, it holds the same uneven surface but has, in addition, a rather deformed surface. The deformed surface is most likely caused by the oil tests and the consequent smoke evolution, but it can also come from the combination of low feed rate with a low sticking factor. Low feed rate and sticking factor lead to more deformation of the material since the screw needs to rotate additional rounds in order to be able to extrude the profile. This, however, is not certain and needs to be further studied to find an answer to.

For this type of alloy to be used as it is in concrete as reinforcement is probably unlikely. Considering the alloys Cu content and the presence of impurities, e.g. Pb particles in the microstructure will this alloy consequentially have a generally lower corrosion resistance than compared to alloys such as Al-Mg and Al-Si. Although the inhibitor shows great potential to give other alloys as good corrosion protection as it gives Al-5Mg in concrete, it may be too much to expect that it will have an equivalent effect on this type of material. It was not expected that this material would yield good results in the hydrogen-evolution test, but it did not perform any worse than the other alloys exposed to the inhibitor for 7

days. After the cement hydration reaction ended, it produced the same total amount of gas as Al-1Mg and had the same evolution rate as the Al-12.7Si. With the finding that a cement sample without an aluminium samples produced gas, it is difficult to conclude the applicability of this type of alloy in concrete with inhibitor. Therefore, a test should be carried out where this alloy is exposed to the environment in the cement for 8 months to conclude its applicability. The hardened cement with the aluminium sample is put in a plastic bag with water so that it does not dry out and after 8 months the cement is split into two and aluminium samples are inspected for corrosion products. Preliminary trials with the same experimental set-up have already been carried out by Prof. Dr Justnes, H. where he has investigated the effectiveness of the inhibitor. Aluminium samples without any inhibitor in concrete with 100% ordinary Portland cement corroded so violently that there were only corrosion products left in the cement after 8 months. Although the engine block material does not corrode as much as an unprotected sample in OPC concrete, there are limitations on how much aluminium can corrode. Limitations lie in the adhesion between the concrete and the aluminium surface where too much corrosion can lead to loss of adhesion, and in the case of larger quantities of corrosion products, it can lead to spalling of the concrete. Organic and metallic coating systems to the aluminium alloy is an option to protect the metal from corroding in the alkaline environment, but due to issues regarding adhesion between the coating surface and concrete, this has shown to be an incompatible solution according to Prof. Dr Justnes, H..

An opportunity to enable the use of engine block material and other recycled secondary alloys in concrete with today's limitations of the inhibitor may be through co-extrusion. Co-extrusion is a process where two or more materials are simultaneously extruded through the same die and becomes metallurgical bonded together during high temperatures and pressure into one single material, [58]. The co-extrusion of different aluminium alloys has already been investigated where e.g. Kazanowski P. *et. al.*, [59] successfully managed to co-extrude an Al-Cu alloy (AA2014) with an Al-Mg-Si alloy (AA6063). This essentially means that it may be possible to co-extruded recycled engine block material together with Al-5Mg. By co-extruding reinforcement rods with recycled engine block material as a core and Al-5Mg as a sleeve around the core may be an opportunity to produce an environmentally-friendly reinforcement material with high strength and excellent corrosion resistance. In a conversation with Prof. Roven H., J., which is one of the inventors of the screw extrusion process together with Prof. II Reiso O., [6] it came to the conclusion that to co-extrude with the screw extrusion process certainly was an opportunity.

6 Conclusion

- Through the trials with the aluminium reinforced concrete beams in the 4 point bend tests and the hydrogen-evolution measurements from aluminium samples in cement paste it may on this basis be concluded that the corrosion-protected Al-5Mg alloy is chemically compatible with concrete where 55% of the cement is replaced with calcined marl as a SCM. To determine whether Al-5Mg can be used as reinforcement material in concrete constructions, further studies have to be performed where the Al-5Mg reinforcement rods have to be manufactured with a deformation pattern to obtain better adhesion to the concrete. The trials carried out up to now seems promising for implementing aluminium as reinforcement in concrete since the aluminium reinforcement behaved mechanically identical to the steel reinforcement before the anchorage failed.
- In addition to prior trials conducted together with Prof. Dr Justnes H., with hydrogen development of aluminium samples in cement paste, an additional independent study was conducted with the objective of investigating the effect of longer exposure time of the aluminium samples in the inhibitor solution. The study revealed that aluminium samples treated in inhibitor solution for 7 days produced a less total volume of gas and at a lower rate than the identical samples treated for 18 hours in the same solution with the same set-up. No particular trends could be identified with respect to the total amount of gas developed and the rate of the development for the 7 days treated samples. A cement paste without an aluminium sample was examined to be used as a benchmark. It was observed that the sample developed a relatively significant amount of gas that did not conform to the theory of cement chemistry. In a discussion with Prof. Dr Justnes H. were several explanations hypothesised, but no final conclusion could be given to this phenomenon. It was initially assumed that all gas developed exclusively was hydrogen from the electrochemical reaction of aluminium in the alkaline environment, but with these new results it may turn out that the assumption was only partially correct. With this in mind, until further investigations have been made, this experimental procedure can be viewed as a relative indicator of the inhibitor's effectiveness on the corrosion resistance to aluminium alloys. According to Prof. Dr Justnes H., it is hypothesised that Al-5Mg, after being treated with inhibitor forms a new oxide layer which may have a spinel crystal structure and a chemical composition of $MgAl_2O_{4(s)}$ which is more stable than the ordinary oxide layer found on the untreated alloy surface in alkaline environments. Further studies to determine the gas composition and the structure and composition of the developed oxide layer on the aluminium surface are advised.
- In the feasibility study with the goal of recycling a used car engine through screw extrusion showed promising results. It was successful in terms of being able to machine an engine block to granulated material and then produce ø10 mm rods of it. However, the surface of this produced profile was quite deformed due to the insufficient cleansing of oil residue from the granulated material and suboptimal run parameters during the screw extrusion operation. This type of material has

previously not been tested in the screw extrusion process, and it was known in advance that this type of alloy due to its mechanical properties would be difficult to process. Further studies to optimise run parameters and upgrades of the extrusion tools are recommended in order to improve the production of this type of alloy through screw extrusion and the quality of the product. Due to the Cu content and the presence of detrimental intermetallic phases such as Pb in the material, the theory indicates that the corrosion resistance of this alloy is relatively low. Nevertheless, the alloy was tested in cement paste with inhibitor protection in the hydrogen development set-up. Compared to the other alloys that were treated for 7 days in the inhibitor solution, the engine block did not develop a significantly greater total volume of gas nor at a higher rate. In order to determine the degree of corrosion of the material in the concrete, a test should be conducted where the material is inspected after being embedded in concrete for 8 months. Co-extrusion may be a possibility to Co-extrusion may be a possibility of implementing recycled secondary aluminium alloys as an environmentally-friendly reinforcement material in concrete. Through co-extruding, the recycled engine block as a core and Al-5Mg as a sleeve into a rod may combine the mechanical properties of the engine block with the excellent corrosion properties of Al-5Mg.

- Different CTE values between reinforcement materials and concrete exposed to large temperature differences can cause the reinforcement material to expand at a higher rate than the concrete which can cause a loss of adhesion between the two materials and cracking and spalling of the concrete. Aluminium has almost twice as high CTE than concrete, but it can be alloyed with elements such as Si in order to lower the CTE. Nevertheless, different CTE values will not be such a big problem as long as the concrete is not exposed to abnormally high temperatures and that larger structures are designed with respect to it, and therefore it should focus on using alloys that are responsive to heat treatment rather than low CTE alloys. Fire safety is an issue with implementing aluminium as reinforcement in concrete constructions, but by rather using this material in marine applications may be a solution to that obstacle. The measurements of CTE obtained using thermodilatometry gave relatively equal values to the literature, but the measurements were influenced by systematic errors which gave uncertainty in the results. The uncertainty may stem from the fact that the dilatometer is mainly calibration for measuring CTE of ceramic materials at high temperatures. It was also discovered that CTE can be estimated through several methods that can give different CTE values depending on the method.

- The hardness of the material is predominately determined by their chemical composition. Higher amounts of elements in solid solution will yield a higher hardness, which was observed in the case for the two Al-Mg alloys. The eutectic Si structure in the Al-Si alloys gave a high hardness to the alloys. The additional amount of Cu seemed to considerably increase the hardness of the engine block when compared to Al-12.7Si with approximately the same composition of Si. For the Al-Mg alloys, the extrusion process seemed to have influenced the hardness minimal, whereas the screw extrusion process decreased the hardness by 35-70 HV for the Al-Si alloys and

the engine block. This may be explained from the particle structure in the as-cast state gets heavily deformed during the thermomechanical processing and leads to smaller and more well-distributed particles in the microstructure.

- The lower stiffness and strength of aluminium compared to carbon steel can be dealt with by allowing the use other alloys to be used in the concrete, with a precipitation-hardenable alloy and by manufacturing these with desirable cross-section geometries. With these measures, aluminium can achieve approximately the same mechanical properties and a twice as high strength to weight ratio as compared to carbon steel. The results showed that more alloying elements in solid solution provide higher strength with the Al-Mg alloys. Since little Si is in solid solution, this means that after the Al-Si alloys were screw extruded, the strength decreased while ductility increased due to the deformed particle morphology and distribution.
- The homogenisation heat treatment prior to the extrusion of the Al-Mg alloys reduced the amount of $\beta - Al_2Mg_3$ and refined the grains in order to obtain better extrudability. Partial melting in the screw extrusion chamber at the screw end, high deformation rate and flow pattern from the screw movement are factors that may explain the microstructure of the screw extruded materials.

7 Recommendation to further work

- Future measurements by using thermodilatometry in accordance with ASTM standard E228, several parallels should be made to exclude systematic errors and CTE should be defined and calculated in several ways to provide an overview of its impact. Otherwise, is it highly recommended to measure CTE with high accuracy by interferometric techniques as described in ASTM standard E289.
- Implement red mud as a SCM and use this concrete mix in further experiments.
- Hot roll the aluminium reinforcement rods so that the extruded profiles obtain ribs and thus better adhesion to the concrete.
- XRD, XRF, XPS SEM and TEM analysis of the acquired protective oxide layer of the aluminium alloys before and after concrete exposure and analyse the importance and functionality of the alloying elements on the developed oxide layers. By gaining a better understanding of the inhibitor, it can be improved so that more alloys can be used in concrete.
- Develop better operation parameters and/or implement new equipment which will ensure effective screw extrusion of Al-Si alloys.
- TEM studies and EBDS in SEM for obtaining better knowledge about the second-phase particles and texture of the materials.
- Examine the effect of anodising the aluminium surface, treat the sample in inhibitor solution and then expose it to cement to determine whether anodising may give better corrosion properties and adhesion to the concrete.
- Conduct studies in which co-extruded reinforcement rods are made with recycled aluminium alloys with Al-5Mg as a sleeve, and also check the possibility of conducting co-extrusion in the screw extruder.
- Perform studies where aluminium reinforced concrete is exposed to high temperatures and use of this material in marine environments.
- Investigate the gas development from the cement paste without an aluminium sample.

References

[1] Jacobsen, S., Maage, M., Smeplass, S., Kjellsen, K. O., Sellevold, E. J., Lindgård, J., ... Geiker, M. (2016). Compendium: TKT4215 Concrete technology 1, Trondheim, Norwegian University of Science and Technology, Faculty of Engineering Science and Technology, Department of Structural Engineering

[2] Justnes, H. (2017): Durable Aluminium Reinforced Environmentally-friendly Concrete Construction – DARE2C: XXIIIth Symposium on Nordic Concrete Research & Development, 21. – 23. August 2017 in Aalborg, Denmark

[3] Carbon capture technology. (n.d.). Retrieved July 16, 2018, from `https://www.norcem.no/no/CCS-aktuelt`

[4] Davis, J. R. (1993). Aluminum and Aluminum Alloys. Materials Park, OH: ASM International.

[5] Cars produced this year:. (n.d.). Retrieved July 16, 2018, from `http://www.worldometers.info/cars/`

[6] J C Werenskiold et.al. Screw extruder for continuous extrusion of materials with high viscosity, 2009. International patent number EP2086697B1 WO2008/063076. Patent reference JP-A-2004 035 961, US-A-2 787 022.

[7] Duflou, J. R., Tekkaya, A. E., Haase, M., Welo, T., Vanmeensel, K., Kellens, K., . . . Paraskevas, D. (2015). Environmental assessment of solid state recycling routes for aluminium alloys: Can solid state processes significantly reduce the environmental impact of aluminium recycling? CIRP Annals, 64(1), 37-40.

[8] Amundsen., H., S., (2017). Screw extrusion of aluminium alloys for use in concrete constructions (Project Thesis), Trondheim, NTNU

[9] Goswami, R., Spanos, G., Pao, P., & Holtz, R. (2010). Precipitation behavior of the β phase in Al-5083. Materials Science and Engineering: A, 527(4-5), 1089-1095.

[10] Engler, O., & Miller-Jupp, S. (2016). Control of second-phase particles in the Al-Mg-Mn alloy AA 5083. Journal of Alloys and Compounds, 689, 998-1010.

[11] Callister William D., Rethwisch David G., Materials Science and Engineering: An Introduction, 9th Edition: Ninth Edition, John Wiley and Sons, Incorporated, 2015

[12] Skorpen, K., G., (2018). Screw Extrusion of Light Metals (Unpublished doctoral dissertation), NTNU, Trondheim

[13] Humphreys, F. J., Rohrer, G. S., & Rollett, A. D. (2017). Recrystallization and Related Annealing Phenomena. Amsterdam: Elsevier.

[14] Lars Lodgaard. Precipitation of dispersoids containing Mn and/or Cr in Al-Mg-Si-alloys. PhD thesis, The Norwegian University of Science and Technology, 2000.

[15] Wei, W., González, S., Hashimoto, T., Babu, R. P., Thompson, G. E., & Zhou, X. (2015). Effect of low temperature sensitization on the susceptibility to intergranular corrosion in AA5083 aluminum alloy. Materials and Corrosion, 67(4), 331-339.

[16] Starink, M. J., & Zahra, A. (1997). Low-temperature decomposition of Al-Mg alloys: Guinier-Preston zones and $L1_2$ ordered precipitates. Philosophical Magazine A, 76(3), 701-714

[17] Baker, Hugh Okamoto, Hiroaki. (1992). ASM Handbook, Volume 03 - Alloy Phase Diagrams. ASM International.

[18] J K Solberg. Teknologiske metaller og legeringer. Tapir forlag, NTNU, 2014.

[19] Oguocha, I. N., Adigun, O. J., & Yannacopoulos, S. (2008). Effect of sensitization heat treatment on properties of Al–Mg alloy AA5083-H116. Journal of Materials Science, 43(12), 4208-4214.

[20] Dybowski, B., Adamczyk-Cieślak, B., Rodak, K., Bednarczyk, I., Kiełbus, A., & Mizera, J. (2015). The Microstructure of AlSi7Mg Alloy in as Cast Condition. Solid State Phenomena, 229, 3-10.

[21] Kovačević, I. (2008). Simulation of spheroidisation of elongated Si-particle in Al–Si alloys by the phase-field model. Materials Science and Engineering: A, 496(1-2), 345-354.

[22] Makhlouf, M., & Guthy, H. (2001). The aluminum–silicon eutectic reaction: mechanisms and crystallography. Journal of Light Metals, 1(4), 199-218

[23] Davis, J. R. (2001). Alloying: understanding the basics. Materials Park, OH: ASM International.

[24] Grosselle, F., Timelli, G., & Bonollo, F. (2010). Doe applied to microstructural and mechanical properties of Al–Si–Cu–Mg casting alloys for automotive applications. Materials Science and Engineering: A, 527(15), 3536-3545.

[25] Lombardi, A., Delia, F., Ravindran, C., & Mackay, R. (2014). Replication of engine block cylinder bridge microstructure and mechanical properties with lab scale 319 Al alloy billet castings. Materials Characterization, 87, 125-137.

[26] Dieter, G. E., & Bacon, D. (2001). Mechanical metallurgy. London: McGraw-Hill

[27] Reiso, O., 2015. Tmt4266, metal fabrication and forming- microstructure and crystal plasticity- extrusion & metallurgy, 2015

[28] Widerøe, F., & Welo, T. (2013). Using contrast material techniques to determine metal flow in screw extrusion of aluminium. Journal of Materials Processing Technology, 213(7), 1007-1018.

[29] Brown, A. A., & Bammann, D. J. (2012). Validation of a model for static and dynamic recrystallization in metals. International Journal of Plasticity, 32-33, 17-35.

[30] Skorpen, K., G., Mauland, E., Reiso, O. & Roven, H., J. (2014) Novel method of screw extrusion for fabricating Al/Mg (macro-) composites from aluminum alloy 6063 and magnesium granules

[31] Banerjee, M. (2017). 2.1 Fundamentals of Heat Treating Metals and Alloys. Comprehensive Materials Finishing, 1-49

[32] Doherty, R., Hughes, D., Humphreys, F., Jonas, J., Jensen, D. J., Kassner, M., . . . Rollett, A. (1998). Current issues in recrystallization: A review. Materials Today, 1(2), 14-15.

[33] Pedersen, K., Lademo, O., Berstad, T., Furu, T., & Hopperstad, O. (2008). Influence of texture and grain structure on strain localisation and formability for AlMgSi alloys. Journal of Materials Processing Technology, 200(1-3), 77-93.

[34] Campbell, F. C. (2013). Inspection of metals: understanding the basics. Materials Park, OH: ASM International.

[35] Hatch, J. E. (1984). Aluminium: properties and physical metallurgy. Materials Park, OH: American Society for metals.

[36] Johansen, I. (1995). Properties, microstructure and modelling of an RS aluminium alloy (Doctoral dissertation)

[37] ASM handbook (Vol. 2, Properties and Selection: Nonferrous Alloys and Special-Purpose Materials). (1990). Materials Park, OH: ASM International

[38] Setina, J., Gabrene, A., & Juhnevica, I. (2013). Effect of Pozzolanic Additives on Structure and Chemical Durability of Concrete. Procedia Engineering, 57, 1005-1012

[39] Ma, S., Wu, Y., & Zhang, H. (2016). Building materials in civil engineering. Oxford: Woodhead Publishing.

[40] Wong, H. S., Matter, K., & Buenfeld, N. R. (2013). Estimating the original cement content and water–cement ratio of Portland cement concrete and mortar using backscattered electron microscopy. Magazine of Concrete Research, 65(11), 693-706.

[41] Behnood, A., Tittelboom, K. V., & Belie, N. D. (2016). Methods for measuring pH in concrete: A review. Construction and Building Materials, 105

[42] Eide Å., E., Kolberg E., M. & Østbye E., M. (2018). "The possibility of using reinforcement bars of aluminium in concrete structures", (Unpublished Master Thesis), Trondheim, NTNU

[43] Nürnberger, U. (2007). Corrosion of metals in contact with mineral building materials. Corrosion of Reinforcement in Concrete, 1-9.

[44] Vargel, C. (2004). Corrosion of aluminium. Amsterdam: Elsevier.

[45] Setiadi, A., Milestone, N. B., Hill, J., & Hayes, M. (2006). Corrosion of aluminium and magnesium in BFS composite cements. Advances in Applied Ceramics, 105(4), 191-196.

[46] Oakes B.D., Historical review inhibitors mechanisms, NACE Corrosion, 1981, paper No. 248.

[47] "How It's Made Engine Blocks." YouTube, How It's Made, Discovery Channel, 24 Sept. 2010, www.youtube.com/watch?v=yXVLbzI3xTE.

[48] J. K. Solberg, Lysmikroskopi. Institutt for Materialteknologi, NTNU, 2010.

[49] J. Hjelen, Scanning Elektron-Mikroskopi. Metallurgisk institutt, NTH, 1989.

[50] ASTM E228-06 Standard Test Method for Linear Thermal Expansion of Solid Materials With a Push-Rod Dilatometer, ASTM International, West Conshohocken, PA, 2006

[51] Justnes, H., Østnor, T., Danner, T.: Calcined marl as effective pozzolana. In: Proceeding of the International RILEM Conference on Advances in Construction Materials through Science and Engineering, RILEM PRO 79, Hong Kong, China, 8 p. 5-7 September 2011

[52] ASTM E112-13 Standard Test Methods for Determining Average Grain Size, ASTM International, West Conshohocken, PA, 2013

[53] ASTM E831-14 Standard Test Method for Linear Thermal Expansion of Solid Materials by Thermomechanical Analysis, ASTM International, West Conshohocken, PA, 2014

[54] ASTM E289-17 Standard Test Method for Linear Thermal Expansion of Rigid Solids with Interferometry, ASTM International, West Conshohocken, PA, 2017

[55] James, J. D., Spittle, J. A., Brown, S. G., & Evans, R. W. (2001). A review of measurement techniques for the thermal expansion coefficient of metals and alloys at elevated temperatures. Measurement Science and Technology, 12(3)

[56] Kong, X., Li, M., Xue, S., Hartley, W., Chen, C., Wu, C., . . . Li, Y. (2017). Acid transformation of bauxite residue: Conversion of its alkaline characteristics. Journal of Hazardous Materials, 324, 382-390.

[57] Cui, J. (2011). Solid state recycling of aluminium scrap and dross characterisation (Doctoral dissertation), NTNU, Trondheim

[58] Thirumurugan, M., Rao, S. A., Kumaran, S., & Rao, T. S. (2011). Improved ductility in ZM21 magnesium–aluminium macrocomposite produced by co-extrusion. Journal of Materials Processing Technology, 211(10), 1637-1642.

[59] Kazanowski, P., Epler, M. E., & Misiolek, W. Z. (2004). Bi-metal rod extrusion—process and product optimization. Materials Science and Engineering: A, 369(1-2), 170-180

Appendices

A Flowchart of the work and results obtained in this thesis

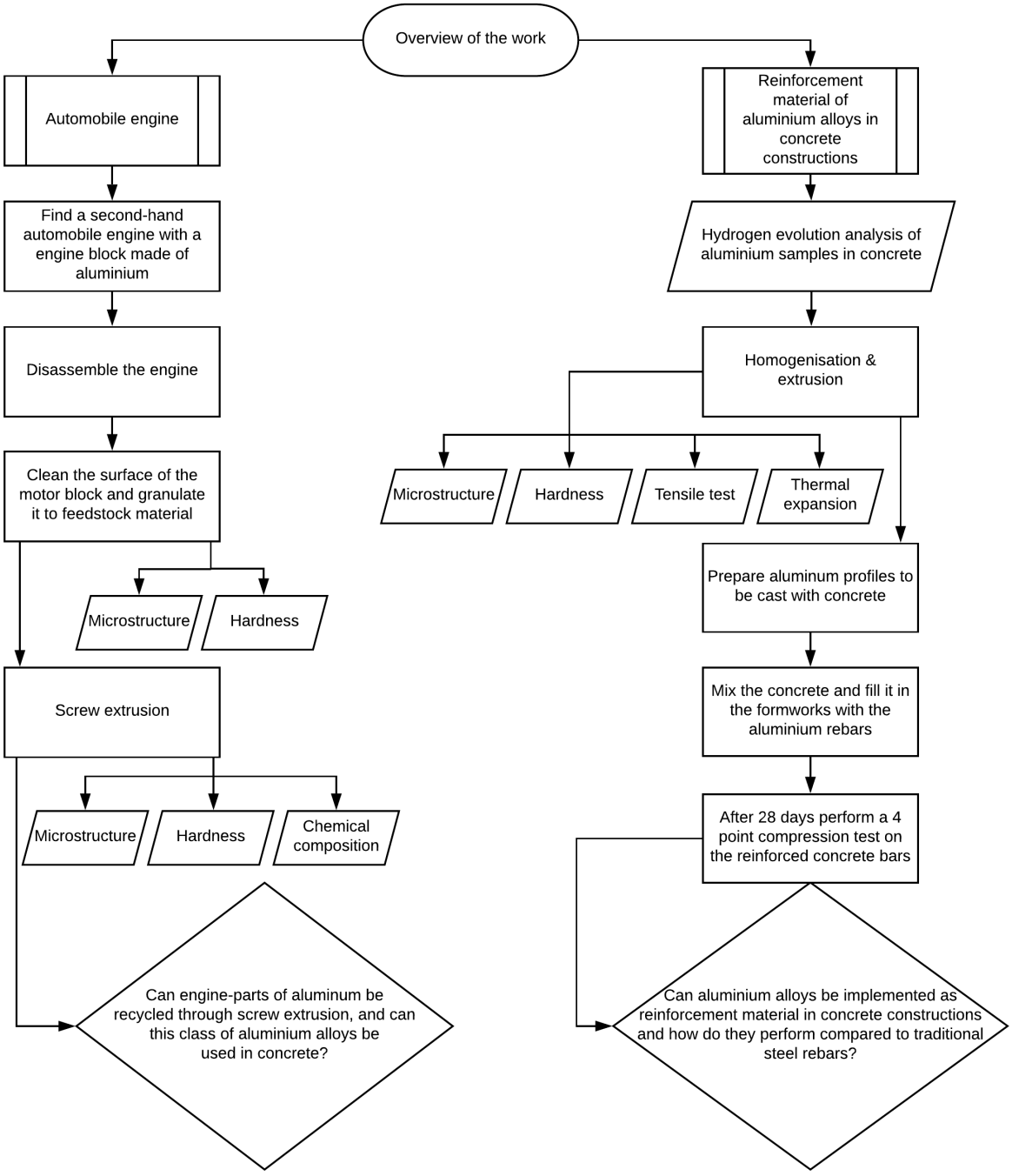

Figure A.0.1: Schematic flow chart representation of the experimental work done in this thesis, of two parallel opportunity studies that can potentially serve the same purpose. The boxes with a rectangular shape represent a process step and the boxes with a rhomboid shape represent which results that were collected from that step.

B Extrusion log

This appendix chapter shows the extrusion log from the extrusion of the Al-5Mg bolt used to extrude the T-beam profile, the two Al-5Mg bolts and the Al-1Mg bolt used to produce the reinforcement material.

Prosjektnummer / navn: 102018127, Ekstrud av T-profil, N5 og stang ø10.0mm, C6 Dato: 2018-03-14
Container / bolster: Ekstrudering 100 mmØ / Vingebolster
Kommentarer: Hans J.R., Oddvin R. og Hans Sigurd (masterstudent)

Bolter forvarmet i ovn. T_{ovn} 445°C, skal gi T_{bolt} ~430 °C etter ca. en time

Log	Forsøk Nr	Materiale	Målte parametre											Kommentarer
			$v_{STEMPEL}$ (mm/s)		T_{BOLT} (°C)			T_{CONT}	T_{STEM}	$T_{ÆREFLATE}$		Kraft (kN)		
			innstilt	ok	ovn	foran	Bak			$T1_{MAX}$	$T2_{MAX}$	Max	Min	
T-prof.	1	Al5Mg	1,0	1,0	tc 430	408	397	433	~30			62960		
Ø10mm	2	"	1,0	1,1	tc 436	410	410	433	~80			7100		OBS skår T-profil i loggefil
"	3	"	"	1,4		410	409	431	~150			7052		15mm bolt
"	4	Al1Mg	1,0	1,0		436	425	432	~~470~~			3947		10mm bolt

Kjørte med presserest på 5mm på T-verktøy og 15mm for Ø10
T-profil fikk en lengde på ca 8m og kunne kjøres i hull i kjeller på ett press
Stang måtte ha to stopp. Stoppet manuelt på 535 m ved ram på 585

SINTEF

Date: 15.08.2002 21:24:31

Exp nr: 1 Ekstrud T-profil, N5, 180314

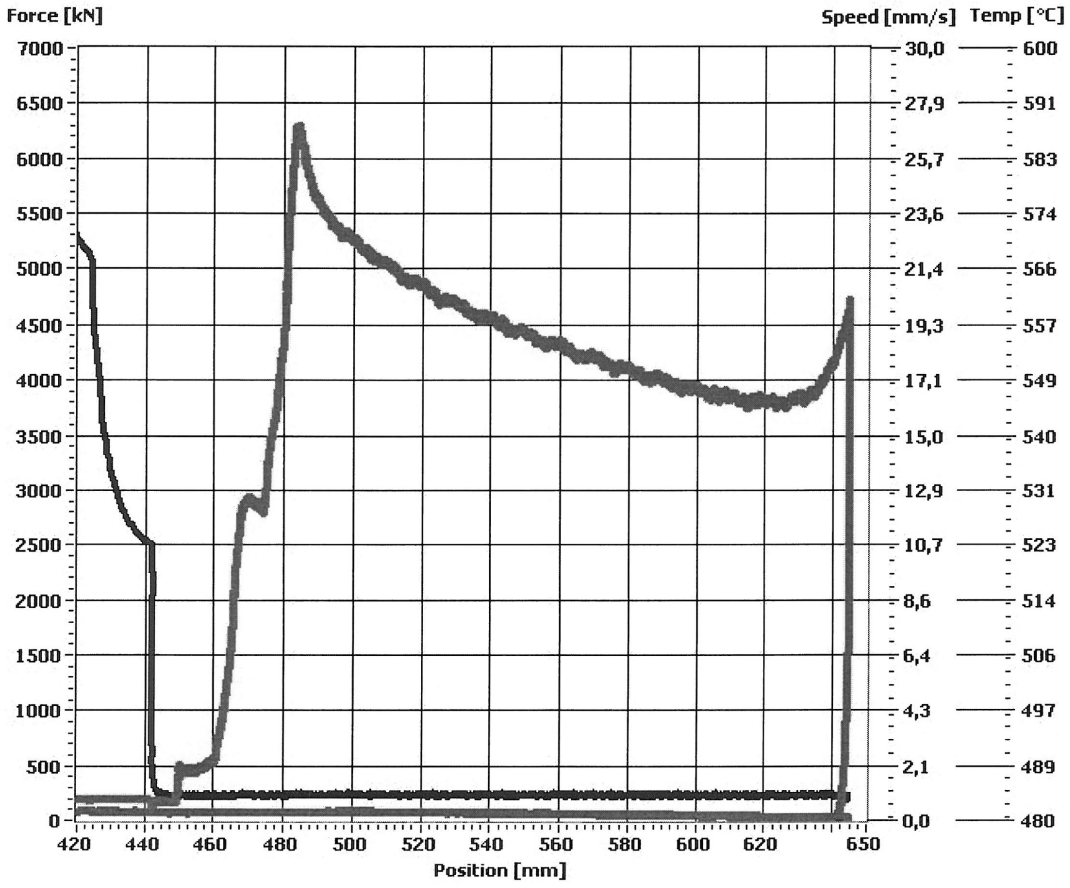

Position [mm]
Force [kN]
Speed [mm/s]
Temp Die [°C]
Temp Container [°C]
Temp 1 [°C]
Temp 2 [°C]
Temp 3 [°C]
Temp 4 [°C]
Temp 5 [°C]
Temp 6 [°C]
Voltage 1 [V]
Voltage 2 [V]
Voltage 3 [V]
Kraft smiverktøy [kN]

Matrix: N5, T-profil

Max Force = 6296
Min Force = 44
Avr Speed = 1,0
Max Temp Die = 481
Max Temp Cont = 433

SINTEF

Ø10mm, C6

Date: ~~15.08.~~2002 23:15:04

Exp nr: 2 **Ekstrud ~~T-profil, N5,~~ 180314**

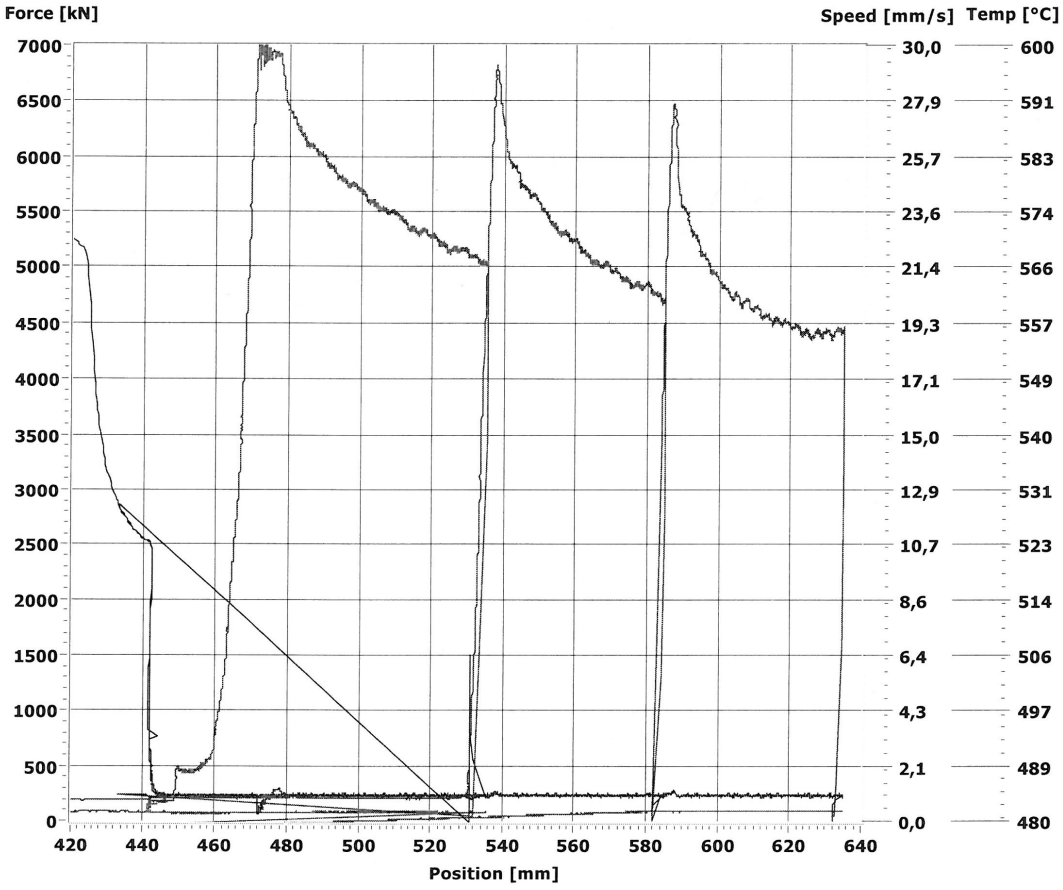

Position [mm]
Force [kN]
Speed [mm/s]
Temp Die [°C]
Temp Container [°C]
Temp 1 [°C]
Temp 2 [°C]
Temp 3 [°C]
Temp 4 [°C]
Temp 5 [°C]
Temp 6 [°C]
Voltage 1 [V]
Voltage 2 [V]
Voltage 3 [V]
Kraft smiverktøy [kN]

C5, Ø10mm

Matrix: ~~N5, T-pro~~

Max Force = 7100
Min Force = 34
Avr Speed = 1,1
Max Temp Die = 482
Max Temp Cont = 433

SINTEF

Ø10mm, C5

Date: 15.08.2002 23:32:21

Exp nr: 3 Ekstrud ~~T-profil, N5~~, 180314

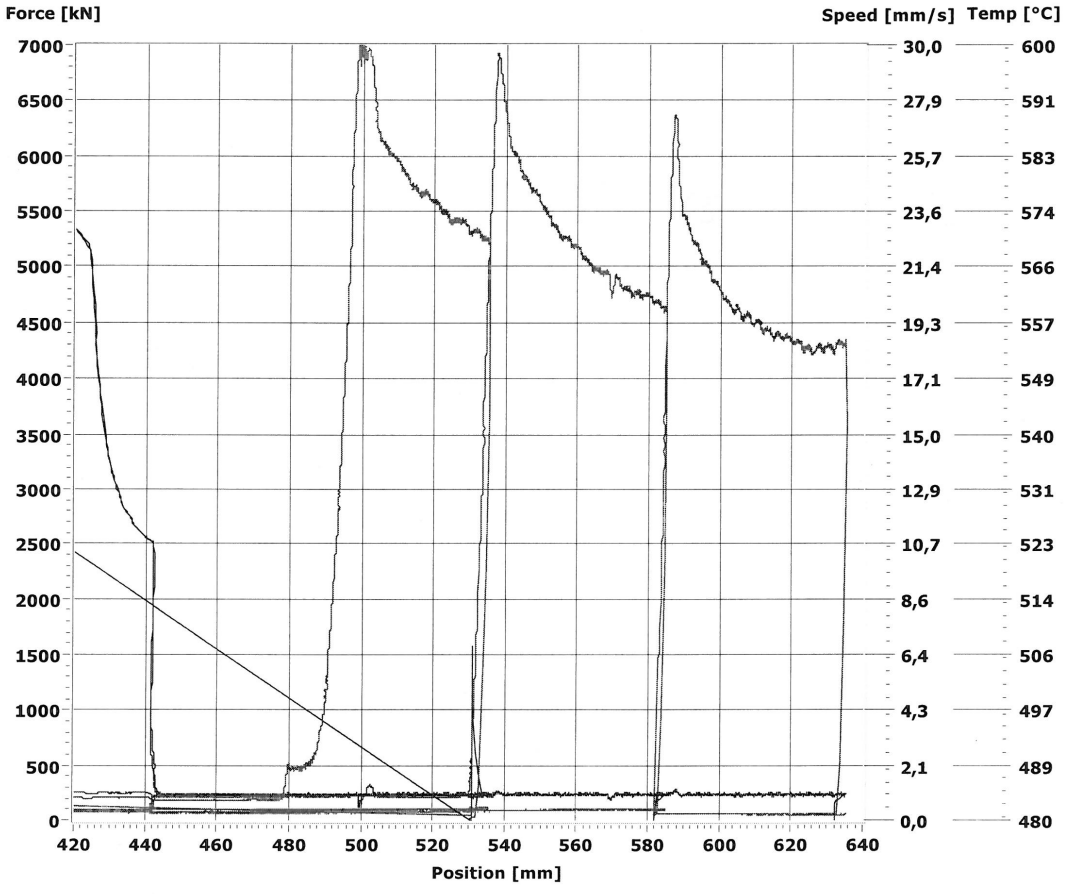

Position [mm]
Force [kN]
Speed [mm/s]
Temp Die [°C]
Temp Container [°C]
Temp 1 [°C]
Temp 2 [°C]
Temp 3 [°C]
Temp 4 [°C]
Temp 5 [°C]
Temp 6 [°C]
Voltage 1 [V]
Voltage 2 [V]
Voltage 3 [V]
Kraft smiverktøy [kN]

C5, Ø10...

Matrix: N5, ~~T-pro~~

Max Force = 7052
Min Force = 28
Avr Speed = 1,4
Max Temp Die = 482
Max Temp Cont = 431

SINTEF

Ø10mm, C5

Date: ~~15.08.2002~~ 23:49:27

Exp nr: 4

Ekstrud ~~T-profil, N5~~, 180314

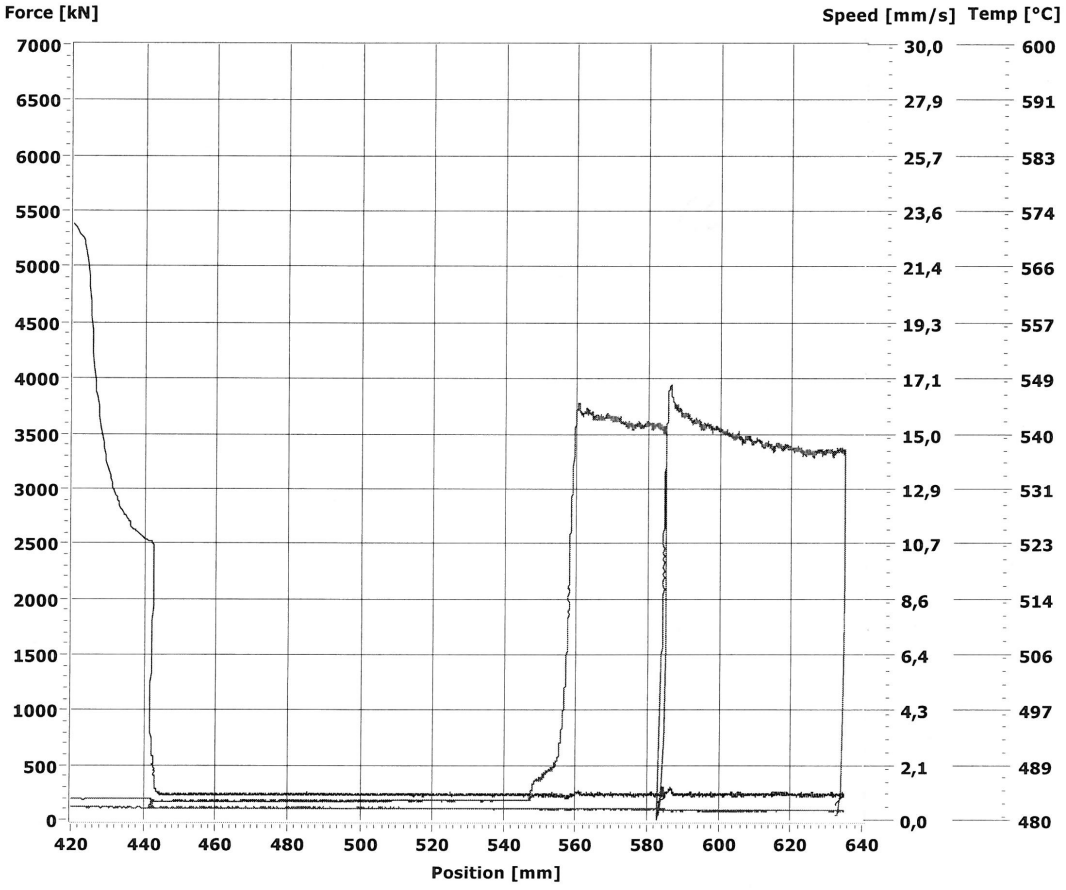

Position [mm]
Force [kN]
Speed [mm/s]
Temp Die [°C]
Temp Container [°C]
Temp 1 [°C]
Temp 2 [°C]
Temp 3 [°C]
Temp 4 [°C]
Temp 5 [°C]
Temp 6 [°C]
Voltage 1 [V]
Voltage 2 [V]
Voltage 3 [V]
Kraft smiverktøy [kN]

C5 ø 10

Matrix: ~~N5, T-pro~~

Max Force = 3942
Min Force = 3278
Avr Speed = 1,0
Max Temp Die = 482
Max Temp Cont = 432

C Micrographs of anodised cross-sections

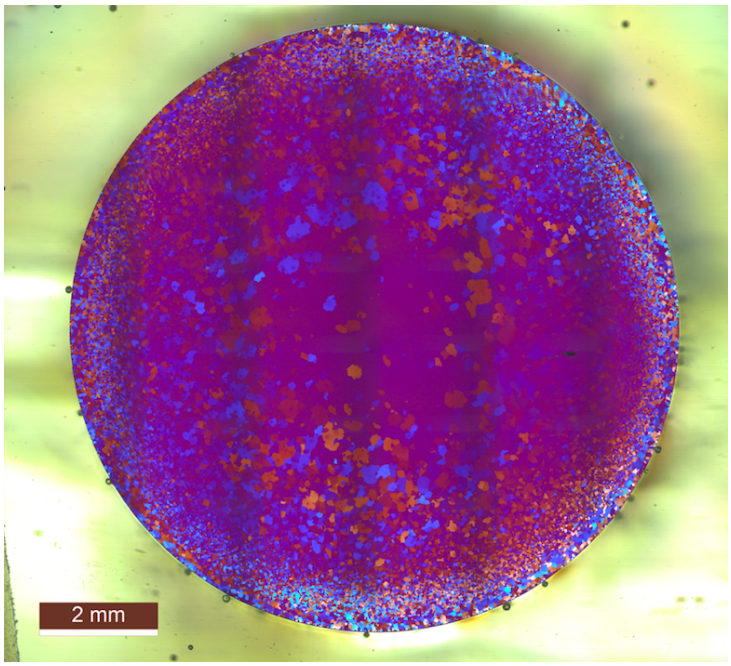

Figure C.0.1: Micrograph of the anodised transverse cross-section of the Al-1Mg alloy.

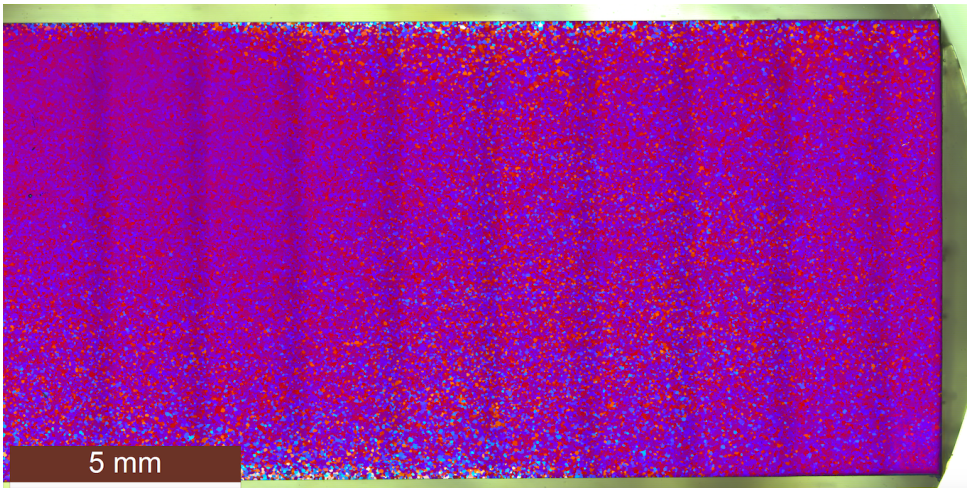

Figure C.0.2: Micrograph of the anodised longitudinal cross-section of the Al-5Mg alloy.

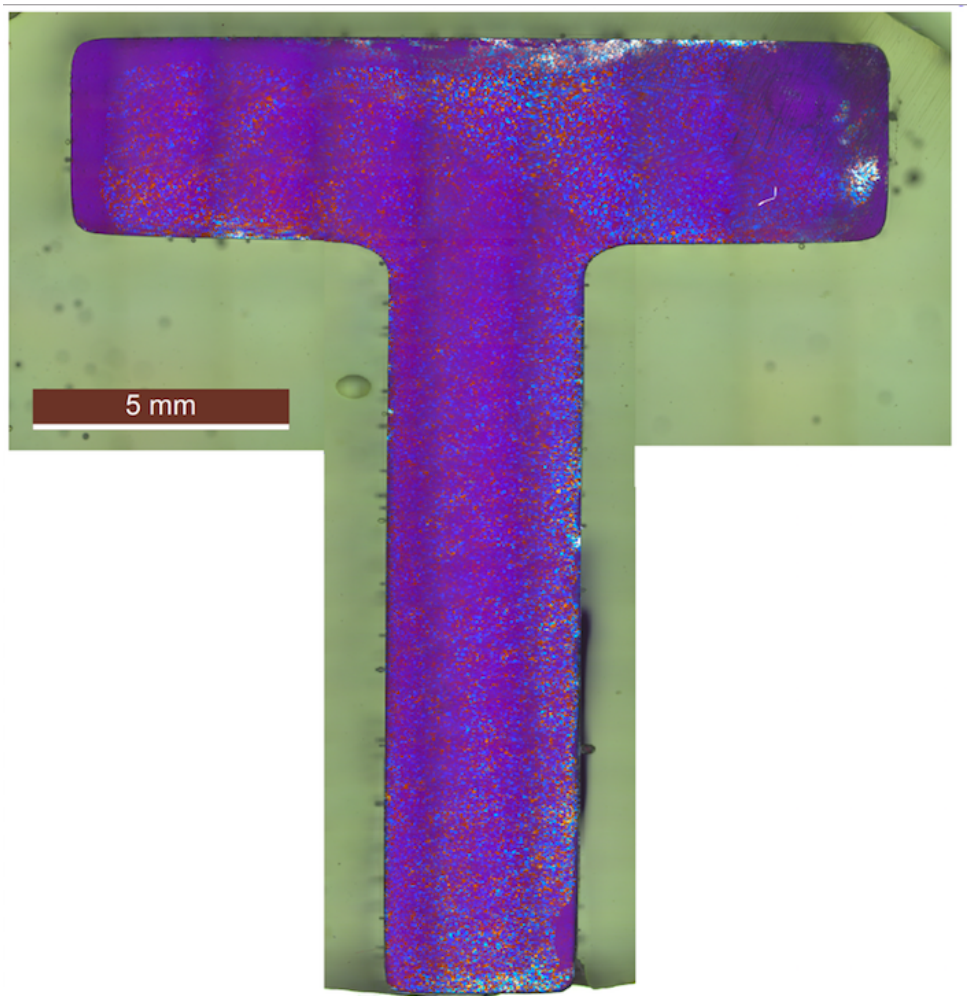

Figure C.0.3: Micrograph of the anodised cross-section of the Al-5Mg T-profile.

D Micrographs of the samples before extrusion

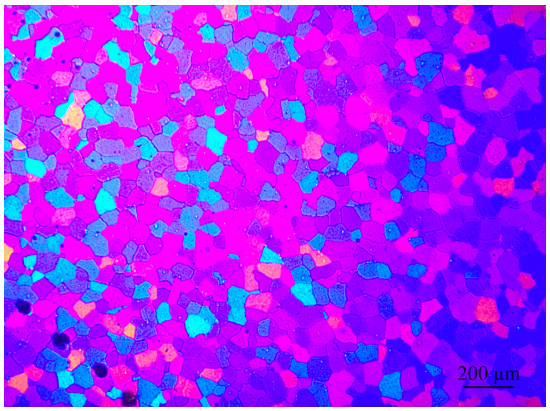

Figure D.0.1: The billet microstructure of the Al-1Mg alloy.

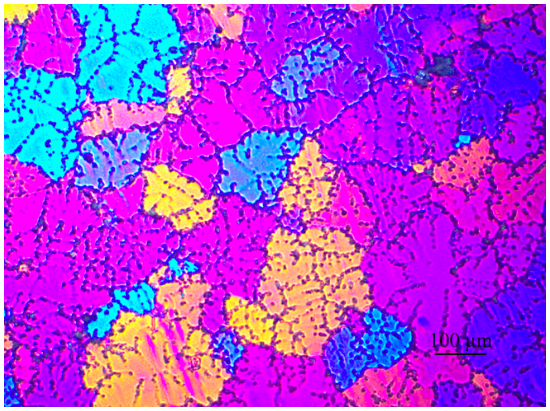

Figure D.0.2: The billet microstructure of the Al-5Mg alloy.

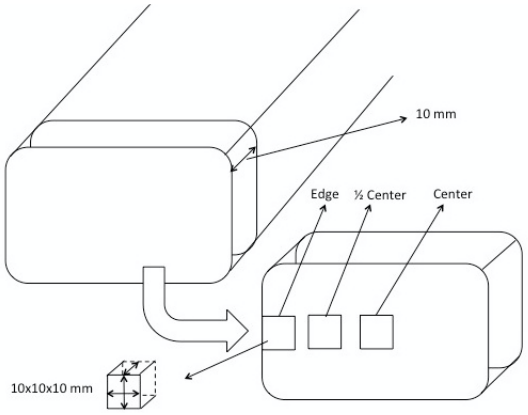

Figure D.0.3: Positions of where the Al-Si micrograph specimens from the billet were collected from.

The micrograph samples of the Al-Si alloy billets were collected from position $\frac{1}{2}$centre as illustrated in figure D.0.3.

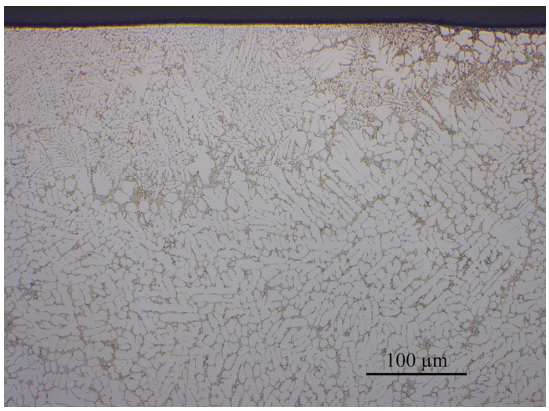

(a) Bright-field illumination and 20x magnification.

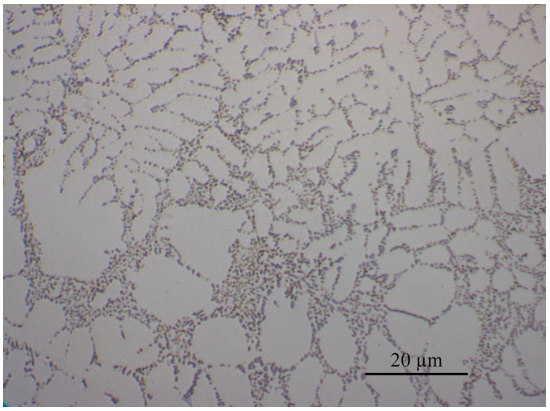

(b) Bright-field illumination and 50x magnification.

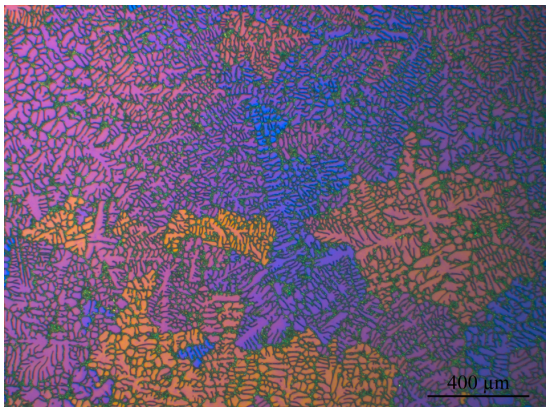

(c) Polarised light illumination and 5x magnification.

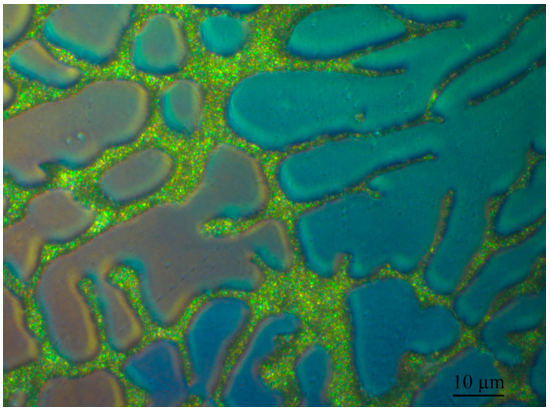

(d) Polarised light illumination and 100x magnification.

Figure D.0.4: LOM micrographs of the Al-7Si-0.3Mg billet before extrusion.

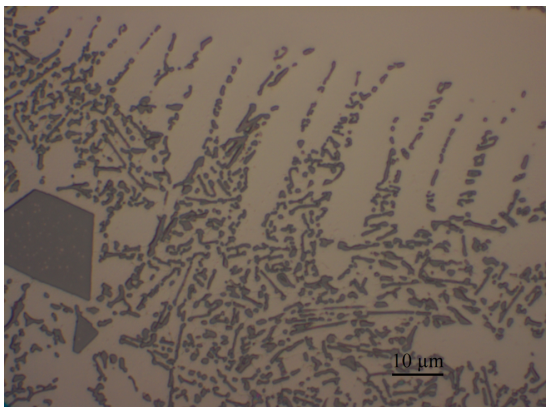

(a) Bright-field illumination and 100x magnification.

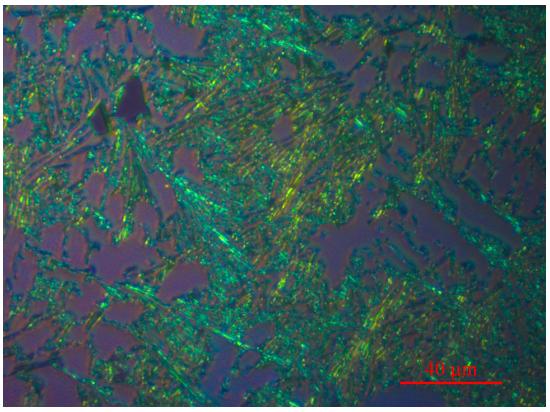

(b) Polarised light illumination and 50x magnification.

Figure D.0.5: LOM micrographs of the Al-12.7Si billet before extrusion.

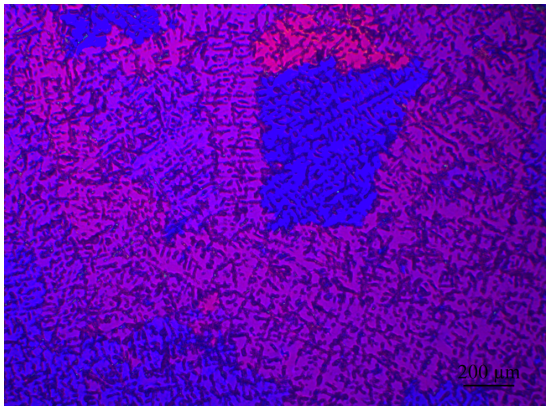

(a) Polarised light illumination and 50x magnification.

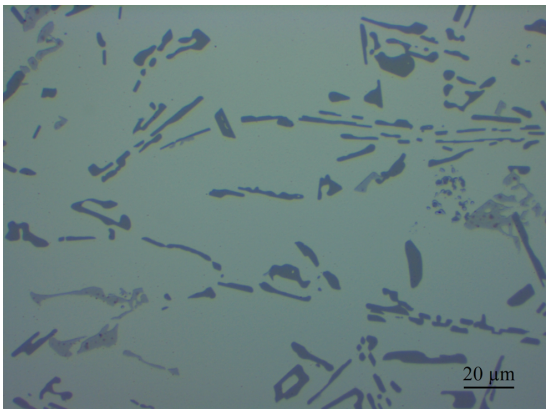

(b) Bright-field illumination and 100x magnification.

Figure D.0.6: LOM micrographs of the car engine before extrusion.

E CTE results

Thermodilatometry

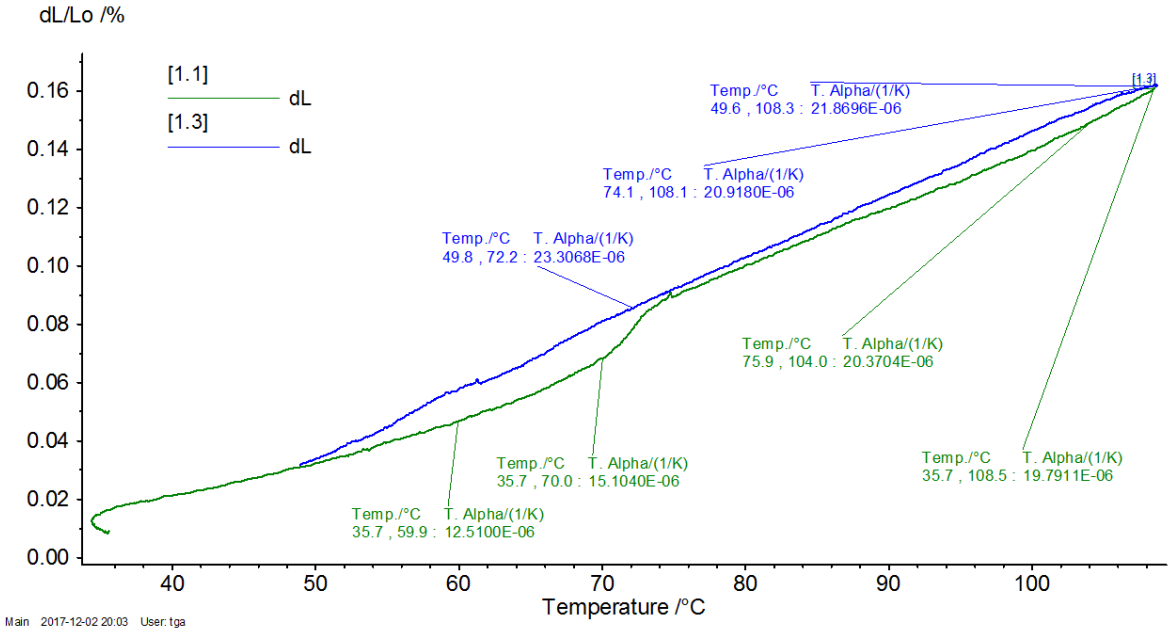

Figure E.0.1: The CTE measurement of the screw extruded Al-12.7Si from 30-100°C.

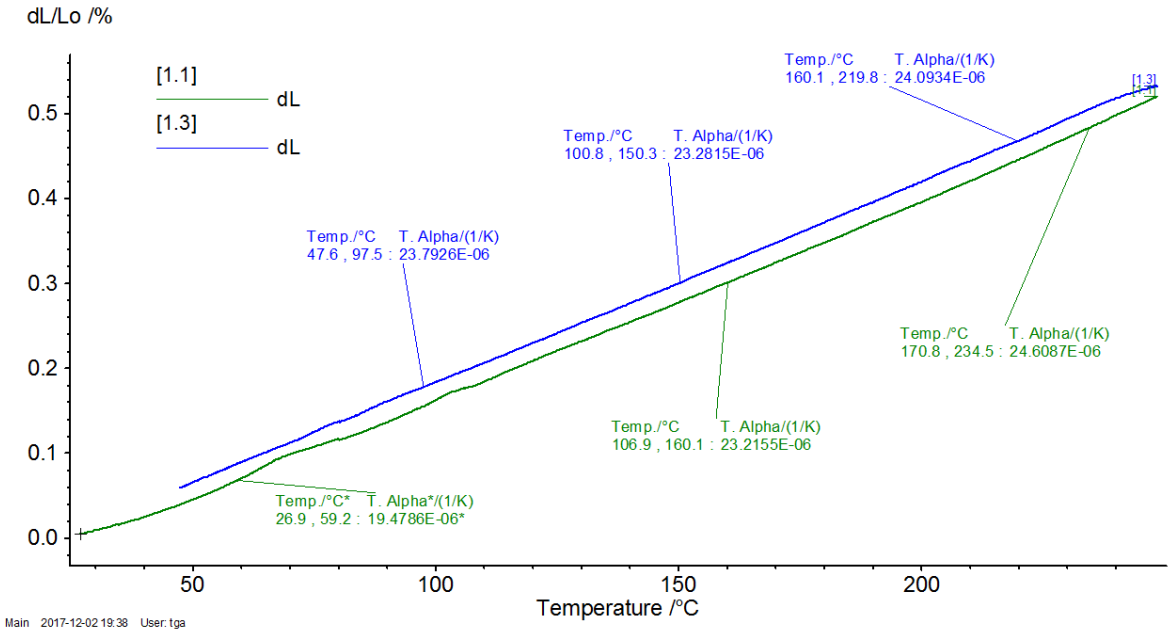

Figure E.0.2: The CTE measurement of the screw extruded Al-7Si-0.3Mg from 30-250°C.

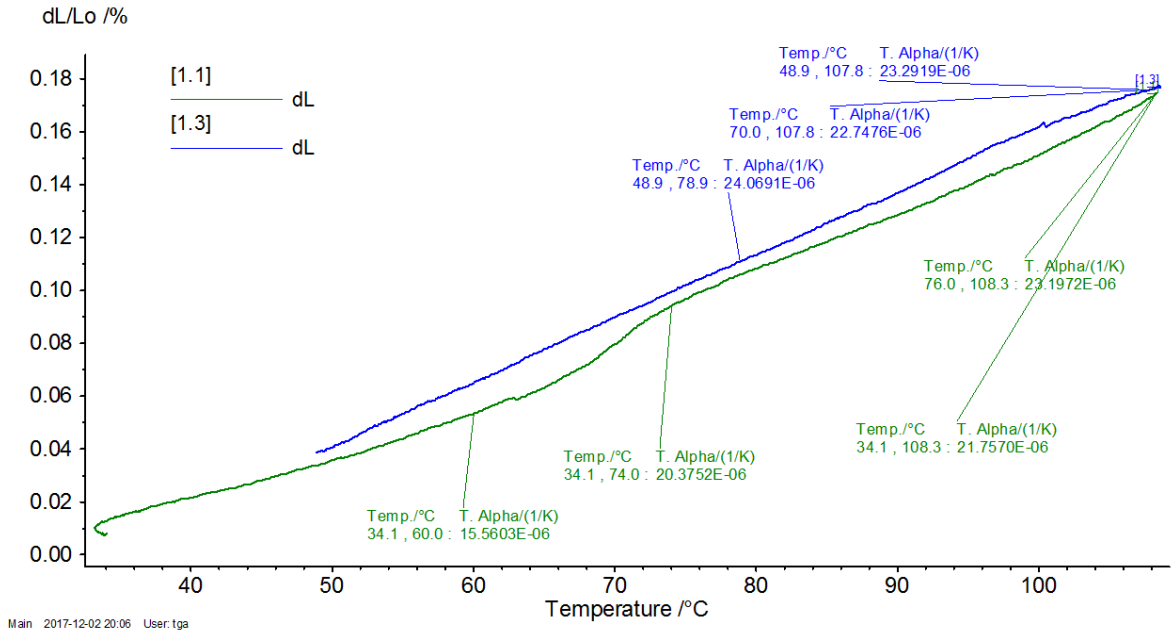

Figure E.0.3: The CTE measurement of the screw extruded Al-7Si-0.3Mg from 30-100°C.

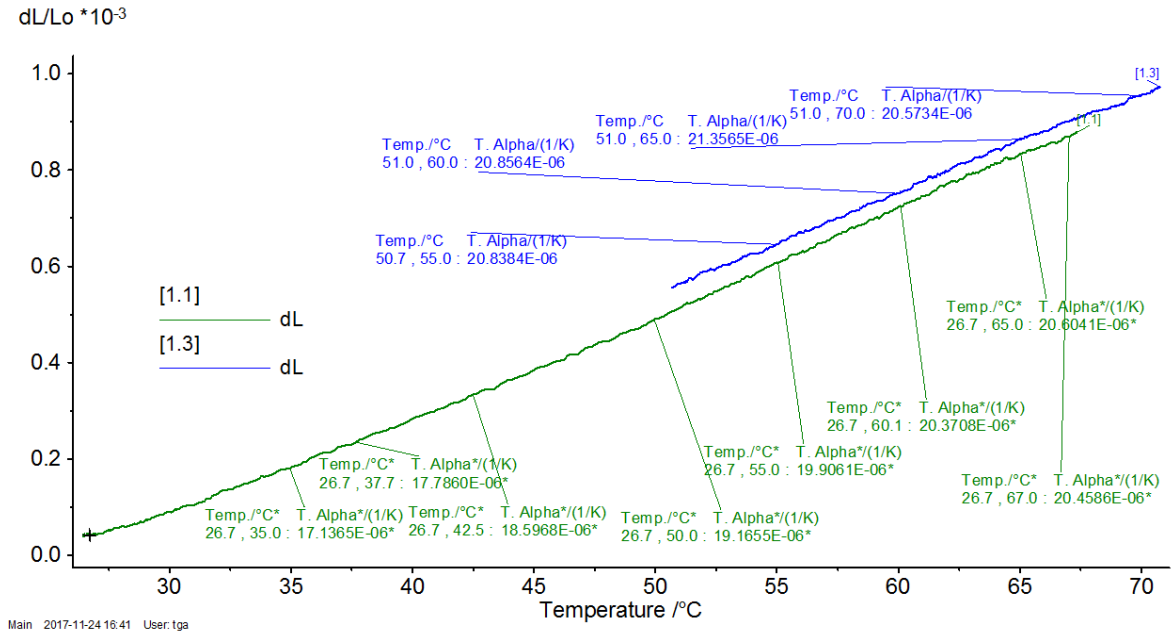

Figure E.0.4: The CTE measurement of the screw extruded Al-12.7Si from 30-70°C.

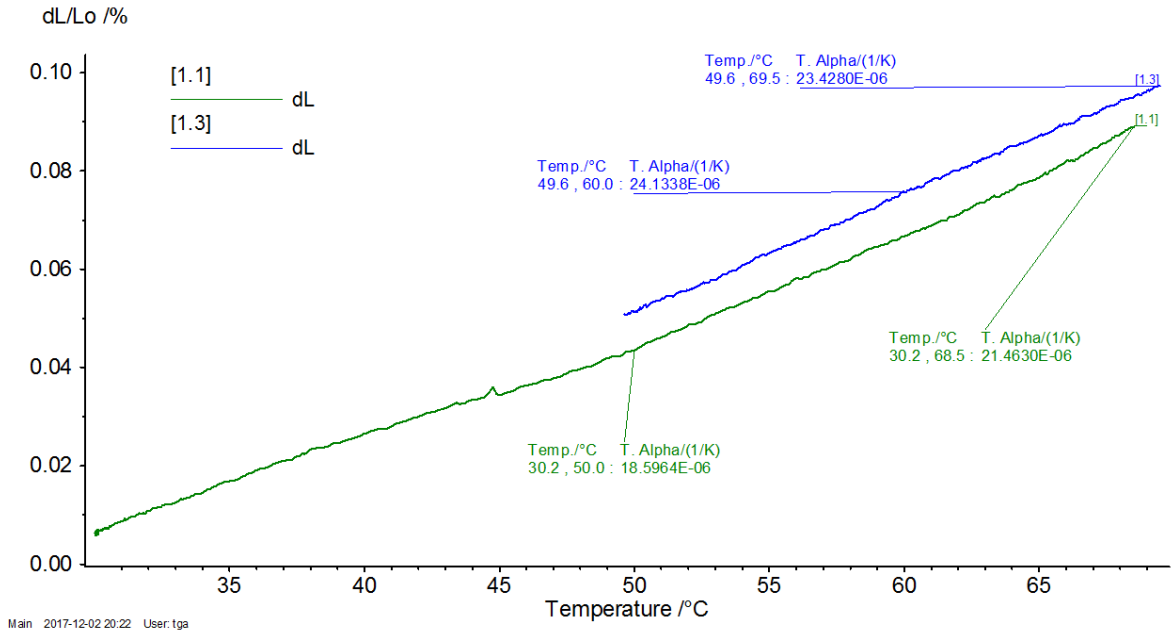

Figure E.0.5: The CTE measurement of the screw extruded Al-7Si-0.3Mg from 30-70°C.

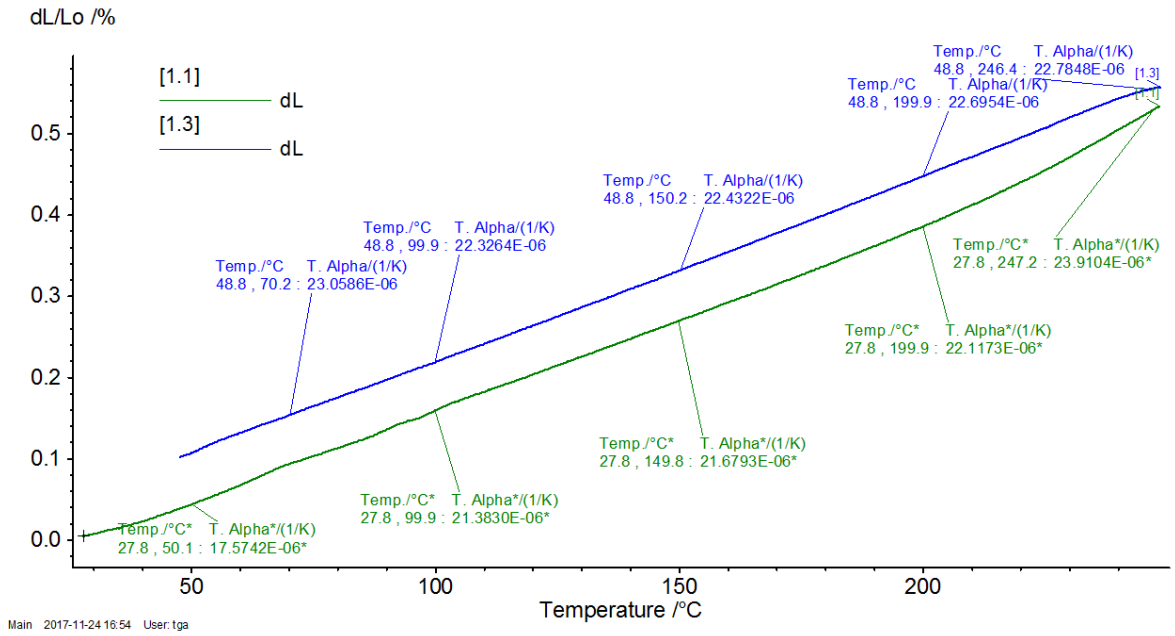

Figure E.0.6: The CTE measurement of Al-12.7Si in as-cast state from 30-250°C.

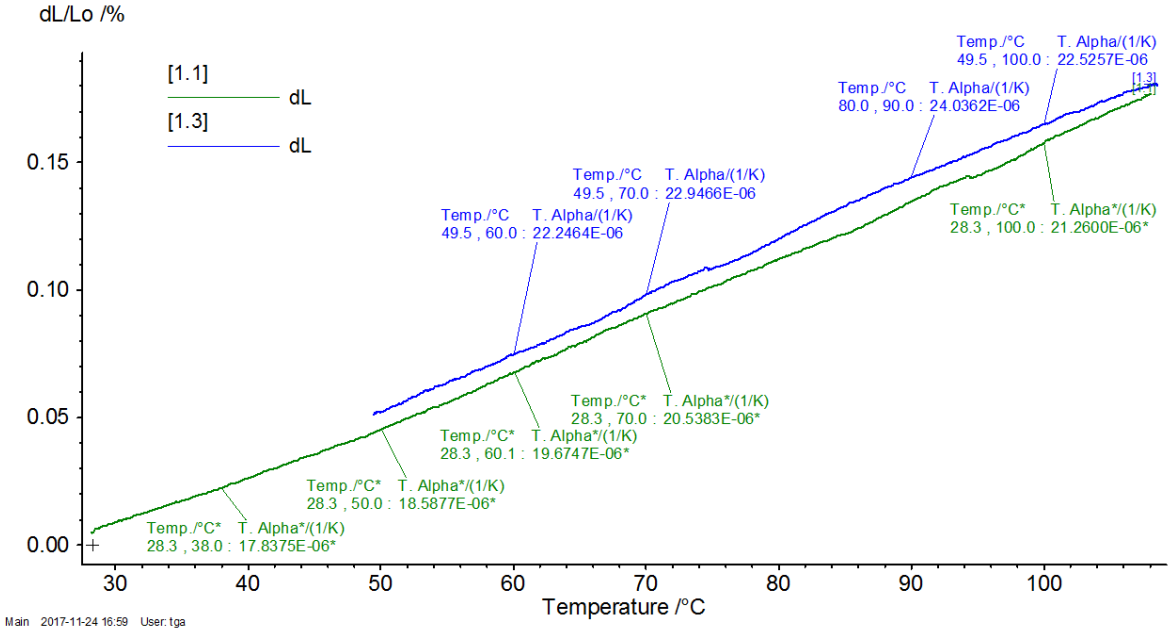

Figure E.0.7: The CTE measurement of Al-12.7Si in as-cast state from 30-100°C.

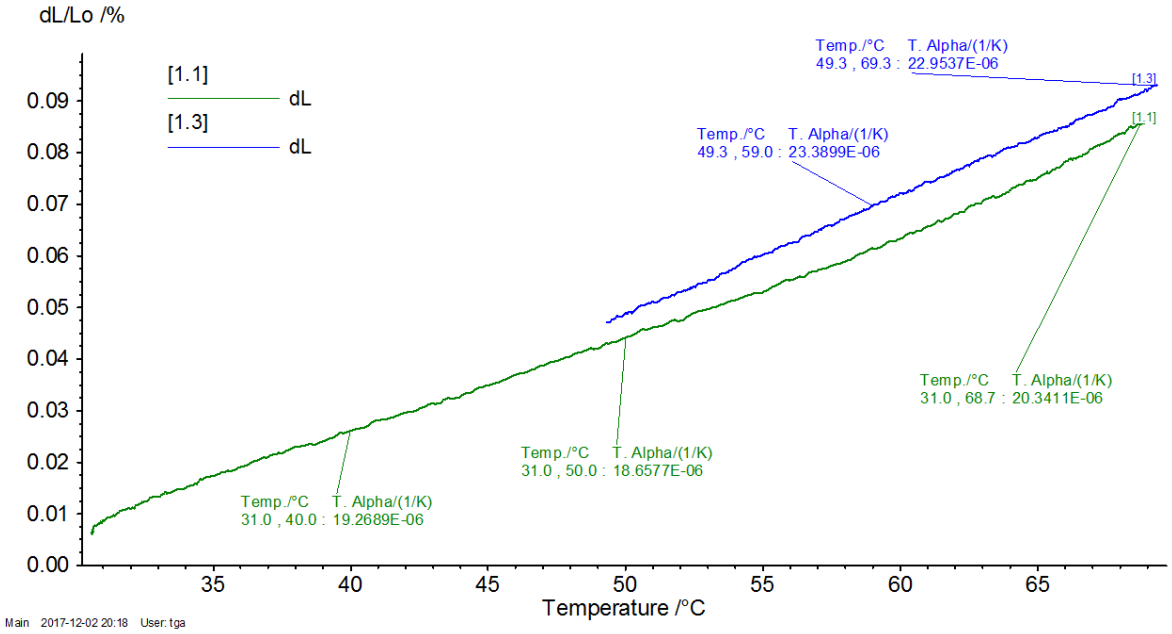

Figure E.0.8: The CTE measurement of Al-12.7Si in as-cast state from 30-70°C.

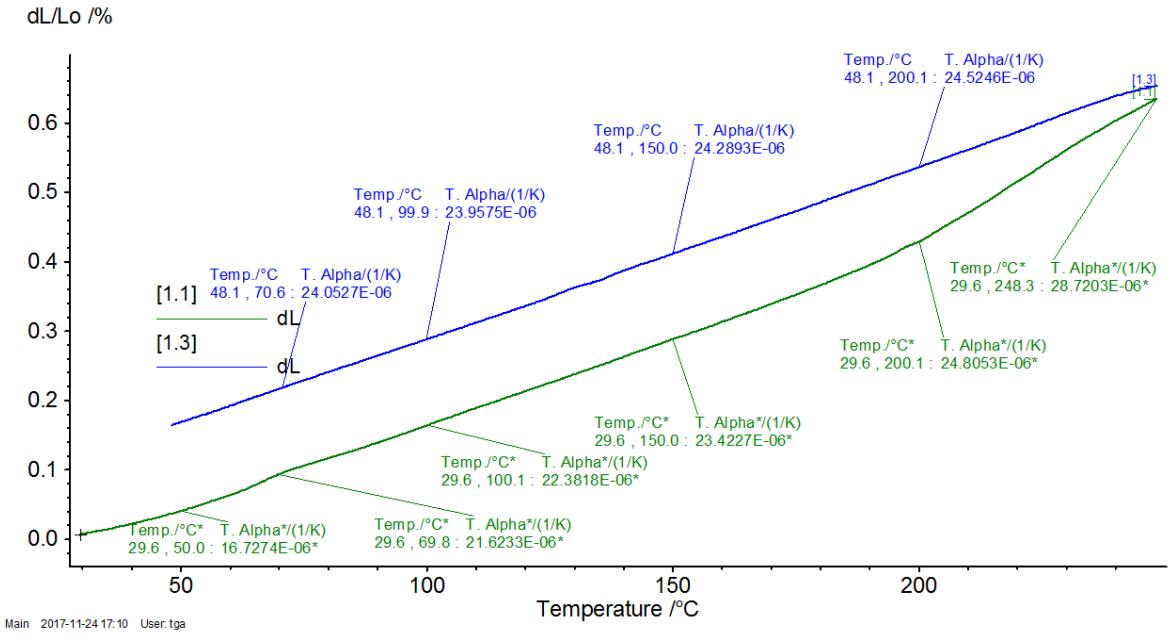

Figure E.0.9: The CTE measurement of Al-7Si-0.3Mg in as-cast state from 30-250°C.

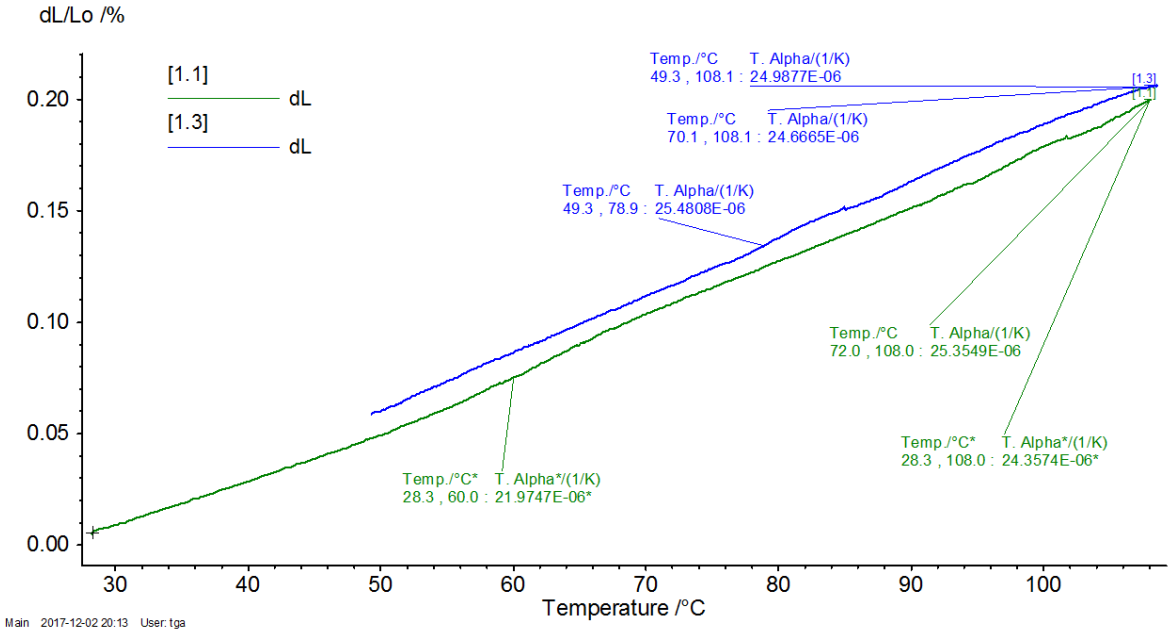

Figure E.0.10: The CTE measurement of Al-7Si-0.3Mg in as-cast state from 30-100°C.

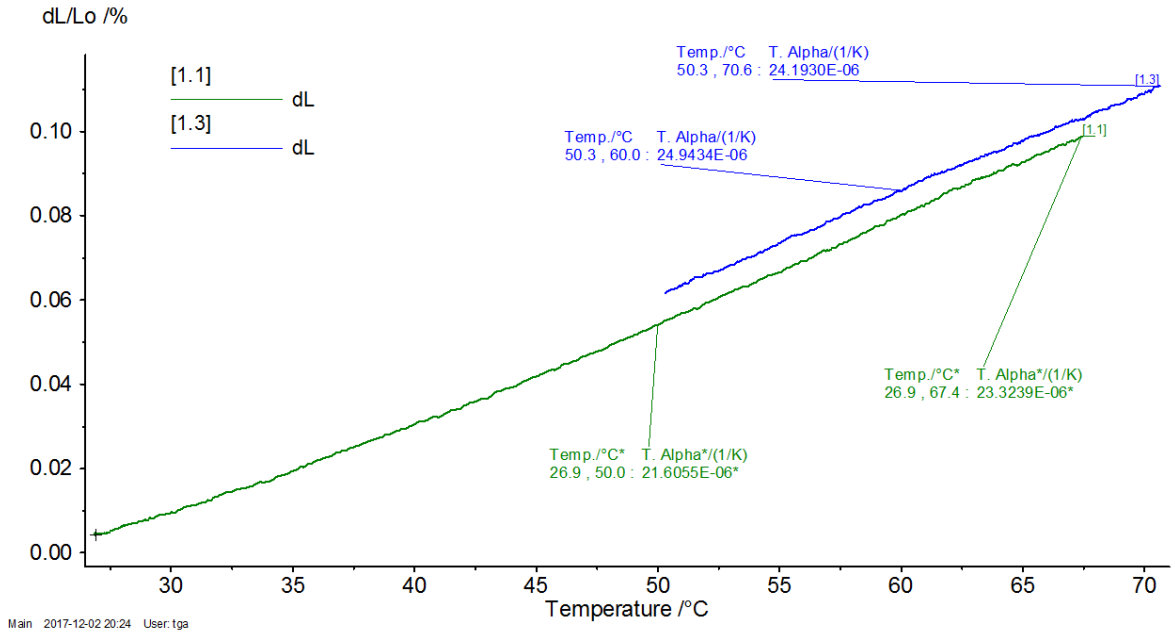

Figure E.0.11: The CTE measurement of Al-7Si-0.3Mg in the as-cast state from 30-70°C.

Manually measuring with extensometer

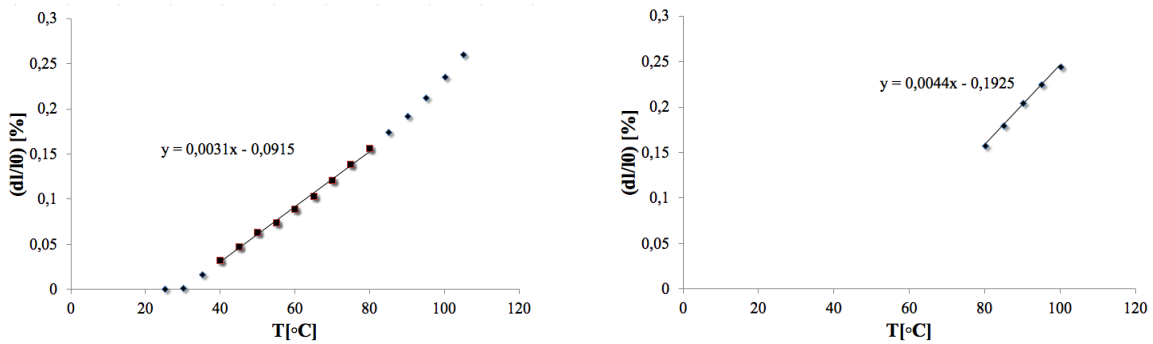

(a) Data collected from heating up the sample.

(b) Data obtained from cooling the sample down from the max temperature.

Figure E.0.12: The measured values of CTE of the Al-5Mg alloy.

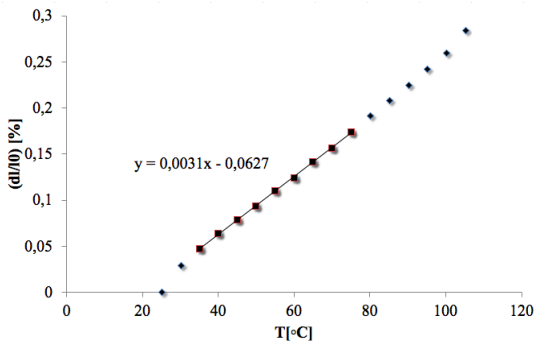

Figure E.0.13: The CTE measurement of the screw extruded Al-7Si-0.3Mg from 30-100°C.

F EDS analysis of the alloys before extrusion

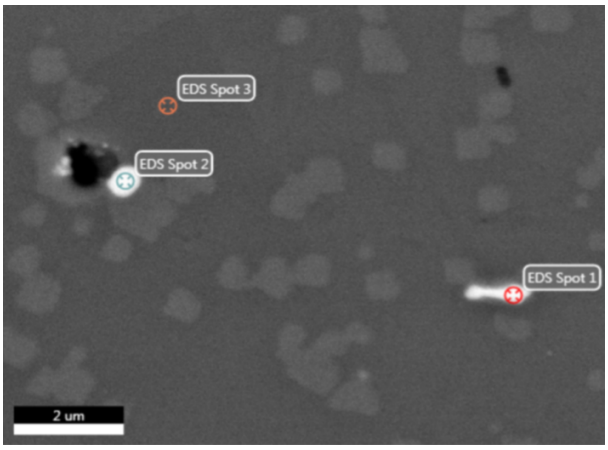

Figure F.0.1: SEM micrographs of the Al-1Mg alloy extrusion profile 10000x magnification. Points indicate where analysis with EDS were taken.

Table F.1: EDS spectrum of the Al-1Mg extrusion profile.

Element	Content [wt.%]	Error [wt.%]
EDS spot 1		
Fe	11.05	2.62
Mg	1.65	5.12
Al	85.14	2.90
Si	2.16	9.06
EDS spot 2		
Fe	9.68	2.88
Mg	4.11	4.06
Al	83.90	2.99
Si	2.31	8.93
EDS spot 3		
Mg	1.75	4.13
Al	98.25	2.29

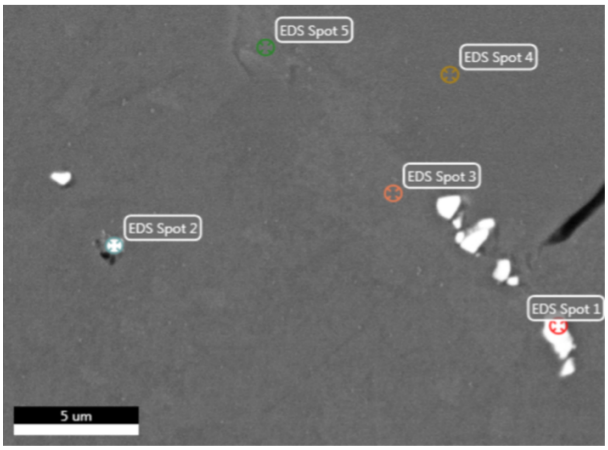

Figure F.0.2: SEM micrograph of the Al-5Mg alloy billet 5000x magnification. Points indicate where analysis with EDS were taken.

Table F.2: EDS spectrum Al-5Mg billet.

Element	Content [wt.%]	Error [wt.%]
EDS spot 1		
Fe	17.13	2.29
Mg	4.79	4.08
Al	70.08	3.31
EDS spot 2		
Fe	7.40	2.73
Mg	18.57	3.01
Al	71.96	3.63
Si	2.07	7.73
EDS spot 3		
Mg	10.82	2.54
Al	89.18	2.81
EDS spot 4		
Mg	5.85	2.63
Al	94.15	2.50
EDS spot 5		
Mg	31.19	2.33
Al	68.81	3.96

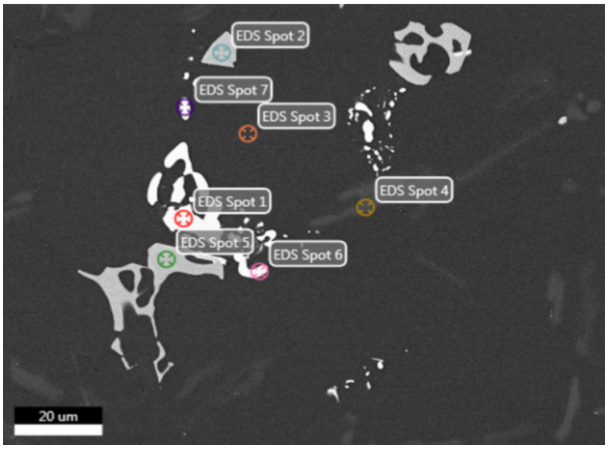

Figure F.0.3: SEM micrograph of the engine block before extrusion 800x magnification. Points indicate where analysis with EDS were taken.

Table F.3: EDS spectrum of the car engine before extrusion.

Element	Content [wt.%]	Error [wt.%]
EDS spot 1		
Cu	32.81	2.72
Al	46.51	5.29
EDS spot 2		
Fe	14.74	2.22
Cu	7.51	3.14
Al	66.42	3.44
Si	11.33	5.80
EDS spot 3		
Cu	1.25	1.54
Al	98.75	2.81
EDS spot 4		
Al	2.25	3.08
Si	97.50	2.30
EDS spot 5		
Fe	15.16	2.21
Cu	7.35	3.26
Al	66.16	3.45
Si	11.33	5.79
EDS spot 6		
Cu	53.33	2.72
Al	46.67	5.29
EDS spot 7		
Cu	53.33	2.72
Al	46.67	5.29